Recent developments in heavy-ion fusion reactions

B. B. Back,* H. Esbensen, C. L. Jiang, and K. E. Rehm

Physics Division, Argonne National Laboratory, Argonne, Illinois 60439, USA

(published 28 March 2014)

In this review the main advances in heavy-ion fusion research that have taken place over the last decade are addressed. During this period, experimental studies have been extended to deep sub-barrier energies to reveal the unexpected phenomenon of fusion hindrance. The coupled-channels descriptions have been refined to include the effects of nucleon transfer and to account for the fusion hindrance in terms of the ion-ion potential in the strongly overlapping region. Substantial progress has been made in time-dependent Hartree-Fock theory to the point that this approach now can make parameter-free predictions of heavy-ion fusion excitation functions. As several heavy-ion fusion reactions are of crucial importance in late-stage giant-star evolution, these reactions continue to be studied with better experimental and theoretical tools in order to provide improved input to astrophysical models. The effects of loosely bound valence nucleons on the fusion cross sections are the focus of a number of experimental studies involving radioactive beams, which have only recently become available. And finally, as the active field of synthesizing superheavy elements relies on heavy-ion fusion to reach the nuclei of interest, it is important to understand the fusion dynamics that plays a crucial role in both the "cold-fusion" and "hot-fusion" approaches to the superheavy island of stability. Also this area has seen significant progress in several different approaches to the problem of predicting the cross sections for formation and survival of these rare nuclei.

DOI: 10.1103/RevModPhys.86.317 PACS numbers: 25.70.Jj, 25.60.Pj, 26.30.Ef, 26.20.Np

CONTENTS

I. INTRODUCTION

The interest in heavy-ion fusion has its roots in the quest to extend the periodic table beyond the elements that can be synthesized using neutrons and light charged particles and

*Corresponding author.
back@anl.gov

heavy actinide targets. Heavier beams of carbon, oxygen, and beyond were needed to reach this new territory via the heavy-ion fusion process in which the beam and target nuclei provided the protons and neutrons to the new element. As several facilities that could provide such beams became available during the late 1960s and during the 1970s, much of the interest in nuclear physics shifted from nuclear excitations that can be induced by light ion beams to those that require the high angular momenta that only the heavy-ion fusion process can reach. As fusion accounts for the major part of the reaction cross section in most cases where above-barrier beam energies are used, it was only natural that a comprehensive study of this reaction became a central focus of nuclear physics research. The theoretical descriptions of the process were initially rather rudimentary, but they gave the essential overall dependence of the cross sections on beam energy, system size, and the range of angular momenta of the fused system. The expression for the fusion cross section is often given as

$$\sigma_{\mathrm{CN}} = \pi\lambda\!\!\!^{-2} \sum_{L=0}^{\infty} (2L+1) T(L) P_{\mathrm{CN}}(L), \tag{1}$$

where $T(L)$ is the normal L-dependent transmission coefficient for the interaction potential and $P_{\mathrm{CN}}(L)$ is the probability that a compound nucleus (CN) is formed. In most cases, the P_{CN} term can safely be assumed to be unity; only in systems leading to very heavy compound systems does the dynamics of forming a compound system from the dinuclear configuration at the interaction barrier cause this factor to fall substantially below unity. Experimentally, what is observed is often the evaporation residues formed after particle and γ emission from the hot compound system that is formed in the fusion process. Again, for relatively light systems this constitutes the main decay cascade that reduces the excitation energy and angular momentum of the system. However, in heavy systems where fission can compete with particle evaporation, this decay branch must also be measured in order to arrive at the total fusion cross section.

The effect of target deformation on the heavy-ion fusion cross sections was recognized in excitation functions on the deformed ^{238}U target (Wong, 1973) and subsequent experimental data on Sm isotopes clearly demonstrated this effect (Stokstad *et al.*, 1976). For the heaviest projectiles, it also became clear that other processes, such as deep-inelastic scattering and quasifission, which lead to two large fragments in the exit channel, became strong competitors to the complete fusion reaction (Gross and Kalinowski, 1978; Świątecki, 1981; Bjørnholm and Świątecki, 1982; Fröbrich, 1984). The notion that intrinsic excitations of the target nucleus affect the fusion process was first proposed by Esbensen (1981). Further development with the coupled-channels (CC) method (MacFarlane and Pieper, 1978; Dasso, Landowne, and Winther, 1983) provided an excellent description of the often very different behavior of the fusion excitation function in the barrier region for even-even neighboring systems, as illustrated in, e.g., the Ni + Ni systems (Beckerman *et al.*, 1980). Inherent in the coupled-channels description of the fusion process is the notion that a multiplet of interaction barriers are involved in the process and it was demonstrated that a double differentiation of high-quality fusion excitation functions directly reflects the distribution of barriers (Rowley, Satchler, and Stelson, 1991). Experimentally, the development of new instrumentation and methods allowed for the extension of measurements to deep sub-barrier energies (Jiang *et al.*, 2002), which revealed an unanticipated drop in the cross sections that could not be explained by the coupled-channels theory with standard ion-ion potentials. In addition, with the availability of radioactive beams it became possible to study the effects of loosely bound valence nucleons on the fusion process and some insight into the reaction mechanism was gained by applying the continuum discretized coupled-channels (CDCC) method to describe the interplay of fusion and breakup. Recently, the description of heavy-ion fusion within the time-dependent Hartree-Fock (TDHF) framework has advanced to the point of being able to provide an essentially parameter-free prediction of this process [see, e.g., Negele (1982) for a general overview of the TDHF method]. Finally, although the basic concept of a strong inhibition of complete fusion in heavy systems has been realized since the early 1980s, the theoretical description of this effect now appears to have reached a level where the observed minute cross sections for synthesizing superheavy elements can be reliably reproduced and predictions for even heavier systems can be made.

In this review, the most recent developments in fusion research will be reviewed. As detailed below, earlier review articles summarize the previous developments. This article therefore attempts to cover the research that has received less attention in earlier works as well as the experimental and theoretical work that has been carried out in the most recent period.

A. Brief history and references to previous reviews

The early experimental data and simple theoretical understanding of heavy-ion fusion reactions were obtained in the 1970s and were reviewed by Birkelund *et al.* (1979) and later by Birkelund and Huizenga (1983) within the context of other reaction channels. The systematic review of heavy-ion fusion by Vaz, Alexander, and Satchler (1981) was concerned with the height of the fusion barrier. This quantity was extracted using a one-dimensional barrier penetration model from cross sections between 100 and 500 mb. It was known that sub-barrier fusion could be enhanced compared to a one-dimensional calculation and therefore that energy regime was excluded. It was suspected that high-energy fusion data may not be reliable as well and cross sections larger than 500 mb were therefore also excluded.

A new generation of experiments was performed after the discovery of the enhancement of sub-barrier fusion. The first review of the subject was published by Beckerman (1985), one of the pioneers in the field. It was followed by a second review a few years later (Beckerman, 1988). In the meantime, the theoretical understanding of the fusion process was discussed by Steadman and Rhoades-Brown (1986).

Better insight into the fusion process can be obtained from the angular momentum dependence of fusion cross sections. This can be probed by measuring the γ multiplicity from fusion-evaporation residues or by measuring the anisotropy in

the angular distribution of fission fragments. The results of these methods were reviewed by Vandenbosch (1992). A more general review of heavy-ion reactions at energies close to the Coulomb barrier was written by Reisdorf (1994). It described many of the experimental and theoretical developments that had taken place since the earlier reviews by Beckerman (1985) and by Steadman and Rhoades-Brown (1986).

Further theoretical understanding of the fusion process was enabled by the high-precision fusion data that were first obtained at the Australian National University. The high precision of the data allowed a determination of the second derivative of the energy-weighted cross section which was interpreted to represent the barrier distribution for fusion (Rowley, Satchler, and Stelson, 1991). A review of these new developments was subsequently published by Dasgupta *et al.* (1998), followed by a dedicated review of the many theoretical developments by Balantekin and Takigawa (1998).

These reviews have been the standard references in the field of heavy-ion fusion reactions for many years.

With the construction of radioactive beam facilities, a renewed interest developed concerning the fusion of weakly bound nuclei. Early theoretical discussions focused on how the coupling to the breakup of weakly bound nuclei would influence the fusion yield and how it would affect the competition between complete and incomplete fusion. This subfield has been reviewed by Liang and Signorini (2005), Canto *et al.* (2006), and Keeley *et al.* (2007).

Quite recently, Hagino and Takigawa (2012) published a new review of sub-barrier fusion reactions. This review primarily concerns the theoretical description of many-particle quantum tunneling and is a useful reference for a more detailed discussion.

Finally, the field of heavy-ion fusion reactions has been the central topic for a series of conferences, namely, FUSION97 (1997), FUSION03 (2004), FUSION06 (2006), FUSION08 (2008), and FUSION11 (2011).

B. Focus of this review

The focus of this review is to summarize new developments that have taken place since the reviews by Dasgupta *et al.* (1998) and Balantekin and Takigawa (1998). These developments include new measurements of fusion reactions with stable beams and with beams of unstable nuclei. Of particular interest are the fusion reactions at very low energies and very small cross sections, some of which are of interest to astrophysics.

New results with stable beams provide a better insight into the reaction mechanisms that can explain the measured fusion cross sections and the extracted barrier distributions. A large effort has been made since the review by Dasgupta *et al.* (1998) to reproduce the observed barrier distributions by considering the influence of an increasing number of multiphonon excitations in coupled-channels calculations. Another important subject has been to demonstrate experimentally the influence of nucleon transfer on fusion by comparing the fusion data obtained with different isotope combinations. These and other subjects that relate to reactions at energies close to the Coulomb barrier are discussed in Sec. II.

In Sec. III we review the progress that has been made in understanding the fusion hindrance which occurs for very small cross sections, at energies far below the Coulomb barrier. The phenomenon was first demonstrated by Jiang *et al.* (2002) who measured the fusion cross sections for $^{60}\mathrm{Ni} + {}^{89}\mathrm{Y}$ down to very small cross sections. It has since been confirmed in fusion measurements of many other light and medium-heavy systems.

In Sec. IV we discuss the inconsistency that exists between the parameters of the ion-ion potential that have been extracted from the analysis of elastic and quasielastic scattering data and from the analysis of fusion data at energies far above the Coulomb barrier. We show that the apparent inconsistency can sometimes be removed by applying an ion-ion potential that has a shallow pocket and a thicker barrier in the entrance channel potential.

In Sec. V we discuss recent developments in the understanding of the fusion reactions of carbon isotopes that take place in type Ia supernovae and other cosmic events such as superbursts in accreting neutron stars. This is followed, in Sec. VI, by a summary of the research in fusion reactions with unstable nuclei that has taken place since the two most recent reviews on this subject by Liang and Signorini (2005) and Canto *et al.* (2006). Finally, the connection between fusion and the production of superheavy elements is discussed in Sec. VII.

II. NEW RESULTS AT ENERGIES NEAR THE COULOMB BARRIER

The experimental study of heavy-ion fusion reactions has continued vigorously since the review by Dasgupta *et al.* (1998). The goal has been to reveal the influence of the nuclear structure of the reacting nuclei on the fusion process. The most obvious effect is the large enhancement of sub-barrier fusion cross sections that is observed in comparison to the predictions of one-dimensional barrier penetration models. The enhancement can often be explained by coupled-channels calculations that include couplings to the low-lying surface modes of the reacting nuclei (Balantekin and Takigawa, 1998). The coupled-channels method and the approximations that are commonly made are summarized in Sec. II.A and a description of the couplings to surface excitations is presented in Sec. II.B.

A major concern in the coupled-channels approach is how many channels one should include in the calculations and which channels can safely be ignored. This is a difficult question but some insight has been obtained by detailed calculations. For example, the excitation of high-lying or giant resonance states can often be ignored because the coupling to such states does not affect the shape (or energy dependence) of the calculated fusion cross section. The coupling to such states results instead in an overall shift in energy of the calculated cross section due to an adiabatic renormalization of the ion-ion potential (Hagino and Takigawa, 2012). The same is true for couplings to transfer channels with large negative Q values. These issues are discussed in Sec. II.B.

A good way to illustrate and amplify the energy dependence of the measured and calculated fusion cross sections at

energies close to the Coulomb barrier is to extract the so-called barrier distribution.

This approach was employed by Keller *et al.* (1986) in the analysis of the fusion-evaporation cross sections for ^{90}Zr + ^{89}Y, ^{90,92,96}Zr, and ^{94}Mo. Subsequently, Rowley, Satchler, and Stelson (1991) derived a closed-form expression that directly relates the barrier distribution to the second derivative of the energy-weighted fusion cross section. The shape of the calculated barrier distribution is sensitive to the nuclear structure of the reacting nuclei and it is sometimes possible to identify structures in the measured barrier distribution that are caused by the coupling to certain reaction channels. Some new results are discussed in Sec. II.C.

A particular issue has been to demonstrate the influence of nucleon transfer and to separate it from the well-known effects of couplings to surface excitations. The influence is most clearly seen in fusion reactions of asymmetric systems, in particular, in cases where the transfer Q values are positive. The approach has mostly been empirical, and some of the many results that have been obtained and the general picture that emerges are discussed in Sec. II.D.

One can also extract a barrier distribution from the measured quasielastic scattering. This concept was introduced by Timmers *et al.* (1995), and an important objective has been to investigate how this distribution compares to the barrier distribution for fusion. This is discussed in Sec. II.E Another issue is the influence of (many) weak reaction channels on the measured cross sections and the extracted barrier distributions, which is discussed in Sec. II.F.

An alternative to the coupled-channels approach is the TDHF method. Much progress has been made in recent years with this method and new results are summarized in Sec. II.G.

A. The coupled-channels approach

The influence of nuclear structure on heavy-ion fusion reactions is commonly studied in the coupled-channels approach using a number of computer codes, e.g., PTOLEMY (MacFarlane and Pieper, 1978), FRESCO (Thompson, 2006), and CCFULL (Hagino, Rowley, and Kruppa, 1999). The number of channels that needs to be included can be enormous. It is therefore necessary to make certain assumptions and approximations that reduce the effective number of channels and thus simplify the calculations. The basic problem is that an excited state with spin I generates $I + 1$ channels when coupled to the orbital angular momentum L of the scattering, with final orbital angular momenta $L' = |L - I|, \ldots, L + I$.

One way to simplify the calculations is to use the so-called rotating frame (or isocentrifugal) approximation, which was developed independently in 1986 by several groups as discussed in the review by Hagino and Takigawa (2012). The basic assumption of this approximation is that the orbital angular momentum L of the heavy-ion collision, or rather the centrifugal potential, is the same in all reaction channels. As a consequence of this assumption, one does not have to worry about the coupling of the spin of a state to the orbital angular momentum, and one has to consider only one effective channel for each excited state (instead of $I + 1$ channels). This reduces the number of coupled equations considerably.

The rotating frame approximation is well justified for heavy-ion fusion reactions. It has been tested in calculations of heavy-ion fusion cross sections on several occasions (Tanimura, 1987a; 1987b; Esbensen and Back, 1996). It has also been tested for inelastic (Esbensen, Landowne, and Price, 1987a, 1987b) and quasielastic scattering (Hagino and Rowley, 2004) as well as for transfer reactions at large scattering angles (Esbensen and Landowne, 1989). The approximation is poor at forward scattering angles, where the long-range Coulomb excitation dominates.

A consequence of the rotating frame approximation is that the magnetic quantum number M of the entrance channel is conserved. In collisions of even-even nuclei, the ground-state spins of the reacting nuclei are zero and the magnetic quantum number remains zero all through the collision. In reactions of an even-even nucleus with an odd-A nucleus with ground-state spin I, one must then repeat the calculation of the fusion cross section for each value of the M quantum number, $M = -I, \ldots, I$, and it is the average cross section that should be compared to the data for an unpolarized beam and target (Esbensen, 2003).

1. Coupled equations

In the rotating frame, the coupled equations are [see, for example, Esbensen (2003) and Hagino and Takigawa (2012)]

$$(h_L + \epsilon_{nI} - E)\phi_{nI}(r) = -\sum_{n'I'} \langle nI|\delta V|n'I'\rangle \phi_{n'I'}(r), \qquad (2)$$

where $\phi_{nI}(r)$ is the radial wave function of the channel $|nI\rangle$ with excitation energy ϵ_{nI}. The conserved magnetic quantum number M of the excited states $|nIM\rangle$ has been suppressed in the notation. The interaction δV that produces the couplings between the different channels is discussed in Sec. II.B. The diagonal part of the radial Hamiltonian is

$$h_L = \frac{\hbar^2}{2\mu}\left(-\frac{d^2}{dr^2} + \frac{L(L+1)}{r^2}\right) + \frac{Z_1 Z_2 e^2}{r} + U(r), \qquad (3)$$

where μ is the reduced mass of the interacting nuclei, $Z_1 Z_2 e^2/r$ is the Coulomb interaction, and $U(r)$ is the ion-ion potential.

The coupled equations are solved with the usual scattering boundary conditions at large separations of projectile and target,

$$\phi_{nI}(r) \to e^{-ikr}\delta_{nI,00} + r_{nI}e^{ik_n r} \quad \text{for } r \to \infty, \qquad (4)$$

with an incoming wave only in the elastic channel $|00\rangle$ and outgoing waves in all channels, with reflection coefficients r_{nI}. The fusion is simulated by ingoing-wave boundary conditions (IWBC),

$$\phi_{nI}(r) = t_{nI}e^{-iq_{nI}r}, \qquad (5)$$

which are imposed after the barrier has been penetrated, conventionally at the minimum of the pocket in the entrance channel potential. Here q_{nI} is the local momentum at the position where the IWBC are imposed and t_{nI} is the

transmission coefficient. The fusion cross section is determined by the ingoing flux at the minimum of the pocket $|t_{nI}|^2\hbar q_{nI}/\mu$ relative to the incoming flux $\hbar k/\mu$ in the entrance channel,

$$\sigma_f = \pi\lambda\!\!\!^{-2}\sum_{nIL}(2L+1)\frac{q_{nI}}{k}|t_{nI}|^2. \tag{6}$$

This implies that the fusion in a certain channel $|nI\rangle$ will vanish whenever the local momentum q_{nI} is zero.

The ingoing-wave boundary conditions are sometimes supplemented with or replaced by the absorption in a weak and short-range imaginary potential that acts near the minimum of the pocket in the entrance channel potential. The fusion cross section is then determined by Eq. (6) plus the absorption in the imaginary potential,

$$\sigma_{\rm abs} = \pi\lambda\!\!\!^{-2}\sum_{nIL}(2L+1)P_{nI}({\rm abs}), \tag{7}$$

where $P_{nI}({\rm abs})$ is the absorption probability of the channel $|nI\rangle$. It is sometimes difficult to account for the fusion data at energies far above the Coulomb barrier and it becomes necessary to apply a stronger and longer-ranged imaginary potential. One reason could be that the number of open channels increases dramatically at high energies and many of them are not considered explicitly in the coupled equations. This problem is discussed in Sec. IV.

2. The ion-ion potential

The ion-ion potential $U(r)$ is a critical ingredient in coupled-channels calculations. It determines not only the height of the Coulomb barrier V_{CB}, but also the nuclear couplings to the excited states of the reacting nuclei. The ion-ion potentials that have been used are often of the Woods-Saxon type

$$U(r) = \frac{U_0}{1+\exp[(r-R)/a]}, \tag{8}$$

where U_0 is the depth, R is the radius, and a is the diffuseness of the potential. A standard set of parameters that are consistent with the analysis of elastic scattering data can be found in the textbook by Broglia and Winther (1991). The empirical potential is a smooth function of the mass numbers of the reacting nuclei and may need small adjustments, for example, of the depth U_0 or the radius R, in order to optimize the fit to fusion data.

In recent years it has been realized that the Woods-Saxon parametrization of the ion-ion potential is unrealistic for overlapping nuclei and provides a poor description of the fusion data at extreme sub-barrier energies (see Sec. III). One way to overcome this problem is to use a double-folding potential and adjust it for overlapping nuclei so that it provides a better description at very low energies. The potential is given by

$$U(\mathbf{r}) = \int d\mathbf{r}_1 \int d\mathbf{r}_2 \rho_1(\mathbf{r}_1)\rho_2(\mathbf{r}_2)v_{NN}(\mathbf{r}+\mathbf{r}_2-\mathbf{r}_1), \tag{9}$$

where ρ_i are the densities of the reacting nuclei, and v_{NN} is an effective, nucleon-nucleon (NN) interaction. An interaction that is often used is the M3Y interaction which was introduced by Bertsch *et al.* (1977). This interaction produces an ion-ion potential outside the barrier region that is in good agreement with the empirical Woods-Saxon potential for elastic scattering discussed above (Akyüz *et al.*, 1981). Moreover, it has proven quite reliable in predicting the height of the Coulomb barrier (Mişicu and Esbensen, 2007). The predicted entrance channel potential is unfortunately unrealistic for overlapping nuclei because it is much deeper than the ground-state energy of the compound nucleus. The effective NN interaction is therefore supplemented with a repulsive contact term,

$$v_{NN}^{\rm rep}(\mathbf{r}) = v_0\delta(\mathbf{r}). \tag{10}$$

The repulsive potential is calculated by inserting the interaction defined in Eq. (10) into the double-folding expression, Eq. (9). The diffuseness a_r of the densities is treated as an adjustable parameter. The strength v_0 of the repulsion is calibrated to produce a reasonable incompressibility for completely overlapping nuclei, for example, the value predicted by Myers and Świątecki (2000). The diffuseness a_r, on the other hand, is adjusted to optimize the fit of coupled-channels calculations to the fusion data (Mişicu and Esbensen, 2007). The total ion-ion potential is referred to as the M3Y + repulsion (M3Y + rep) potential. There are essentially two kinds of adjustable parameters in this potential: the radii of the reacting nuclei and the diffuseness a_r, which controls the depth of the pocket in the entrance channel potential.

Examples of entrance channel potentials for the fusion of ^{48}Ca + ^{48}Ca are shown in Fig. 1. The M3Y + repulsion potential was adjusted to reproduce the data of Stefanini *et al.* (2007a), whereas the Woods-Saxon (WS) potential was

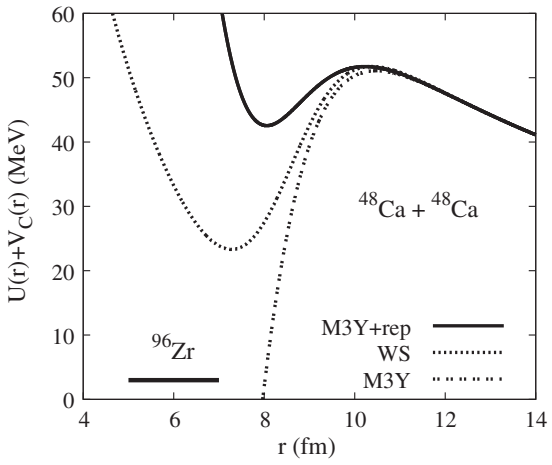

FIG. 1. Entrance channel potentials for the fusion of ^{48}Ca + ^{48}Ca. The Woods-Saxon potential (dotted curve) is compared to the M3Y potential with (solid curve) and without (dashed curve) repulsion. The corresponding ground-state energy of the fused system ^{96}Zr is also indicated by the horizontal bar. From Esbensen, Jiang, and Stefanini, 2010.

adjusted to fit the high energy data (Esbensen, Jiang, and Stefanini, 2010). These data are discussed in more detail in Sec. II.D.

B. Excitations of surface modes

The most important excitations that can influence the fusion of heavy, spherical nuclei are usually the low-lying 2^+ and 3^- states of projectile and target, but low-lying 4^+ and 5^- states can occasionally also play a role. However, if one wants to account for the large enhancement of sub-barrier fusion cross sections compared to one-dimensional barrier penetration calculations, it is often important to include the influence of the two-phonon and mutual excitations of the low-lying 2^+ and 3^- states in projectile and target. In the rotating frame approximation discussed above, that implies a total of 15 coupled channels which are illustrated schematically in Fig. 2. Without the rotating frame approximation, the total number of channels would be over 100.

The nuclear couplings to surface excitations of a nucleus are generated by the interaction $U(r-\delta R)$, where $U(r)$ is the ion-ion potential, δR is the surface distortion

$$\delta R = \sum_{n\lambda\mu} R\alpha_{n\lambda\mu} Y_{\lambda\mu}(\hat{r}), \tag{11}$$

and $\alpha_{n\lambda\mu}$ is the static or dynamic deformation amplitude. In the rotating frame, the direction $\hat{r}$ between the colliding nuclei defines the z axis. That implies that $\mu = 0$ and

$$\delta R = \sum_{n\lambda} R\alpha_{n\lambda 0}\sqrt{\frac{2\lambda+1}{4\pi}}. \tag{12}$$

The matrix element of the surface distortion amplitude between the ground state and the first excited state is

$$\langle n\lambda|\delta R|00\rangle = \frac{\beta_{n\lambda}R}{\sqrt{4\pi}}. \tag{13}$$

This expression holds for both static and dynamic deformations, i.e., rotational and vibrational excitations of the reacting nuclei.

The Coulomb interaction between the reacting nuclei can safely be truncated to first order in deformation amplitudes.

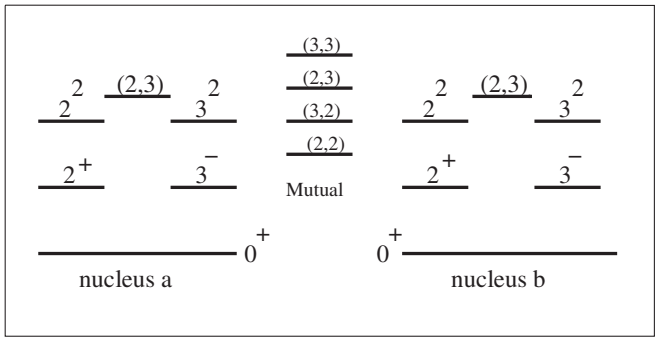

FIG. 2. States included in standard two-phonon coupled-channels calculations of fusion of even-even nuclei.

The off-diagonal part of the Coulomb interaction which generates the coupling matrix elements in the coupled equations, Eq. (2), is

$$\delta V_C = \sum_{n\lambda} \frac{3Z_1Z_2e^2}{2\lambda+1}\frac{R^\lambda}{r^{\lambda+1}}\alpha_{n\lambda 0}\sqrt{\frac{2\lambda+1}{4\pi}}. \tag{14}$$

The structure input to the coupled-channels calculations are the excitation energies, and the strengths β_λ of the couplings which are extracted from the measured $B(E\lambda)$ values for the electromagnetic decay from the excited state λ^π to the 0^+ ground state,

$$B(E\lambda) = \left(\frac{3Ze^2R^\lambda}{4\pi}\right)^2\frac{\beta_\lambda^2}{4\pi}. \tag{15}$$

The value of β_λ is usually assumed to be the same for Coulomb and nuclear induced excitations. However, this is not necessarily correct, and different values are sometimes used if the nuclear coupling strength can be determined from the analysis of inelastic scattering data.

The nuclear interaction has in the past been calculated to first order in the surface distortion δR. It was pointed out by Hagino *et al.* (1997a) that it is important to include surface distortions to all orders when calculating the coupling matrix elements in the coupled equations. A simple model was developed by Esbensen and Landowne (1987) in which the nuclear interaction $U(r-\delta R)$ is expanded up to second order in δR,

$$U(r-\delta R) \approx U(r) + \delta V_N,$$

where

$$\delta V_N = -\frac{dU}{dr}\delta R + \frac{1}{2}\frac{d^2U}{dr^2}[(\delta R)^2 - \langle 0|(\delta R)^2|0\rangle]. \tag{16}$$

The last term of second order in δR is constructed in such a way that it vanishes in the ground state of a nucleus. The first-order term in δR will also vanish in the 0^+ ground state of a nucleus so $U(r)$ remains the ion-ion potential for elastic scattering and needs not be renormalized. The renormalization may become a problem if one includes the interaction to all orders in δR.

The matrix elements of the second-order interaction, Eq. (16), can easily be calculated for a vibrational nucleus and the model has been applied consistently up to two-phonon excitations (Esbensen, 2003).

The computer code CCFULL (Hagino, Rowley, and Kruppa, 1999) is based on an approach that is very similar to what is described above since it makes use of the ingoing-wave boundary conditions that are imposed at the minimum of the pocket of the entrance potential. The calculations are also performed in the rotating frame (no Coriolis) approximation in order to limit the number of coupled equations. The ion-ion potential is always parametrized as a Woods-Saxon form and imaginary potentials cannot be employed. One major difference is that the couplings to rotational as well as surface excitations are calculated to all orders in the static and

dynamic deformation amplitudes, respectively, instead of truncating the expansion of the interaction to second order in α_λ as done in Eq. (16). The code is therefore better suited to describe the fusion of heavy and soft systems, where multiphonon excitations play a role. Finally, the code also includes the pair transfer between the ground states of the reacting nuclei and is described by a macroscopic form factor introduced by Dasso and Vitturi (1986) [see Eq. (24)].

1. Simplified models

It is useful to have simplified models of the fusion process that can easily be used to calculate the cross sections. For example, in the fusion of a spherical nucleus with a deformed target one can sometimes ignore the rotational excitation energies of the target and calculate the fusion cross section in the static approximation $\sigma_f(\hat{e})$ as a function of the orientation $\hat{e}$ of the deformed nucleus relative to the center axis. The average cross section, obtained by averaging over all orientations $\hat{e}$ of the target

$$\langle \sigma_f \rangle = \int \frac{d\Omega}{4\pi} \sigma_f(\hat{e}), \tag{17}$$

can be obtained from the computer code CCDEF developed by Fernandez-Niello, Dasso, and Landowne (1989).

Another useful computer code is CCFUS, which diagonalizes the interaction Hamiltonian at the position of the Coulomb barrier. It was developed by Dasso and Landowne (1987b) and is often referred to as the constant-coupling model because the coupling matrix elements on the right-hand side of Eq. (2) are assumed to be constants. This allows us to diagonalize the matrix

$$M_{nn'} = \epsilon_{nI}\delta_{nn'} + \langle nI|\delta V|n'I'\rangle \tag{18}$$

with a unitary transformation U,

$$\sum_{ij} U_{ni} M_{ij} (U^{-1})_{jm} = \lambda_n \delta_{nm}.$$

The diagonalized Hamiltonian then takes the form

$$(h_L + \lambda_{nI} - E)\phi_{nI}(r) = 0. \tag{19}$$

The fusion cross section for each individual eigenchannel $\sigma(E-\lambda_n)$ is a function (here the same function) of the energy E minus the eigenvalue λ_n, and the total cross section is given by the weighted sum,

$$\sigma_f = \sum_n |U_{n0}|^2 \sigma(E-\lambda_n), \tag{20}$$

where $|U_{n0}|^2$ is the weight of the eigenchannel n, which is expressed in terms of the matrix elements U_{n0} of the unitary transformation U.

It was realized early on by Dasso and Landowne (1987a) that there are important corrections to the constant-coupling model, due to the difference in the location of the different eigenbarriers. These corrections were implemented in their computer code CCFUS (Dasso and Landowne, 1987b). The computer code CCMOD (Dasgupta *et al.*, 1992) is a modified version of CCFUS that considers the effect of deformation on fusion. It also takes into account the difference in the radial location of the barriers in the different eigenchannels. Couplings of the ground states to excited states are calculated to first order in the (static or dynamic) deformation amplitudes.

2. Effects of high-lying states

A critical issue is how many channels should one include in the coupled-channels calculations in order to produce a converged result. This issue has been investigated in several publications that are discussed next.

The first example is the question of the influence of a high-lying state that may have a strong coupling to the ground state but very large and negative Q value. It has been shown by Takigawa *et al.* (1994) that the effect of couplings to high-lying states is mainly an adiabatic polarization which does not influence the shape of the calculated cross section (or barrier distribution) but produces an overall shift of the cross section to slightly lower energies. In the language of the constant-coupling model discussed above, the coupling to a high-lying state produces two eigenbarriers, one that is shifted slightly below the unperturbed barrier and carries most of the weight, and one that is shifted far above the unperturbed barrier and carriers a small weight.

The effect of the coupling to the relatively high-lying 3^- state in ^{16}O was discussed by Hagino *et al.* (1997a) in connection with the fusion of $^{16}\mathrm{O} + {}^{144}\mathrm{Sm}$. The dependence on the excitation energy of the 3^- state is nicely illustrated in Fig. 10 of the review by Hagino and Takigawa (2012). The coupling to the 3^- state in ^{16}O is relatively strong and produces a shift of the cross section (and barrier distribution) of about 1–2 MeV but the energy-dependent shape of the cross section is not much affected. The reason is (in the language of the constant-coupling model) that the 6.13 MeV excitation energy of the 3^- state is so high that there is no sign of a second, weaker barrier at higher energies.

Thus it appears that the coupling to high-lying states can be simulated by an adiabatic renormalization of the ion-ion potential. The simplest approach is to ignore the high-lying states and calibrate the ion-ion potential, for example, of the Woods-Saxon type, so that the measured cross sections are reproduced. This approach would not be satisfactory if a double-folding potential was used because one would have to use densities with larger radii in order to simulate the effect of the adiabatic polarization of the state that has been left out.

C. Barrier distributions from high precision fusion data

A good way to reveal detailed structures in the energy dependence of the measured fusion cross sections at energies close to the Coulomb barrier is to plot the so-called barrier distribution, which is defined as the second derivative of the energy-weighted cross section (Rowley, Satchler, and Stelson, 1991),

$$B(E) = \frac{d^2(E\sigma_f)}{dE^2}. \quad (21)$$

The experimental barrier distribution is calculated using the finite difference method and the energy step ΔE that is used is usually of the order of 2 MeV. Since the barrier distribution is sensitive to the value of ΔE it is important to choose the same energy step when calculating and comparing to the theoretical barrier distributions. For a single barrier (i.e., without any couplings) the definition, Eq. (21), produces a distribution that is peaked at the Coulomb barrier and has a width that is determined by the "diffuseness" of the barrier penetration probability.

In the constant-coupling model, Eq. (20), the definition Eq. (21) of the barrier distribution produces a weighted sum of eigenbarrier distributions,

$$B_f(E) = \sum_n W_n B(E - \lambda_n). \quad (22)$$

The position of a peak in the barrier distribution can therefore be identified with the energy of the eigenbarriers, $V_n = V_{CB} + \lambda_n$, where V_{CB} is the Coulomb barrier associated with the unperturbed Hamiltonian h_L (for $L = 0$) as defined in Eq. (3). The overall width of the theoretical barrier distribution obtained from coupled-channels calculations is therefore expected to reflect the strengths of the couplings and the excitation energies of the states that are included in the calculations.

Several examples of barrier distributions were presented in the review by Dasgupta *et al.* (1998). Some showed a clear signature of the effect of deformation on the shape of the barrier distribution, and others illustrated the influence of couplings to excitations of surface modes that can produce several peaks in the barrier distribution. For example, in the fusion of $^{16}O + ^{144}Sm$, the coupling to the 3^- state of ^{144}Sm produces two well-separated peaks and such peaks are clearly observed in the measured barrier distribution (Hagino and Takigawa, 2012).

The influence on the barrier distribution of two-phonon excitations and higher-order couplings was investigated by Newton *et al.* (2001) in a systematic study of high precision fusion data for lighter projectiles reacting with a ^{92}Zr target. It was shown that two-phonon excitations of the low-lying target states influence the barrier distribution and that a better fit to the data was obtained by applying a nuclear coupling parameter β_2^N that is larger than the adopted and better known value of the Coulomb parameter β_2^C. Finally, the fits to the high-energy fusion data improved by applying a large diffuseness of the ion-ion potential. Moreover, the best value of the diffuseness seemed to increase with increasing values of the product Z_1Z_2 of the atomic numbers of projectile and target. This feature is discussed in more detail in Sec. IV.B.

In the fusion of systems with very strong couplings involving heavy soft or strongly deformed nuclei, it is necessary to consider excitations to multiphonon or high-spin states in order to make the calculations converge. Couplings to such high-lying states are often required to reproduce the data. A good example is the fusion of $^{58}Ni + ^{60}Ni$, which was measured by Stefanini *et al.* (1995). In that work it was necessary to include up to four-phonon excitations, in order to reproduce the structures that were observed in the measured barrier distribution. However, it seems unlikely that the harmonic approximation provides a realistic description of such high-lying states.

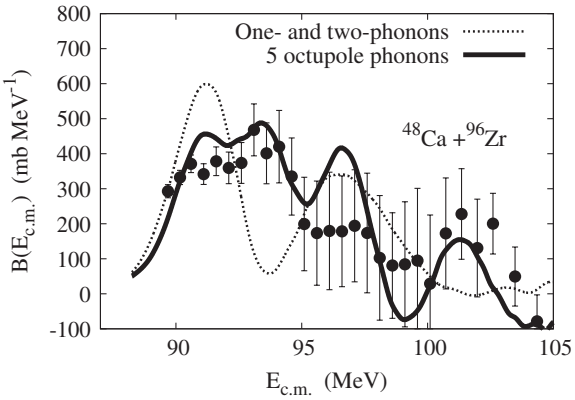

FIG. 3. Barrier distributions for the fusion of $^{48}Ca + ^{96}Zr$ calculated by Esbensen and Jiang (2009), including one- and two-phonon (dotted curve), or up to five-phonon excitations (solid curve), are compared to the experimental distribution extracted from the data of Stefanini *et al.* (2006).

A more recent example is the fusion of $^{48}Ca + ^{96}Zr$, which was measured by Stefanini *et al.* (2006). The measured and calculated barrier distributions obtained for this system are illustrated in Fig. 3. Here the coupling to the octupole excitation of ^{96}Zr is particularly strong and by considering up to five-phonon excitations of this surface mode, in addition to the one- and two-phonon excitations of other low-lying surface modes, it is possible to describe the measured barrier distribution fairly well (Esbensen and Jiang, 2009). The good agreement with the measured distribution could be accidental because the couplings to and among such high-lying states are poorly known. On the other hand, the data offer the opportunity to test specific nuclear structure models, and it appears that the vibrational model used here works quite well.

D. Influence of breakup reactions

The influence of breakup on fusion is in general difficult to calculate within the coupled-channels approach because of the large number of channels that are needed to describe the breakup process. The issue has been discussed, in particular, in connection with the fusion of weakly bound nuclei and some of the reactions that have been measured are summarized in Sec. VI.

A coupled-channels technique known as the CDCC has been developed to describe the two-body breakup of a weakly bound nuclei in the Coulomb and nuclear fields from a target nucleus (Sakuragi, Yahiro, and Kamimura, 1986). The continuum wave function for the breakup is described by a large number of discretized states that are not true continuum states but are localized in space. The method has mostly been used to describe two-body breakup reactions at intermediate energies but it has also been used to study the fusion of $^{6,7}Li$ (described as two-body systems) with a heavy target nucleus (Diaz-Torres, Thompson, and Beck, 2003). It was found that the

breakup enhances the total fusion cross section at energies near the Coulomb barrier, whereas it has hardly any effect at high energies.

The CDCC method has also been applied to calculate the fusion of ^{6}He with a heavy target, describing the ^{6}He as ^{4}He plus a dineutron two-body system (Beck, Keeley, and Diaz-Torres, 2007). They found also in this case an enhancement of the total fusion of ^{6}He due to the coupling to breakup channels. In this work measurements of the elastic scattering of ^{6,7}Li on ^{59}Co were compared to CDCC calculations. The calculations showed a clear influence of the breakup and good agreement with the data was achieved.

The CDCC method has, unfortunately, not been applied extensively to calculate the fusion of other weakly bound nuclei with stable targets, although many experiments have been performed. A major limitation of the CDCC method is that the weakly bound nucleus must be described as a two-body system. Moreover, it is difficult to include other excitations in the calculations besides the breakup because it would make the calculations much more time consuming. An extended CDCC method, which includes core excitations in addition to the breakup, has been developed (Summers, Nunes, and Thompson, 2006) but it has not been applied to fusion.

One can also calculate the two-body breakup of weakly bound nuclei and their fusion with an inert target nucleus by using the time-dependent wave-packet method developed by Ito *et al.* (2006, 2007). They applied the method to calculate the fusion of ^{11}Be and ^{6}He with heavy targets and found that the fusion cross section is slightly hindered by the presence of weakly bound neutrons. They showed that this conclusion is sensitive to the maximum angular momentum used in the calculation, and they argued that this sensitivity can explain differences with CDCC calculations discussed above. They also argued that the influence of a weakly bound proton is to enhance the cross section for the fusion of the core with the target nucleus.

It is difficult to judge how well the calculations described above agree with measurements because the calculated effects are relatively small and the experimental error bars are relatively large. It would therefore be useful to apply the methods to other systems, where measurements have been performed and error bars are smaller. Some of these systems are discussed in Sec. VI.

Further theoretical development of the CDCC approach has been carried out by Diaz-Torres *et al.* (2007) and Diaz-Torres (2010b, 2011) and important data on incomplete fusion and break-up reactions have recently become available; see, e.g., Souza *et al.* (2009, 2010a, 2010b) and Shrivastava *et al.* (2013).

E. Influence of transfer reactions

The influence of couplings to transfer channels on heavy-ion fusion cross sections has been much debated since the early measurements for the nickel isotopes by Beckerman *et al.* (1980). The data for the symmetric ^{58}Ni + ^{58}Ni and ^{64}Ni + ^{64}Ni systems can be explained fairly well by coupled-channels calculations that include couplings to one- and two-phonon excitations of low-lying surface modes (Mişicu and Esbensen, 2007). The fusion of the asymmetric ^{58}Ni + ^{64}Ni system, on the other hand, is enhanced at low energy and suppressed at high energy compared to coupled-channels calculations that include only couplings to low-lying surface modes. It was proposed early on by Broglia *et al.* (1983) that the coupling to transfer channels with positive Q values would explain the data.

A schematic model of the influence of transfer on fusion was developed early on by Stelson (1988). It related the enhancement of sub-barrier fusion to the onset of a neutron flow between the reacting nuclei, and parametrized the cross section in terms of a barrier distribution for fusion several years before this concept was introduced by Rowley, Satchler, and Stelson (1991). Stelson found that a rather flat and broad barrier distribution was required to fit the Ni + Ni fusion data discussed above. The model has had a lot of appeal over the years because a neutron flow must definitely have an influence on the fusion of asymmetric systems that have positive Q values for neutron transfer. However, the application of the model to the fusion of symmetric systems, where the Q values for transfer are large and negative, is questionable.

The influence of transfer on fusion can qualitatively be understood from the work of Dasso, Landowne, and Winther (1983). They showed that the coupling to a channel with positive Q value enhances the fusion cross section at low energy, whereas the coupling to a channel with large negative Q values has a much smaller effect. This is exactly the situation for the nickel isotopes, where the Q values for pair transfer (both two-neutron and two-proton) are positive for the asymmetric ^{58}Ni + ^{64}Ni system, whereas they are negative in the two symmetric systems. Actually, what matters most according to Broglia *et al.* (1983) is not the Q value itself but rather the effective Q value,

$$Q_{\text{eff}} = Q + \Delta V_{CB}, \tag{23}$$

where ΔV_{CB} is the height of the Coulomb barrier in the entrance minus the height in the exit channel.

A similar trend was observed in the fusion of ^{40}Ca with the ^{40,44,48}Ca isotopes by Aljuwair *et al.* (1984), where the fusion of the asymmetric systems was enhanced compared to the fusion of the symmetric ^{40}Ca + ^{40}Ca system.

The fusion of ^{48}Ca + ^{48}Ca was recently measured by Stefanini *et al.* (2009), and the fusion of ^{40}Ca + ^{48}Ca and ^{40}Ca + ^{40}Ca was remeasured down to much smaller cross sections by Jiang *et al.* (2010b) and Montagnoli *et al.* (2012), respectively. The new data sets are shown in Fig. 4. They exhibit a trend similar to what was observed for the nickel isotopes, namely, that the fusion of the asymmetric system is enhanced at low energy and suppressed at high energies compared to a smooth interpolation between the data for the two symmetric systems.

A characteristic feature of the effect of couplings to transfer channels with positive Q values is that the coupling to the pair transfer has the largest influence, whereas the coupling to single-nucleon transfer channels usually has a smaller effect on the calculated sub-barrier fusion cross section. The qualitative reason for this feature is that the form factors $F_{1N}(r)$ for single-nucleon transfer are long ranged, $F_{1N}(r) \propto \exp(-r/a)$ with $a \approx 1.2$ fm, whereas the pair-transfer form factor $F_{2N}(r)$ is proportional to the square of single-nucleon

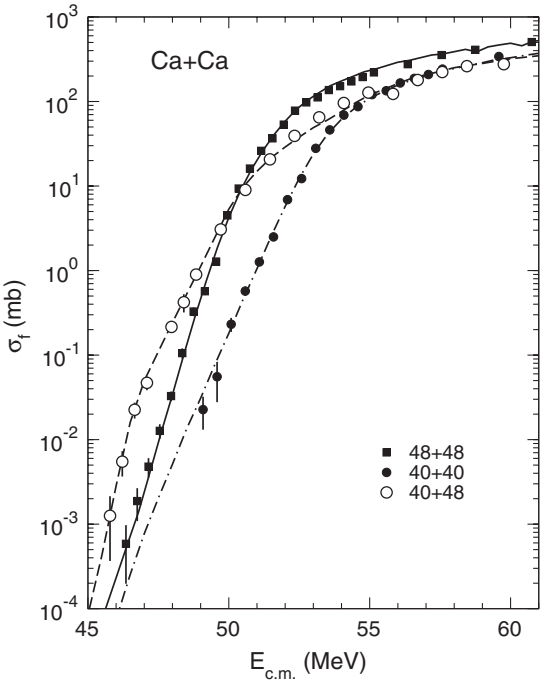

FIG. 4. Fusion cross section for the $^{40}Ca + {}^{40}Ca$ by Montagnoli *et al.* (2012) is compared to $^{48}Ca + {}^{48}Ca$ (Stefanini *et al.*, 2009) and $^{40}Ca + {}^{48}Ca$ (Jiang *et al.*, 2010b). The curves represent coupled-channels calculations using the $M3Y +$ rep potential. From Montagnoli *et al.*, 2012.

transfer form factors and is therefore of shorter range, $F_{2N}(r) \propto |F_{1N}(r)|^2 \propto \exp(-2r/a)$. In other words, the single-nucleon transfer cross sections may be large because the form factors are long ranged but the strength of the couplings may still be relatively small at the Coulomb barrier and the effect on fusion will therefore be modest, according to the constant-coupling model of Dasso, Landowne, and Winther (1983).

The fusion data for the two symmetric calcium systems shown in Fig. 4 were explained by coupled-channels calculations that included couplings to the one- and two-phonon, and mutual excitations of the low-lying surface modes (Montagnoli *et al.*, 2012). The M3Y + repulsion, double-folding potential that was used (see Sec. II.A.2) was adjusted for each symmetric system to optimize the fit to the data. The low-energy region for these systems will be discussed in more detail in Sec. III.C. This calibration made it possible to predict the double-folding potential for the asymmetric $^{40}Ca + {}^{48}Ca$ system. However, in order to explain the data for the asymmetric system, it was necessary to include couplings to transfer channels, the most important being the two-neutron and two-proton transfer channels which both have positive Q values. The two-nucleon transfer was simulated by the form factor originally proposed by Dasso and Pollarolo (1985),

$$F_{2N}(r) = -\sigma_t \frac{dU(r)}{dr}, \tag{24}$$

where $U(r)$ is the ion-ion potential. The coupled-channels calculations of the fusion of $^{40}Ca + {}^{48}Ca$ were performed within a model introduced by Esbensen, Jiang, and Rehm (1998) that treats the excitation of nuclei and the transfer of nucleons as two independent degrees of freedom. The effective Q value for the pair transfer was set to $Q_{2N} = +1$ MeV [which is close to the optimum Q value, see Rehm (1991)], and the strength of the pair-transfer σ_t coupling was adjusted to optimize the fit to the fusion data of Jiang *et al.* (2010b). The results of the calculations were discussed by Montagnoli *et al.* (2012) and are shown in Fig. 4. It should be mentioned that a similar approach by Broglia, Dasso, and Landowne (1985) made it possible to qualitatively explain the $^{58}Ni + {}^{64}Ni$ fusion data.

Another example where couplings to transfer channels are needed is the fusion of $^{40}Ca + {}^{96}Zr$. This was measured together with the fusion of $^{40}Ca + {}^{90}Zr$ by Timmers *et al.* (1998). The data are shown in Fig. 5, together with coupled-channels calculations that include couplings to one- and two-phonon excitations as well as mutual excitations of the one-phonon states. The calculation for $^{40}Ca + {}^{90}Zr$ reproduces the data for this system quite well, whereas a similar calculation for $^{40}Ca + {}^{96}Zr$ falls short of explaining the data at low energies. The most likely reason is that the effective Q values for one- and two-nucleon transfer are all positive for the latter system, and couplings to transfer channels should therefore be considered. The effective Q values for the first system $^{40}Ca + {}^{90}Zr$ are mostly negative, except for the two-proton transfer which has an effective Q value of 3 MeV. The good agreement between the data and the calculation suggests that the influence of transfer must be small in this case. A similar trend was observed in the fusion of $^{32}S + {}^{90,96}Zr$ by Zhang *et al.* (2010).

The ^{48}Ca induced fusion on $^{90,96}Zr$ was measured by Stefanini *et al.* (2006). The data appear to be more "well behaved" at low energies than the $^{40}Ca + {}^{96}Zr$ data discussed above. This is illustrated in Fig. 6 where data for the latter system exhibit the strongest enhancement and the smallest logarithmic slope at low energies. The steeper falloff for the ^{48}Ca induced reactions correlates with a weak influence of couplings to transfer reactions because most of the effective Q values are negative.

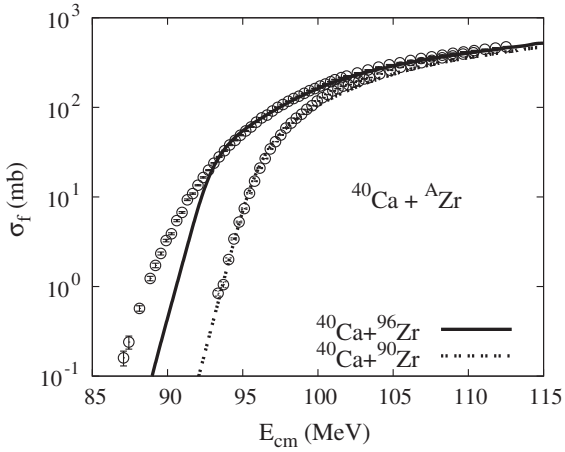

FIG. 5. Fusion cross sections for $^{40}Ca + {}^{90,96}Zr$ measured by Timmers *et al.* (1998) are compared to calculations that include one- and two-phonon excitations of the low-lying states in projectile and target.

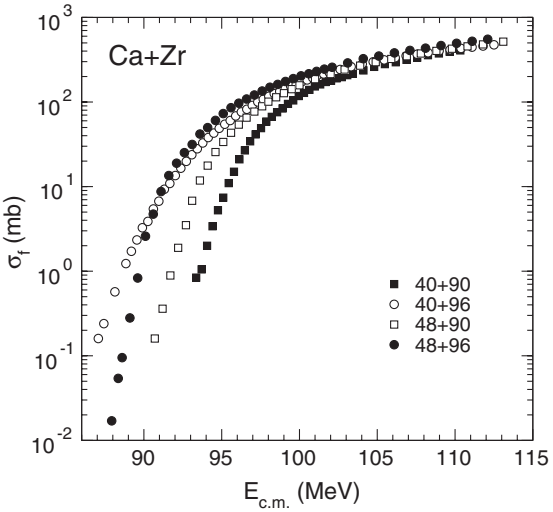

FIG. 6. Comparison of the measured fusion excitation functions for the Ca + Zr systems. The ^{40}Ca data were measured by Timmers *et al.* (1998) and the ^{48}Ca data by Stefanini *et al.* (2006).

Another correlation between the fusion enhancement and nuclear structure effects is discussed by Kalkal *et al.* (2010). Measurements of fusion cross sections induced by beams ranging from ^{28}Si to ^{58}Ni on ^{90}Zr point toward a strong increase of the fusion enhancement for systems with heavier deformed nuclei.

The results of additional systematic studies of the isotope effects on the fusion excitation function are shown in Fig. 7 for the systems Si + Ni, S + Ni, S + Zr, and Ni + Ni. These data clearly demonstrate the influence of nucleon transfer on the fusion excitation function in the near-barrier region. Fusion between the most neutron-poor isotopes (solid circles) as well as those for the most neutron-rich (solid squares) combinations exhibit a steep falloff of the cross section below the Coulomb barrier. These systems all have negative Q values for nucleon transfer between the reaction partners. Conversely, the intermediate systems shown as open circles in Fig. 7 have positive Q values for transfer reactions. This contributes to the coupled-channels effect on the fusion of these systems and leads to less steep excitation functions. This situation is very similar to that of the Ca + Ca and Ca + Zr discussed above and it has also been observed in some light systems (Jiang, 2011).

Fusion data for ^{32}S + ^{48}Ca were recently analyzed by Montagnoli *et al.* (2013). They found that the barrier distribution for this system is much broader than observed in the fusion of ^{36}S + ^{48}Ca, which had been measured previously by Stefanini *et al.* (2008). The coupling to the 3^- state is similar in the two sulfur isotopes but the 2^+ excitation is much stronger in ^{32}S than in ^{36}S. However, that difference in structure does not explain the large difference between the barrier distributions that are shown in Fig. 8. It is more likely that transfer has a large impact on the fusion of ^{32}S + ^{48}Ca because the effective Q values for pair transfer are positive for this system, whereas they are negative for ^{36}S + ^{48}Ca.

The influence of neutron transfer on sub-barrier fusion in the Ca + Ca and Ca + Zr systems has been considered by Zagrebaev (2003). In this analysis, the enhancement of the

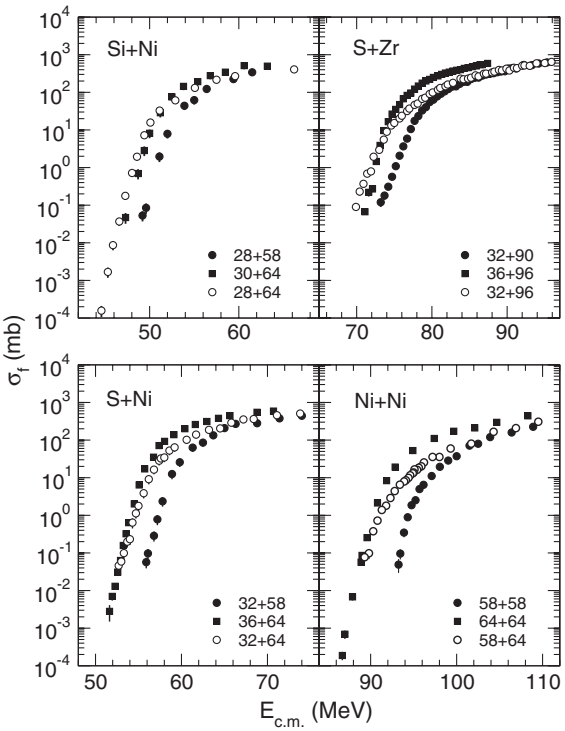

FIG. 7. Fusion cross sections are shown for the systems S + Ni, S + Zr, Si + Ni, and Ni + Ni. The data shown are from ^{28}Si + ^{64}Ni, (Jiang *et al.*, 2006); ^{28}Si + ^{58}Ni, ^{30}Si + ^{64}Ni (Stefanini *et al.*, 1986), ^{32}S + ^{64}Ni, and ^{32}S + ^{58}Ni (Stefanini *et al.*, 2000); ^{36}S + ^{64}Ni (Montagnoli *et al.*, 2010); ^{36}S + ^{96}Zr (Stefanini *et al.*, 2000); ^{32}S + ^{90}Zr and ^{32}S + ^{96}Zr (Zhang *et al.*, 2010); ^{58}Ni + ^{58}Ni and ^{58}Ni + ^{64}Ni (Beckerman *et al.*, 1980); and ^{64}Ni + ^{64}Ni Jiang *et al.*, 2004).

fusion cross section is caused by neutron transfers with positive Q values. Similar to an earlier study in the ^{58}Ni + ^{124}Sn system using a coupled-channels description by Esbensen, Jiang, and Rehm (1998), good agreement with the observed yields for elastic scattering, transfer, and fusion has been achieved.

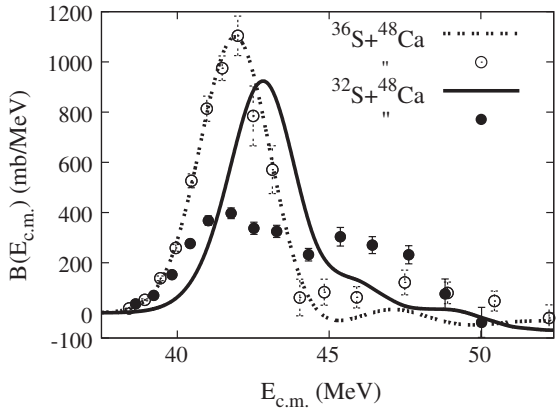

FIG. 8. Barrier distributions for the fusion of ^{32}S + ^{48}Ca and ^{36}S + ^{48}Ca. The coupled-channels calculations include coupling to one- and two-phonon as well as mutual excitations of the low-lying 2^+ and 3^- states in projectile and target. From Montagnoli *et al.*, 2013.

The correlation between a positive effective Q value for transfer and a large enhancement of sub-barrier fusion cross sections was investigated by Scarlassara *et al.* (2000). They pointed out that the Q values for neutron transfer are positive in $^{40}Ca + ^{116}Sn$ and $^{40}Ca + ^{124}Sn$ collisions. This correlates with the fact that the fusion cross sections for these two systems show a large enhancement at sub-barrier energies. However, a somewhat surprising feature is that the neutron transfer Q values are generally smaller in $^{40}Ca + ^{116}Sn$ than in $^{40}Ca + ^{124}Sn$ collisions but that does apparently not have any effect because the sub-barrier enhancements are surprisingly similar for the two systems. The correlation between the enhancement of sub-barrier fusion and the presence of positive Q-value neutron transfer channels was recently confirmed by Kohley *et al.* (2013) who measured the fusion of ^{40}Ca with the radioactive ^{134}Te nucleus.

A more surprising result was observed in the fusion of Ni + Sn isotopes by Kohley *et al.* (2011). Although the Q values for neutron transfer range from negative to large and positive values for the isotopes considered, the reduced fusion cross sections appear to be the same. A similar result was observed for the fusion of Ni + Te isotopes (Kohley *et al.*, 2011). It is presently not clear why the strong influence of transfer with positive Q values observed in the fusion of medium heavy systems (e.g., S + Ca, Ca + Ca, Ni + Ni, Ca + Zr) seems to disappear in the fusion of the heavier Ni + Sn and Ni + Te systems.

F. Influence of weak reaction channels

Coupled-channels calculations that include one- and two-phonon as well as mutual excitations of the low-lying collective states in projectile and target are usually quite successful in reproducing the measured fusion cross sections. However, there are exceptions and it is sometimes difficult to identify what causes the discrepancy between theory and experiment. One example is the fusion and quasielastic scattering of $^{16}O + ^{208}Pb$, where it is very difficult to reproduce the barrier distributions extracted from measurements. It turns out that the distributions extracted from the measured fusion and quasielastic scattering are both broader than predicted by coupled-channels calculations. This problem was recently addressed by Yusa, Hagino, and Rowley (2012). They investigated the influence of 70 non-collective excitations in ^{208}Pb that are known from inelastic proton scattering. Although the couplings to the many noncollective excitations do affect the centroid of the barrier distributions, they do not affect the shape of the barrier distributions and so the discrepancy with the measurements remains.

G. Barrier distributions from quasielastic scattering

A barrier distribution can also be extracted from quasielastic scattering data. It is defined by

$$B_{\mathrm{qel}}(E) = -\frac{d}{dE}\left(\frac{\sigma_{\mathrm{qel}}}{\sigma_R}\right), \tag{25}$$

according to Timmers *et al.* (1995), and it can be compared to the barrier distribution for fusion. An interesting feature is that the two distributions are not always identical. The barrier distribution for quasielastic scattering can be explained fairly well by coupled-channels calculations that use an ion-ion potential of the Woods-Saxon type with a "realistic" diffuseness of 0.6 to 0.7 fm, according to Washiyama, Hagino, and Dasgupta (2006), Gasques, Evers *et al.* (2007) and Evers *et al.* (2008). The analysis of fusion data, on the other hand, often requires a larger diffuseness of the ion-ion potential.

It can be difficult to explain why there are pronounced structures in the measured barrier distribution for one system, while such structures disappear in a neighboring system. This problem was investigated by Piasecki *et al.* (2009) who studied the quasielastic scattering of ^{20}Ne on ^{90}Zr and ^{92}Zr. They found that the barrier distribution for the ^{90}Zr target contained two peaks, whereas the one for the ^{92}Zr target consisted of one broad peak as shown in Fig. 9. It was suggested that the two-peaked structure had been washed out in the quasielastic scattering on ^{92}Zr by a broadening of the individual peaks. The extra broadening was expected to be caused by the absorption into a large number of noncollective, single-particle excitations that exist in ^{92}Zr. This interpretation is supported by the calculations performed by Yusa, Hagino, and Rowley (2010), who described the influence of single-particle excitations by random matrix theory.

Piasecki *et al.* (2012) recently showed that the structures that appear in the calculated barrier distributions for the fusion and quasielastic scattering of $^{20}Ne + ^{208}Pb$ are washed out in the experiment. The disappearance of the structures in the

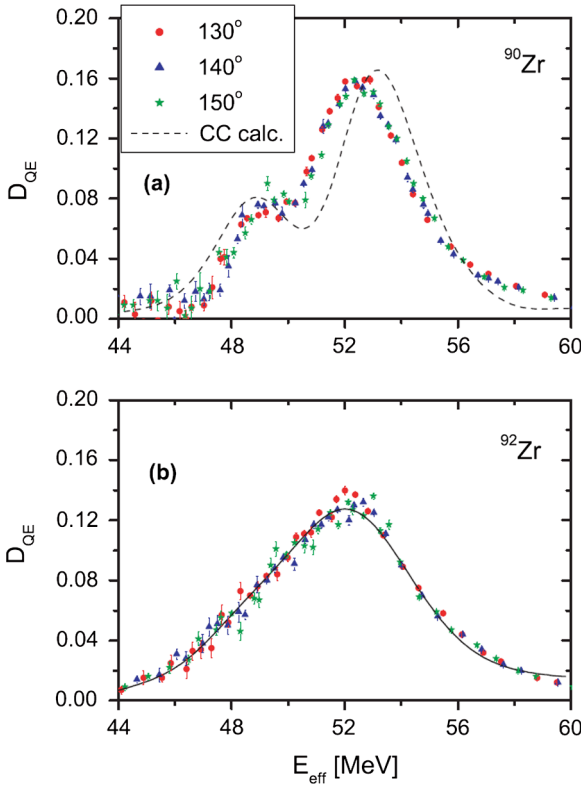

FIG. 9 (color online). Barrier distributions obtained by Piasecki *et al.* (2009) from quasielastic scattering of ^{20}Ne on ^{90}Zr and ^{92}Zr.

experiment is ascribed to a strong influence of transfer channels.

H. Other methods: TDHF calculations

A different approach to describe heavy-ion reactions is the time-dependent Hartree-Fock method. A great advantage of this method, compared to the coupled-channels approach, is that one does not have to worry about which channels one should include because they are all automatically included at the mean field level, both surface excitations as well as nucleon transfer. For a recent review of the TDHF method as it applies to heavy-ion fusion and other reaction channels, see Simenel and Beck (2014), and references therein.

Another advantage is that the TDHF method allows the response of the reacting nuclei to change self-consistently as the nuclei start to overlap, whereas the coupled-channels method usually assumes that the excitation energies and coupling strengths of the surface modes are constant. The TDHF calculation can therefore provide insight into different reaction mechanisms and give guidance for coupled-channels calculations.

Much progress has been made in recent years by Umar and Oberacker and their collaborators in the application of the TDHF method to heavy-ion fusion reactions. The calculations can now be performed in three dimensions without restrictions (Umar and Oberacker, 2006a). They cannot describe the barrier penetration of the full many-body system but it is possible to extract the interaction potential between the colliding nuclei as well as a coordinate dependent mass (Umar and Oberacker, 2008) from the density-constrained TDHF calculations they developed (Umar and Oberacker, 2006b). These potentials and masses can then be applied to calculate the fusion cross section in a one-dimensional barrier-penetration model. Recent theoretical work by Washiyama and Lacroix (2008) explores the effects of dynamical reorganization of internal degrees of freedom within the TDHF framework and finds a reduction of the fusion barrier compared to the frozen density approximation.

The method described above has been applied to calculate the fusion of several heavy-ion systems. A particular application, which relates to the earlier discussion in this section, is to the fusion of calcium isotopes (Keser, Umar, and Oberacker, 2012). The cross sections that were obtained from density-constrained TDHF calculations performed for head-on collisions at three center-of-mass energies are compared in Fig. 10 to the $^{40}Ca + ^{40}Ca$ data of Montagnoli *et al.* (2012). Although the extracted density-constrained interaction potentials and masses depend on the energy at which they are calculated, the calculated fusion cross sections are seen to be in fairly good agreement with the data. This is very encouraging because the calculated cross sections are essentially predictions once the Skyrme force and the energy, at which the interaction potential is calculated, has been chosen.

The fusion of the asymmetric system $^{40}Ca + ^{48}Ca$ is particularly interesting because it provides information about the influence of particle transfer. The calculations show that the neutron transfer from ^{48}Ca to ^{40}Ca and the proton transfer in the opposite direction both take place but they set in primarily after the Coulomb barrier has been penetrated. This

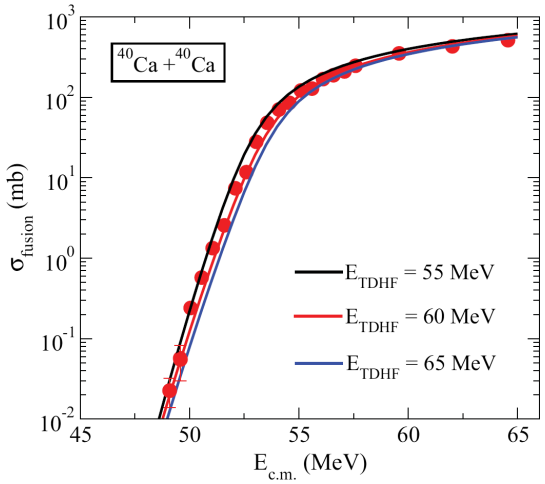

FIG. 10 (color online). Cross sections for the fusion of $^{40}Ca + ^{40}Ca$ calculated by Keser, Umar, and Oberacker (2012) are compared to the data of Montagnoli *et al.* (2012). The three one-dimensional barrier penetration calculations are based on the density-constrained TDHF ion-ion potentials obtained for head-on collision at the center-of-mass energies $E_{TDHF} = 55$, 60, and 65 MeV.

is illustrated in Fig. 11 where the average number of neutrons and protons are plotted as functions of the separation distance R between the reacting nuclei. The main effect of transfer is to modify the inner part of the barrier and increase the depth of the pocket in the entrance channel potential, whereas the barrier height is not so much affected. The result is an enhancement of the fusion cross sections for the asymmetric system, which explains the sub-barrier data quite well. The data are, however, suppressed compared to the calculation by up to a factor of 2 at energies far above the Coulomb barrier.

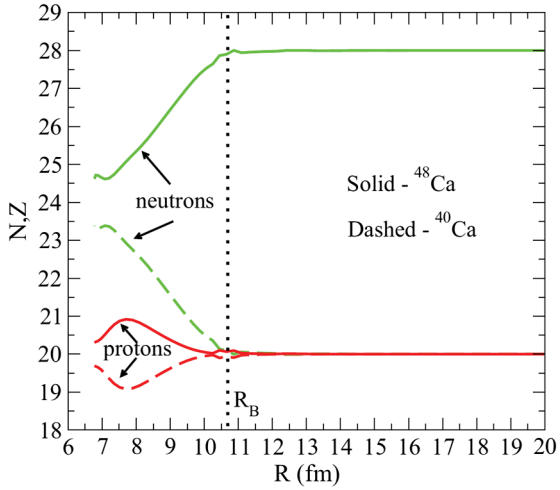

FIG. 11 (color online). Average number of neutrons and protons of the projectile and targetlike fragments obtained in TDHF calculations of collisions between ^{40}Ca and ^{48}Ca at 60 MeV center-of-mass energy. The results are shown as functions of the separation distance R between the two fragments in the entrance channel. The solid lines denote particles that originally belong to ^{48}Ca, whereas the dashed lines refer to ^{40}Ca. The location R_B of the peak of the potential barrier is indicated by the vertical dotted line. From Keser, Umar, and Oberacker, 2012.

The influence of neutron transfer in the fusion of different oxygen isotopes was recently studied in similar density-constrained THDF calculations (Umar, Oberacker, and Horowitz, 2012). It was found that the fusion of the very asymmetric system $^{16}O + ^{24}O$ was enhanced by an order of magnitude compared to predictions based on the São Paulo potential (Beard *et al.*, 2010). The enhancement is caused by neutron transfer which modifies the extracted interaction potential dramatically inside the barrier and even reduces the barrier height.

The fusion of the two neutron-rich isotopes $^{24}O + ^{24}O$, on the other hand, was found to be suppressed in the density-constrained TDHF calculation compared to the calculation in the São Paulo model. As such exotic reactions can play an important role in neutron stars, it is important to settle these questions theoretically because an experimental verification is not possible.

III. HINDRANCE OF FUSION FAR BELOW THE COULOMB BARRIER

In most of the earlier experiments, fusion cross sections were measured down to the 0.1–1 mb level, and standard coupled-channels calculations using Woods-Saxon potentials were quite successful in reproducing the general trends of the excitation functions (Hagino *et al.*, 1997b). The first publications, in which the ability of CC calculations for describing the low-energy fusion data was questioned, were published about 10 years ago (Jiang *et al.*, 2002, 2004; Jiang, Esbensen *et al.*, 2004). In these and subsequent papers fusion excitation functions of the systems $^{60}Ni + ^{89}Y$, $^{64}Ni + ^{64}Ni$, etc. were measured down to the nb region and data for other systems published earlier were reanalyzed.

The main goal of these studies was to measure the fusion cross sections at energies below the lowest barrier that is generated by coupling to the intrinsic modes of excitation of the two reaction partners, i.e., below the region that is well described by standard coupled-channels theory. In this energy region one is thus able to probe the effects of the interaction potential itself, which is the main focus of this section.

Precise measurements of very small fusion cross sections are experimentally very challenging as they are often plagued by various backgrounds in the detector systems. In addition, reactions on minute amounts of heavier isotopic target contaminants or rare isobaric contaminants with lower Z in the beam (e.g., a ^{58}Fe contamination in a ^{58}Ni beam) can dominate the low-energy yields due to their higher center-of-mass energies or lower Coulomb barriers. These backgrounds often reveal themselves as an abnormal change in slope of the excitation functions at the lowest energies.

In order to avoid such difficulties, the $^{64}Ni + ^{64}Ni$ system was studied experimentally by Jiang *et al.* (2004) at Argonne National Laboratory using the fragmentation mass analyzer (Davids and Larson, 1989, 1994). In this system, neither beam nor target had contaminants that could pollute the low-energy cross sections and it was possible to measure the excitation function for evaporation residues from about 400 mb down to less than 6 nb as shown in Fig. 12(a). The comparison with CC calculations using a Woods-Saxon potential (dash-dotted curve) allowed them to cleanly identify the fusion hindrance

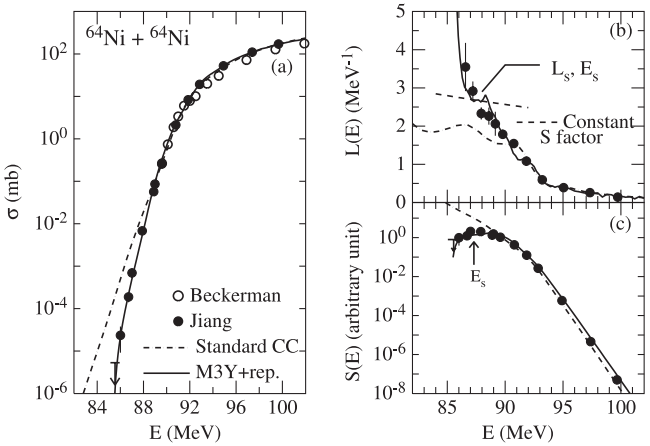

FIG. 12. (a) The experimental fusion cross section, (b) the logarithmic derivative, and the (c) S factor are shown for $^{64}Ni + ^{64}Ni$ as solid circles (Jiang *et al.*, 2004) and open triangles (Beckerman *et al.*, 1980). The dash-dotted curves represent a standard coupled-channels calculation using a Woods-Saxon potential, whereas the solid curves use the M3Y + rep. potential. The dashed curve in (b) corresponds to the constant S factor. See Eq. (30) for the definitions of E_s and L_s.

at the lowest energies. Subsequently, a similar behavior was found for other systems measured previously. These are discussed below.

A. Signatures of fusion hindrance

The $^{64}Ni + ^{64}Ni$ system provides a clear example of fusion hindrance as the deep sub-barrier region cannot be described by CC calculations that use a standard Woods-Saxon potential. There are several other experiments that have been measured to cross sections low enough to reveal this hindrance behavior. Two of these cases are discussed below.

Fusion between the two closed-shell nuclei $^{16}O + ^{208}Pb$ has been measured around the Coulomb barrier (Morton *et al.*, 1999) and at deep sub-barrier energies (Dasgupta *et al.*, 2007). The lowest fusion cross sections obtained in these experiments were about 10 nb. The cross sections are shown in Fig. 13(a),

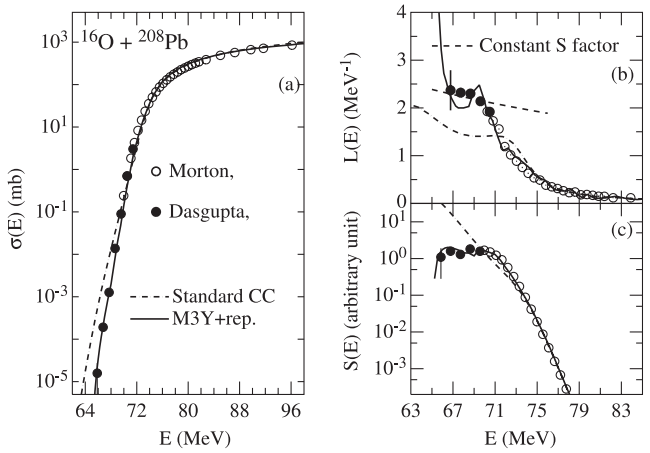

FIG. 13. Same as Fig. 12 but for $^{16}O + ^{208}Pb$. From Morton *et al.*, 1999 and Dasgupta *et al.*, 2007.

together with standard coupled-channels calculations by Morton *et al.* (1999) and Esbensen and Mişicu (2007). These calculations are discussed in more detail in Sec. IV.B.2.

The fusion reaction ^{58}Ni + ^{54}Fe was measured by Stefanini *et al.* (2010) down to the ~μb region. The experimental results are given in Fig. 14(a) together with coupled-channels calculations that use a diffuseness of $a = 0.66$ fm. Again, one observes a clear cross section deficit at the lowest energies.

Although the measured cross sections in these cases clearly fall below the theoretical curves, the conclusion about fusion hindrance is dependent on the various parameters used in the coupled-channels calculations. It is therefore advantageous to seek a representation of the measured cross section that will show this effect without invoking model calculations. Two different representations of the measured cross sections have been therefore introduced by Jiang *et al.* (2002) and Jiang, Esbensen *et al.* (2004).

One approach is to display the logarithmic derivative of the energy-weighted cross section, namely,

$$L(E) = d[\ln(E\sigma)]/dE = \frac{1}{E\sigma}\frac{d(E\sigma)}{dE}, \tag{26}$$

where E is the center-of-mass energy (Jiang *et al.*, 2002). The logarithmic derivative for ^{64}Ni + ^{64}Ni is presented in Fig. 12(b). While the slopes of coupled-channels calculations approach a constant value of ~1.5 MeV^{-1}, the experimental data exhibit a continuous increase with decreasing energy.

An alternative representation uses the so-called S factor (Jiang, Esbensen *et al.*, 2004). This representation is frequently used in nuclear astrophysics to predict the low-energy behavior of nuclear reactions. The S factor is defined as (Burbidge *et al.*, 1957)

$$S(E) = E\sigma(E)\exp(2\,\pi\eta), \tag{27}$$

where $\eta = Z_1Z_2e^2/\hbar v$ is the Sommerfeld parameter and v is the beam velocity. The Gamow factor $\exp(-2\,\pi\eta)$ accounts for the main part of the strong energy dependence of the fusion cross section in light-ion reactions, such that the S factor exhibits only a weak energy dependence far below the Coulomb barrier. This feature is often used to extrapolate the cross section into the region of the Gamow window, in order to predict the astrophysical reaction rates.

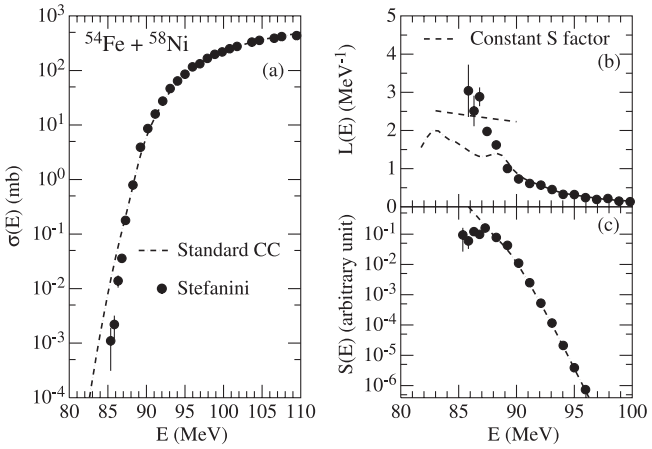

FIG. 14. Same as Fig. 12 but for ^{54}Fe + ^{58}Ni. Only a standard coupled-channels calculation using a Woods-Saxon potential is shown. From Stefanini *et al.*, 2010.

For heavy-ion induced fusion reactions the S factor exhibits a strong energy dependence just below the Coulomb barrier: it increases steeply with decreasing energy [see Figs. 12(c), 13(c), and 14(c)], reflecting the weaker energy dependence of the $E\sigma(E)$ product when compared to that predicted by the Gamow factor. However, at even lower beam energies, the S factor ceases to increase and exhibits a clear maximum in some cases, which is taken as a signature of the fusion hindrance.

The relation between the S factor and the logarithmic derivative can be understood by examining the derivative of the S factor. From Eqs. (26) and (27), one obtains

$$\frac{dS}{dE} = S(E)\left[L(E) - \frac{\pi\eta}{E}\right]. \tag{28}$$

A maximum in the S factor corresponds to $dS/dE = 0$ which occurs when the logarithmic derivative is

$$L_{CS}(E) = \frac{\pi\eta}{E} = \frac{\pi Z_1Z_2e^2}{E^{3/2}\hbar}\sqrt{\frac{m_N}{2}\frac{A_1A_2}{A_1+A_2}}. \tag{29}$$

Here A_1 and A_2 are the mass numbers of the reaction partners and m_N is the nucleon mass. This function, which is the logarithmic derivative for a constant S factor, is shown by the black dashed curves in Figs. 12(b), 13(b), and 14(b). The logarithmic derivative $L(E)$ extracted from the experimental data will intersect the curve $L_{CS}(E)$ exactly at the energy where the experimental S factor exhibits a maximum. We denote the energy and logarithmic derivative where this intersection occurs by E_s and $L_s = L(E_s)$, respectively. These two quantities are then related by the equation:

$$L_s = \frac{\pi Z_1Z_2e^2}{E_s^{3/2}\hbar}\sqrt{\frac{m_N}{2}\frac{A_1A_2}{A_1+A_2}} = 0.4948\zeta/E_s^{3/2}, \tag{30}$$

where L_s is in units of MeV^{-1}, E_s is in MeV, and

$$\zeta = Z_1Z_2\sqrt{\mu} \tag{31}$$

is a parameter characterizing the size of the colliding system in terms of Z_1, Z_2, and the reduced mass $\mu = A_1A_2/(A_1+A_2)$. In principle, there is nothing special about the constant S factor, nor about the relation between values of E_s and L_s, where the logarithmic derivative extracted from measurements intersects with the logarithmic derivative for a constant S factor. It is simply a convenient way of characterizing the unexpected steep falloff of the measured fusion cross sections. Thus, when the S factor reaches a maximum, the logarithmic derivative will have reached a value that exceeds the expectations based on the standard, Woods-Saxon–based coupled-channels calculations. The advantage of the S factor is that it gives a simple and direct representation of the fusion cross

section, whereas the logarithmic derivatives, Eq. (26), as well as the barrier distributions $B(E)$ are more indirectly derived quantities relying on derivatives of the measured fusion cross section.

As mentioned above, the S factor representation is often used to extrapolate the measured cross section to low energy. A positive Q value ensures that fusion is possible, albeit strongly suppressed by virtue of barrier penetration, even at extemely low center-of-mass energies, because the levels in the compound nucleus would still be populated at a finite excitation energy $E_{\rm exc} = Q$.

On the other hand, the Q value for fusion is usually negative for systems with $\zeta > 1500$. This means that the center-of-mass energy corresponding to the ground state of the fused system $E_{\rm c.m.} = -Q$ is positive and that the cross section, and with it the S factor, must vanish at even lower energies. The S factor must therefore have a maximum. From the definition given in Eq. (27), it therefore follows that

$$S(E) \to 0, \quad \text{for } E \to -Q, \quad \text{when} \quad Q < 0. \tag{32}$$

It is an interesting question whether the S factor maximum observed in, ^{64}Ni + ^{64}Ni and many other medium-heavy systems is a reflection of the static property of these systems ($Q < 0$) or whether the dynamics of the fusion reaction as described by the theories discussed in Sec. II are responsible for the fusion hindrance. This question has spurred much interest in measuring deep sub-barrier cross sections in light systems with $Q > 0$ in a search for fusion hindrance, i.e., an S factor maximum in such systems, as this would point to a dynamical origin of this phenomenon. This issue is discussed further in Sec. III.E.

B. Systematics of fusion hindrance in medium-heavy systems

Fusion reactions between relatively "soft" nuclei exhibit a strong effect of the couplings to intrinsic excitation modes of the interacting nuclei leading to a relatively wide distribution of fusion barriers as discussed in Sec. II. This situation tends to obscure the sub-barrier fusion hindrance in such systems and push the effect to even deeper sub-barrier energies while impeding detection. The fusion hindrance is thus, in general, most readily observed in reactions between "stiff" reaction partners. It is therefore natural to include only such systems in a search for general systematics of the onset of this phenomenon.

Until now, the sub-barrier fusion hindrance has been observed in ten systems involving stiff reaction partners. These are listed in the first part of Table I. Each of these systems exhibits a maximum in the S factor and a crossing of the logarithmic derivative at L_s with that expected for a constant S factor, both of which are taken as a signature of sub-barrier fusion hindrance. The derived values of L_s for these systems are shown as solid circles in Fig. 15(d) (see linear scale inset for enhanced detail) as a function of the system parameter $\zeta = Z_1 Z_2 \sqrt{\mu}$. The data points scatter closely around an average value of

$$L_s^{\rm ref} = 2.33 \text{ MeV}^{-1}, \tag{33}$$

which is represented by the dashed curve. The corresponding center-of-mass energies E_s are given as solid circles in Fig. 15(c). The dashed curve represents

$$E_s^{\rm ref} = 0.356\zeta^{2/3} \text{ MeV}, \tag{34}$$

derived from Eqs. (30) and (33).

At the time when the hindrance phenomenon was discovered (Jiang *et al.*, 2002), there was not yet any evidence of S-factor maxima in systems that included soft or well-deformed reacting partners. As mentioned above, it may be expected that the broadening of the effective barrier distribution, caused by strong coupled-channels effects for such systems, substantially lowers the energy where the steep rise in the logarithmic derivative occurs. Subsequently, fusion hindrance has been found in some soft systems by extending the measurements to deep sub-barrier energies. Although both ^{40}Ca and ^{48}Ca are normally considered closed-shell nuclei, we list the ^{40}Ca + ^{48}Ca system among the soft systems because of its fusion behavior that is strongly affected by nucleon transfer reactions. These systems are listed in the second part of Table I and given as open squares in Fig. 15.

In addition, estimates of the onset of fusion hindrance have been made for a number of mostly lighter systems taken from the literature or subsequently measured. In some cases these estimates are based on an extrapolation procedure discussed in Sec. III.C. In the remaining systems, only upper limits can be given. These systems are also listed in Table I and plotted in Fig. 15 as solid squares and open circles for medium-light and light systems, respectively.

By examining the overall trend of the data shown in Fig. 15, it is clear that the simple systematics derived from the stiff systems given in Eqs. (33) and (34) are inadequate for the lighter systems. Subsequently, it was found (Jiang, Back *et al.*, 2006; Jiang, Rehm *et al.*, 2007; Jiang *et al.*, 2009) that a better overall representation is given by

$$L_s^{\rm emp} = 2.33 + 580/\zeta(\text{MeV}^{-1}), \tag{35}$$

$$E_s^{\rm emp} = [0.495\zeta/L_s^{\rm emp}(\zeta)]^{2/3}(\text{MeV}). \tag{36}$$

The shift in the onset of fusion hindrance between stiff (black points) and soft (open squares) fusion systems is clearly seen in the inset of Fig. 15(d) in terms of the L_s and in Fig. 15(b) for E_s. This shows that the fusion hindrance for soft systems occurs at center-of-mass energies E_s that are 7–15 MeV lower than the systematics established for the stiff systems represented by the dashed curves. One should keep in mind that these differences are much larger than the differences of Coulomb barriers.

A quantitative relation between the stiffness and the deviation from $E_s^{\rm emp}$ has not yet been established. It is customary to associate the stiffness of a nucleus to its proximity to closed proton or neutron shells and define the number of "valence nucleons" N_{ph} as the sum of particles and holes outside the nearest closed shells. A discussion of this dependence for reactions with Ni projectiles has been given by Jiang *et al.* (2005) and for Ca + Zr systems by Esbensen and Jiang (2009).

TABLE I. The parameter $\zeta = Z_1 Z_2 \sqrt{A_1 A_2/(A_1+A_2)}$, the energy E_s, and the logarithmic derivative L_s that characterize the maximum of the S factor for different systems. Also given are the corresponding lowest cross sections measured and the ground-state fusion Q value. The first section is for medium-heavy stiff systems, while the second section lists soft systems. S-factor maxima have been identified for systems listed in these two sections. The third section includes medium-light systems and light systems are given in the fourth section. No S-factor maximum has been seen yet for systems in the last two sections, and the values of E_s and L_s are obtained with an extrapolation method. For systems with a positive fusion Q value, the extrapolation parameters A_0, B_0, and σ_s are given.

System	ζ	E_s (MeV)	L_s (MeV^{-1})	A_0 (MeV^{-1})	B_0 (MeV$^{1/2}$)	σ_s (μb)	$\sigma_{\min}$ (μb)	Q (MeV)	Reference
Medium-heavy, stiff systems									
^{50}Ti + ^{208}Pb	11448	18.2 ± 2.7	2.32 ± 0.05				0.00001	−169.6	Hofmann *et al.* (1997)
^{90}Zr + ^{92}Zr	10786	170.7 ± 1.7	2.39 ± 0.04				0.12	−169.6	Keller *et al.* (1986)
^{90}Zr + ^{90}Zr	10727	175.2 ± 1.8	2.29 ± 0.03				0.08	−153.7	Keller *et al.* (1986)
^{90}Zr + ^{89}Y	10430	170.8 ± 1.7	2.31 ± 0.03				0.34	−170.5	Keller *et al.* (1986)
^{60}Ni + ^{89}Y	6534	122.9 ± 1.3	2.37 ± 0.04				< 0.07	−90.49	Jiang *et al.* (2002)
^{58}Ni + ^{58}Ni	4220	94.0 ± 0.9	2.29 ± 0.03				49	−65.85	Beckerman *et al.* (1982)
^{54}Fe + ^{58}Ni	3848	86.7 ± 0.9	2.36 ± 0.04				1.1	−56.51	Stefanini *et al.* (2010)
^{19}F + ^{208}Pb	3079	75.5 ± 1.1	2.32 ± 0.05				23	−50.07	Hinde *et al.* (1999)
^{32}S + ^{89}Y	3026	73.1 ± 0.7	2.40 ± 0.04				60	−36.62	Mukherjee *et al.* (2002)
^{16}O + ^{208}Pb	2528	68.0 ± 2.0	2.23 ± 0.10				16	−36.62	Dasgupta *et al.* (2007)
Medium-heavy, soft systems									
^{64}Ni + ^{100}Mo	7343	120.6 ± 1.8	2.73 ± 0.06				< 0.0046	−92.26	Jiang *et al.* (2005)
^{48}Ca + ^{96}Zr	4523	88.1 ± 1.3	2.71 ± 0.06				17	−45.90	Stefanini *et al.* (2007)
^{64}Ni + ^{64}Ni	4433	87.5 ± 0.9	2.69 ± 0.04				< 0.0054	−48.80	Jiang *et al.* (2004)
^{40}Ca + ^{48}Ca	1868	47.0 ± 0.5	2.87 ± 0.04	−16.4 ± 7.7	6000 ± 2500	6800	1.3	4.563	Jiang *et al.* (2010a)
^{28}Si + ^{64}Ni	1729	45.6 ± 0.5	2.78 ± 0.20				0.027	−1.787	Jiang *et al.* (2006)
Medium-light systems									
^{36}S + ^{64}Ni	2149	< 51.	> 2..9				2.8	−8.544	Montagnoli *et al.* (2010)
^{48}Ca + ^{48}Ca	1959	< 43.	> 3.4				0.59	−2.986	Stefanini *et al.* (2009)
^{40}Ca + ^{40}Ca	1788	48.0 ± 1.0	2.66 ± 0.08				23	−14.176	Montagnoli *et al.* (2012)
^{36}S + ^{48}Ca	1451	< 33.	> 3.7				0.62	7.552	Stefanini *et al.* (2008)
^{32}S + ^{48}Ca	1402	< 31.	> 4.0				0.78	7.663	Montagnoli *et al.* (2013)
^{27}Al + ^{45}Sc	1121	32.4 ± 1.3	3.01 ± 0.18	−8.13 ± 0.93	2052 ± 198.	1560	0.31	9.630	Jiang *et al.* (2010a)
^{16}O + ^{76}Ge	930.7	< 29.	> 2.9				600	10.504	Aguilera *et al.* (1995)
^{28}Si + ^{30}Si	745.6	24.2 ± 3.6	3.10 ± 0.70	−6.48 ± 0.95	1141 ± 132	12	42	14.302	Jiang *et al.* (2008)
^{24}Mg + ^{30}Si	613.2	20.8 ± 0.7	3.20 ± 0.16	−6.6 ± 0.7	932 ± 80	36	73	17.886	Morsad *et al.* (1990)
Light systems									
^{16}O + ^{18}O	186.2	6.51 ± 0.35	5.54 ± 0.50	−3.24 ± 0.13	146.1 ± 3.8	3	7	24.413	Thomas *et al.* (1985)
^{16}O + ^{16}O	180.1	6.78 ± 0.62	5.07 ± 0.69	−4.11 ± 0.71	162.1 ± 15.4	8	5.2	16.542	Spinka and Winkler (1974), Wu (1978), Hulke, Rolfs, and Trautvetter (1980), Wu and Barnes (1984), and Thomas *et al.* (1985)
^{12}C + ^{20}Ne	164.3	5.85 ± 0.56	5.74 ± 0.83	−2.20 ± 0.21	112.4 ± 6.7	0.46	5.3	18.974	Hulke, Rolfs, and Trautvetter (1980)
^{14}N + ^{16}O	153.0	5.39 ± 0.58	6.04 ± 0.97	−2.25 ± 0.27	103.9 ± 6.8	0.52	1.7	18.327	Switkowski, Stokstad, and Wieland (1977)
^{14}N + ^{14}N	129.6	4.15 ± 0.31	7.59 ± 0.82	−2.00 ± 0.06	81.03 ± 1.62	0.048	1.5	27.220	Switkowski, Stokstad, and Wieland (1976)
^{13}C + ^{16}O	128.6	4.00 ± 0.16	7.9 ± 3.2	−2.06 ± 0.35	80.17 ± 6.10	0.064	3.5	20.283	Dasmahapatra, Cujec, and Lahlou (1983b)
^{12}C + ^{16}O	125.7	4.54 ± 0.27	6.43 ± 0.57	−2.08 ± 0.12	82.35 ± 2.90	1.2	0.026	16.756	Patterson *et al.* (1971), Cujec and Barnes (1976), and Christensen, Switkowski, and Dayras (1977)
^{12}C + ^{14}N	106.8	3.49 ± 0.71	8.1 ± 2.5	−1.80 ± 0.43	64.56 ± 6.79	0.15	0.36	15.074	Stokstad *et al.* (1976)
^{12}C + ^{13}C	89.9	3.45 ± 0.37	6.9 ± 1.1	−2.32 ± 0.24	59.37 ± 2.25	15	0.020	16.318	Dayras*et al.* (1976), Notani *et al.* (2012)
^{12}C + ^{12}C	88.2	3.68 ± 0.38	6.18 ± 0.95	−1.32 ± 0.12	52.93 ± 1.15	23	0.0051	13.934	Patterson *et al.* (1969), Mazarakis and Stephens (1973), High and Cujec (1977), Becker *et al.* (1981), and Barron-Palos *et al.* (2006)
^{11}B + ^{14}N	86.9	2.90 ± 0.47	8.7 ± 2.1	−1.75 ± 0.18	51.64 ± 1.90	.57	0.6	24,724	Dasmahapatra, Cujec, and Lahlou (1983a)
^{11}B + ^{12}C	71.9	2.12 ± 0.38	11.5 ± 3.1		41.17 ± 1.37	0.093	0.52	18.198	Stokstad *et al.* (1976)
^{10}B + ^{10}B	55.9	1.47 ± 0.38	15.5 ± 5.9	−2.17 ± 0.70	31.55 ± 10.8	0.022	1.9	31.143	Stokstad *et al.* (1976)

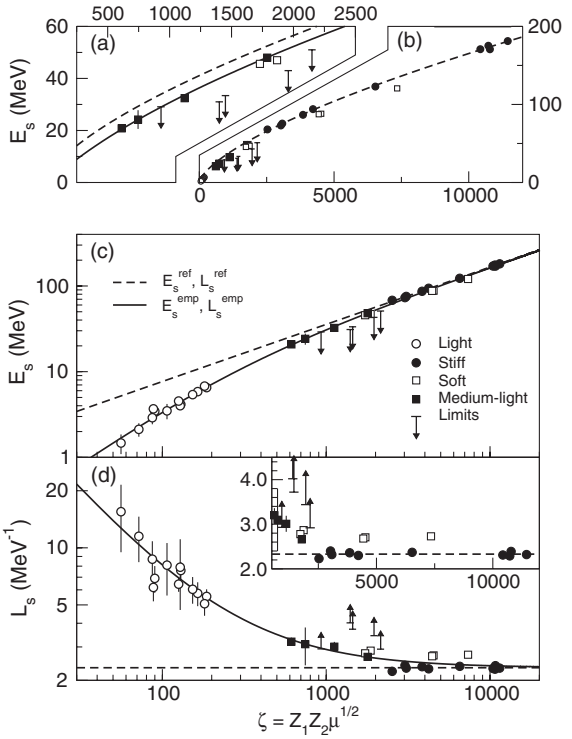

FIG. 15. Systematics of the center-of-mass energy E_s and the logarithmetic derivative L_s, where the S factor has a maximum and the $L_S = L_{CS}$ is plotted as a function of the parameter ζ for light (open circles), "stiff" (solid circles), "soft" (open squares), and medium-light (solid squares) systems. For some medium-light systems only upper limits on E_S and lower limits for L_S can be derived from the data. The solid curves are calculated with the empirical expression given by Eqs. (35) and (36), whereas the dashed curves represent Eqs. (33) and (34).

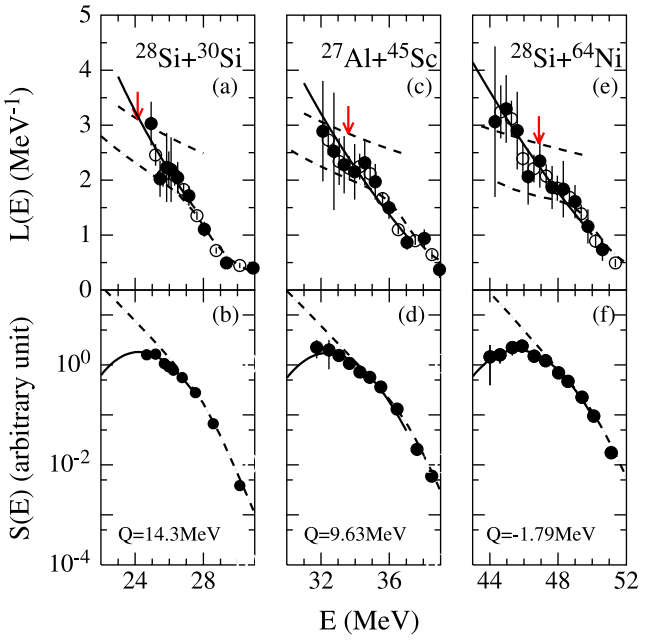

FIG. 16 (color online). Experimental S factors and logarithmetic derivatives are shown for $^{28}\mathrm{Si} + {}^{30}\mathrm{Si}$ (Jiang *et al.*, 2008), $^{27}\mathrm{Al} + {}^{45}\mathrm{Sc}$ (Jiang *et al.*, 2010a), and $^{28}\mathrm{Si} + {}^{64}\mathrm{Ni}$ (Jiang *et al.*, 2006). The dash-dotted curves represent standard coupled-channels calculations, whereas the dashed curves are the constant S factor, Eq. (29). The solid curves represent a fit to the data using Eqs. (39) and (40) for the $^{28}\mathrm{Si} + {}^{30}\mathrm{Si}$ and $^{27}\mathrm{Al} + {}^{45}\mathrm{Sc}$ positive Q-value data, whereas Eqs. (37) and (38) are used for $^{28}\mathrm{Si} + {}^{64}\mathrm{Ni}$ that has a negative Q value. The arrows indicate the location of E_s^{emp}.

C. Fusion hindrance in medium-light systems

In systems with $\zeta \geq 1500$ that have been discussed so far, the ground-state Q value for fusion is negative. On the other hand, most of the fusion reactions that are of astrophysical interest, such as carbon burning, oxygen burning, etc., have positive Q values. As pointed out in Sec. III.A, whereas the S factor for fusion must have a maximum at low energy for systems with a negative Q value, this is not necessarily true for the light, positive-Q-value systems.

It has been observed that current standard theoretical calculations often overpredict the experimental cross sections in light systems and at low energies (Jiang, Rehm *et al.*, 2007) and it is therefore of interest to determine whether light systems also exhibit fusion hindrance in order to better constrain the extrapolation to low energies.

Five fusion reactions with positive Q values have recently been measured at Argonne National Laboratory and Laboratori Nazionali di Legnaro. They are $^{28}\mathrm{Si} + {}^{30}\mathrm{Si}$ (Jiang *et al.*, 2008), $^{27}\mathrm{Al} + {}^{45}\mathrm{Sc}$ (Jiang *et al.*, 2010b), $^{32,36}\mathrm{S} + {}^{48}\mathrm{Ca}$ (Stefanini *et al.*, 2008), and $^{40}\mathrm{Ca} + {}^{48}\mathrm{Ca}$ (Jiang, 2011) with fusion Q values of 14.3, 9.63, 7.66, 7.55, and 4.56 MeV, respectively.

In Fig. 16, we show the results for $^{28}\mathrm{Si} + {}^{30}\mathrm{Si}$ (Jiang *et al.*, 2008) and $^{27}\mathrm{Al} + {}^{45}\mathrm{Sc}$ (Jiang *et al.*, 2010b), as well as $^{28}\mathrm{Si} + {}^{64}\mathrm{Ni}$ (Jiang *et al.*, 2006) which has a slightly negative Q value of -1.79 MeV. These measurements were performed with the ATLAS fragment mass analyzer detector system. In general, the background is higher for light evaporation residues. The lowest cross sections (σ_{min}) that were measured in these experiments are 26 nb for $^{28}\mathrm{Si} + {}^{64}\mathrm{Ni}$, 307 nb for $^{27}\mathrm{Al} + {}^{45}\mathrm{Sc}$, and 42 μb for $^{28}\mathrm{Si} + {}^{30}\mathrm{Si}$. The $L(E)$ values all reach the constant S-factor curve and one observes that the behavior of $L(E)$ and $S(E)$ is very similar for these three systems. At the lowest energies, standard CC calculations (shown by the dash-dotted curves) overpredict the cross sections. A well-defined S-factor maximum is observed only for the system $^{28}\mathrm{Si} + {}^{64}\mathrm{Ni}$, where the Q value is slightly negative. For the other two systems, $^{28}\mathrm{Si} + {}^{30}\mathrm{Si}$ and $^{27}\mathrm{Al} + {}^{45}\mathrm{Sc}$, measurements need to be extended to lower energies before a clear conclusion concerning the existence of a maximum S factor can be reached.

A new extrapolation method which is based on the experimental logarithmic derivative $L(E)$ of the energy-weighted fusion cross section has been developed (Jiang, Rehm *et al.*, 2007; Esbensen and Jiang, 2009). For systems with a negative Q value for fusion, the experimental $L(E)$ data can be reproduced at low energies by (Esbensen and Jiang, 2009)

$$L(E) = A_0 + \frac{B_0}{(E+Q)^{3/2}}. \tag{37}$$

For these negative Q-value systems, Eq. (37) implies that $L(E) \to \infty$ for $E \to -Q$, in agreement with the constraint that the cross section must go to zero when the center-of-mass energy E approaches the ground-state energy of the compound nucleus at $E = -Q$.

Once the parameters A_0 and B_0 in Eq. (37) have been determined from the low-energy data of $L(E)$, it is straightforward to extrapolate the cross sections and find the energy E_s, where $L(E)$ intersects the constant S-factor function and the $S(E)$ factor has a maximum. The solid curves in Fig. 16(e) have been obtained in this way and are seen to describe the $L(E)$ data quite well.

From the parametrization, Eq. (37), one obtains the analytic expression for the cross section

$$\sigma(E) = \sigma_s \frac{E_s}{E} \exp\left(A_0(E - E_s) - \frac{2B_0}{(E_s + Q)^{1/2}}\left[\left(\frac{E_s + Q}{E + Q}\right)^{1/2} - 1\right]\right). \quad (38)$$

The only unknown parameter in Eq. (38) is the normalization factor σ_s, which can be obtained by fitting the low-energy data of the excitation function. The cross sections one obtains for $^{28}\mathrm{Si} + {}^{64}\mathrm{Ni}$, and expressed in terms of the $S(E)$ factor, are shown in Fig. 16(f).

For systems with a positive Q value, the parametrization of the extrapolation should be changed to

$$L(E) = A_0 + \frac{B_0}{E^{3/2}} \quad (39)$$

(Jiang, Rehm *et al.*, 2007). The corresponding expression for the cross section is

$$\sigma(E) = \sigma_s \frac{E_s}{E} e^{\{A_0(E-E_s) - (B_0/0.5E_s^{1/2})[(E_s/E)^{1/2} - 1]\}}, \quad (40)$$

which is independent of the Q value for fusion. Equation (39) implies that $L(E) \to \infty$ for $E \to 0$, in agreement with the constraints on $L(E)$ for systems with a positive Q value. The solid curves in Figs. 16(a)–16(d) were obtained from Eqs. (39) and (40). The values of E_s^{emp} [Eq. (36)] for the three systems are shown for reference in Fig. 16 as arrows. They agree fairly well with the energy E_s where the $L(E)$ data intersect with the constant S-factor curve although some are slightly larger.

A series of measurements have recently been performed with sulfur and calcium isotopes down to very small cross sections in order to study possible effects of the sign of the fusion Q value. The values of $L(E)$ are shown for these systems in Fig. 17 which indicates that there is no obvious dependence on the sign of the fusion Q value. The dash-dotted curves are standard CC calculations, the solid curves correspond to CC calculations using the M3Y + repulsion potential, and the dashed curves show the constant S-factor value, Eq. (29). Arrows indicate the location of E_s^{emp}, which in some cases represents an upper value, especially for soft reaction partners such as those with large neutron excess, $N - Z$, e.g., ^{48}Ca and ^{36}S. It appears that this pushes the fusion hindrance to lower energies, as seen also for soft systems in the medium-heavy mass region as discussed in Sec. III.B.

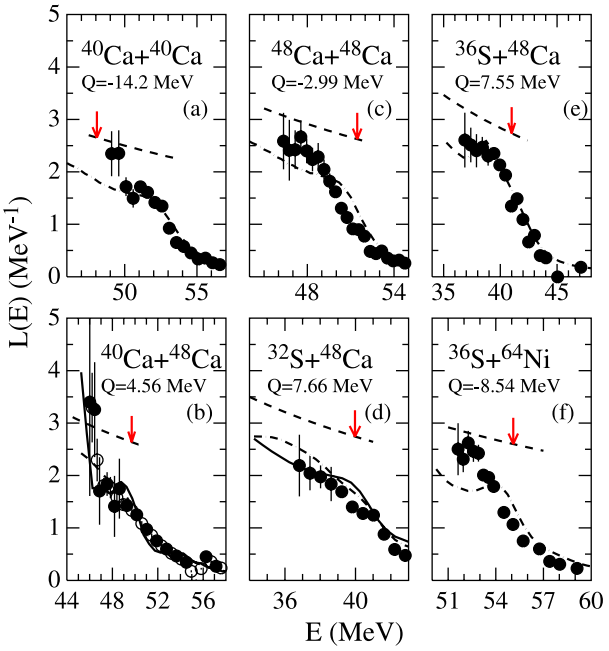

FIG. 17 (color online). The logarithmic derivative is shown for $^{40}\mathrm{Ca} + {}^{40}\mathrm{Ca}$ (Montagnoli *et al.*, 2012), $^{40}\mathrm{Ca} + {}^{48}\mathrm{Ca}$ (Jiang *et al.*, 2010a), $^{48}\mathrm{Ca} + {}^{48}\mathrm{Ca}$ (Stefanini *et al.*, 2008), $^{32}\mathrm{S} + {}^{48}\mathrm{Ca}$ (Montagnoli *et al.*, 2010), $^{36}\mathrm{S} + {}^{48}\mathrm{Ca}$ (Stefanini *et al.*, 2008), and $^{36}\mathrm{S} + {}^{64}\mathrm{Ni}$ (Montagnoli *et al.*, 2010). The dash-dotted curves are standard coupled-channels calculations using the Woods-Saxon potential, whereas the solid curves are based on the $M3Y$ + rep. potential. The dashed curves are the constant S factor, Eq. (29). The arrows indicate the location of E_s^{emp}.

In addition, the systems $^{32}\mathrm{S} + {}^{48}\mathrm{Ca}$ and $^{40}\mathrm{Ca} + {}^{48}\mathrm{Ca}$ shown in Figs. 17(b) and 17(d) are both expected to be influenced by couplings to transfer channels because of positive transfer Q values. While fusion hindrance is seen in $^{40}\mathrm{Ca} + {}^{48}\mathrm{Ca}$ and is well described by CC calculations with the M3Y + repulsion potential, the measurements for $^{32}\mathrm{S} + {}^{48}\mathrm{Ca}$ can be represented quite well by standard CC calculations. This may be a consequence of the fact that the measurements for the latter system have not been extended to sufficiently small cross sections to observe the hindrance. The abnormally low onset of fusion hindrance in $^{40}\mathrm{Ca} + {}^{48}\mathrm{Ca}$ along with $^{32}\mathrm{S} + {}^{48}\mathrm{Ca}$, $^{32}\mathrm{S} + {}^{48}\mathrm{Ca}$, $^{48}\mathrm{Ca} + {}^{48}\mathrm{Ca}$, and $^{36}\mathrm{S} + {}^{64}\mathrm{Ni}$, for which only upper limits for E_s can be established, are illustrated in Fig. 15(a) in relation to the E_s^{emp} systematics.

Thus, the ratio of E_s/E_s^{emp} for the system $^{32}\mathrm{S} + {}^{48}\mathrm{Ca}$ is very small (< 0.78), and so are the ratios for the systems that involve the nucleus ^{36}S, whereas this ratio is ~0.9 for the heavier $^{64}\mathrm{Ni} + {}^{100}\mathrm{Mo}$ system, which also involves soft reaction partners (see Table I). Maybe the ^{32}S and ^{36}S nuclei are indeed special, as first noticed by Montagnoli *et al.* (2013). Measurements of fusion to even lower energies are urgently needed for reactions induced by sulfur and ^{48}Ca nuclei.

D. Fusion hindrance in light systems

Fusion between light nuclei is of interest not only because of the fusion dynamics but also because some of these systems play important roles in the late stages of massive star evolution

as discussed further in Sec. V. In this section we discuss how these systems fit into the global fusion hindrance systematics, including attempts to improve the extrapolation to center-of-mass energies that are of interest to astrophysical applications.

In Fig. 18, the logarithmic derivatives are shown for four light systems, which all have large positive fusion Q values. The solid curves are extrapolations obtained with Eq. (39), the dashed curves are constant S-factor functions, $L_{CS}(E)$, and the dash-dotted curves are standard CC calculations.

For the lightest system, $^{10}B + ^{10}B$, shown in Fig. 18(a), the slopes of both the $L(E)$ and $L_{CS}(E)$ increase and the two curves become nearly parallel, such that the S factor becomes nearly flat (Jiang, Rehm *et al.*, 2007) at the lowest energies. As a consequence, the identification of the onset of fusion hindrance becomes difficult or impossible for this system.

Because of experimental difficulties, the fusion cross sections measured for light systems at low energies in different experiments often show relatively large deviations. The deviations often exceed the experimental uncertainties given in the papers. One example is shown in Fig. 19 for $^{16}O + ^{16}O$, where five measurements are displayed with different scaling factors. Analyzing each data set separately, one observes that the majority of the S-factor data show a maximum as indicated by the dashed curves, but the maxima occur at different center-of-mass energies. Thus, the solid curve in Fig. 18 for $^{16}O + ^{16}O$ represents an average extrapolation with Eq. (39).

Using the two-center shell model to compute the ion-ion potential and the mass parameter in the $^{16}O + ^{16}O$ system, Diaz-Torres, Gasques, and Wiescher (2007) found that the S factor for this system does not decline with decreasing center-of-mass energy. This is probably not a surprising result because this model assumes that the single-particle structure evolves adiabatically as the two nuclei approach in contrast with the diabatic assumption that is the basis for the potential derived by Mişicu and Esbensen (2006), which leads to strong fusion hindrance at sub-barrier energies. For the $^{16}O + ^{16}O$ system, the experimental data do not extend to sufficiently low energies to discriminate between these two approaches.

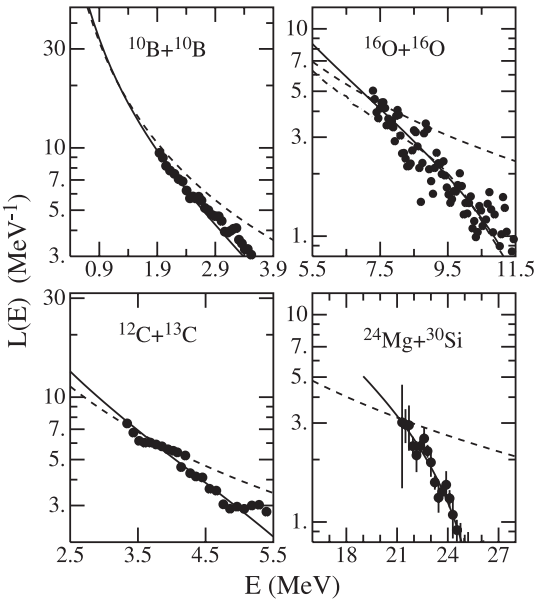

FIG. 18. Logarithmic derivative representation for four light systems with positive Q value. The dashed curves correspond to a constant S factor, whereas the dash-dotted curves display results of coupled-channels calculations. The solid curves represent fits to the low energy data using Eq. (39). The data are from $^{10}B + ^{10}B$ (High and Cujec, 1976), $^{12}C + ^{13}C$ (Dayras *et al.*, 1976; Notani *et al.*, 2012), $^{16}O + ^{16}O$ (Spinka and Winkler, 1974; Wu (1978); Hulke, Rolfs, and Trautvetter, 1980; Wu and Barnes, 1984; Thomas *et al.*, 1985), and $^{24}Mg + ^{30}Si$ (Morsad *et al.*, 1990).

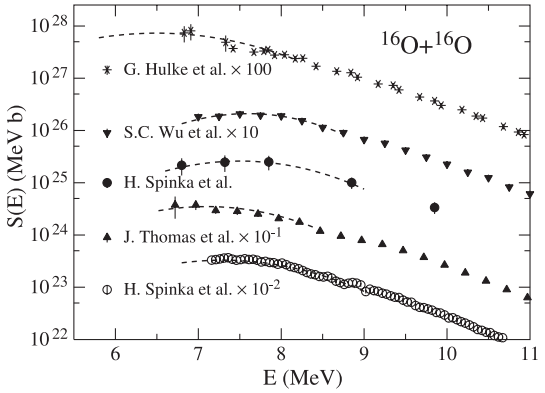

FIG. 19. Experimental S factors are shown for $^{16}O + ^{16}O$. Data from Spinka and Winkler (1974), Wu (1978), Hulke, Rolfs, and Trautvetter (1980), Wu and Barnes (1984), and Thomas *et al.* (1985) are multiplied by different scaling factors as indicated in the plot. The dashed curves serve only to guide the eye.

Another example is shown in Fig. 20 for $^{12}C + ^{12}C$ fusion. Again, the cross sections obtained in various experiments differ considerably. In this system, fluctuations in the cross section lead to a more complex situation, which will be discussed in Sec. V. Because of the importance of this reaction in the late stages of giant-star evolution several attempts have been made to extrapolate down to the energy region of astrophysical interest. Two such extrapolations by Fowler, Caughlan, and Zimmerman (1975) and Gasques *et al.* (2005) are shown as colored and dashed curves in Fig. 20,

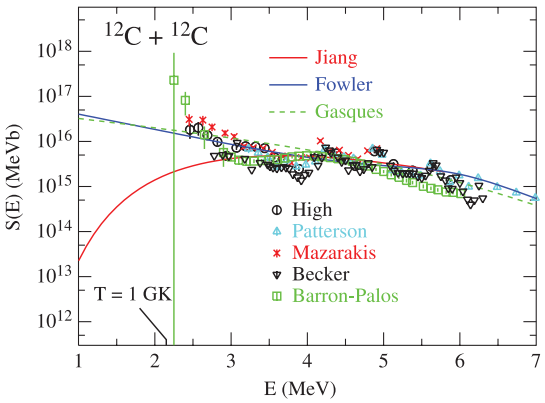

FIG. 20 (color). Experimental S factors for $^{12}C + ^{12}C$ fusion by Patterson *et al.* (1969), Mazarakis and Stephens (1973), High and Cujec (1977), Becker *et al.* (1981), and Barron-Palos *et al.* (2006) are compared with extrapolations suggested by Fowler, Caughlan, and Zimmerman (1975), Gasques, Brown *et al.* (2007), and Jiang, Rehm *et al.* (2007).

respectively. The center-of-mass energy corresponding to a stellar temperature of $T = 1 \times 10^9$ K is also indicated. The extrapolation method developed above [see Eq. (40)], given by the bottom curve, provides a substantially lower estimate of the S factor at the lowest measured energies. Obviously, estimates of the expected cross section at this energy and below differ substantially for the various recipes, resulting in large differences in the predicted isotopic abundances in the astrophysics simulations as discussed in Sec. V.E.; see also Gasques, Brown *et al.* (2007).

While one may be able to discern the intersection between the $L(E)$ and $L_{CS}(E)$ curves for $^{12}C + {}^{13}C$, this crossing point becomes rather ill determined for $^{10}B + {}^{10}B$. For even lighter systems, the data of $L(E)$ in the literature have not been measured to sufficiently low center-of-mass energies to reach the constant S-factor curve $L_{CS}(E)$. It should be pointed out that sub-barrier fusion cross sections are rare for systems between $^{16}O + {}^{16}O$ and $^{28}Si + {}^{30}Si$ (corresponding to $\zeta = 200$–700). Only data around the Coulomb barrier are available in the literature.

The extrapolation and fitting method, Eqs. (39) and (40), have been applied to many other light systems with positive Q values (Jiang, Rehm *et al.*, 2007; Jiang *et al.*, 2009) and it was seen that the experimental data can be accounted for quite well. The parameters obtained for systems with positive Q values can be found in the tables given by Jiang, Rehm *et al.* (2007) and Jiang *et al.* (2009).

The parameters A_0 and B_0 obtained from fits to E_s and L_s data are shown as a function of the entrance channel parameter $\zeta = Z_1 Z_2 \sqrt{\mu}$ in Fig. 21 for light and some medium-light systems. One finds systematic trends for both A_0 and B_0 as functions of ζ, which are well represented by

$$A_0^{\mathrm{emp}} = -10/\zeta - 1.13 - 0.0065\zeta \ (\mathrm{MeV}^{-1}), \qquad (41)$$

whereas the trend for B_0 is given by

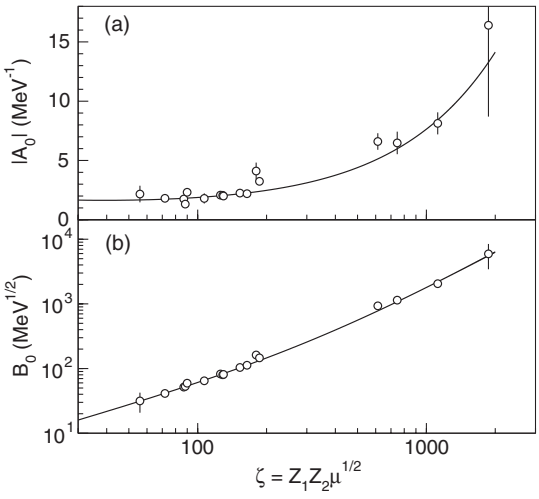

FIG. 21. The parameters (a) A_0 and (b) B_0 shown as a function of ζ for light and for medium-light systems. Only systems with positive Q values are included. The solid curves are given by Eqs. (41) and (42) for A_0 and B_0, respectively.

$$B_0^{\mathrm{emp}} = 0.495\zeta[1 - A_0^{\mathrm{emp}}(\zeta)/L_s^{\mathrm{emp}}(\zeta)](\mathrm{MeV}^{1/2}), \qquad (42)$$

noting that the A_0 and B_0 are correlated by Eq. (39) such that the expression for B_0^{emp} can be derived from Eqs. (35), (36), and (41). Note that Eqs. (41) and (42) as well as (39) and (40) can be used only for systems with positive Q values. In addition, Eqs. (35), (36), (41), and (42) form a set of functions $E_s^{\mathrm{emp}}(\zeta)$, $L_s^{\mathrm{emp}}(\zeta)$, $A_0^{\mathrm{emp}}(\zeta)$, and $B_0^{\mathrm{emp}}(\zeta)$, which can be used to predict the shape of the excitation function at very low energies, including the contributions from fusion hindrance. However, among these four equations, only Eqs. (35) and (41) are independent.

One additional parameter σ_s is needed to obtain the absolute cross section of the extrapolated part of the excitation function. It naturally shows variations by as much as 3 orders of magnitude for various systems. These variations arise since $\sigma(E)$ depends linearly on σ_s but exponentially on the parameters E_s, A_0, and B_0; see Eq. (40). Nuclear structure effects can easily lead to small deviations of E_s from the empirical curve $E_s^{\mathrm{emp}}(\zeta)$ as indicated in Fig. 15(a), which, when magnified through the exponential behavior, lead to a strong correlation between σ_s and $E_s - E_s^{\mathrm{emp}}$.

At this point, the influence of nuclear structure on fusion hindrance (e.g., the α-cluster structure and the odd-even mass effects) is not well understood. Furthermore, contributions from fluctuations are important for some reactions and are not included in this global analysis. Therefore, only the shape of the low energy part of the excitation function can be predicted approximately by this parametrization.

Finally, we emphasize that the question of whether an S-factor maximum exists for light systems is still an open one. Also, the value of the parameter $n = 1.5$ used in the empirical Eqs. (39) and (37) is somewhat arbitrary. This value was introduced by Fowler, Caughlan, and Zimmerman (1975) and Jiang, Rehm *et al.* (2007) and is discussed further by Jiang (2011). Additional data are required in order to better determine the value of this parameter.

E. Theoretical explanations of fusion hindrance

Brink (2004) pointed out that the anomaly in the fusion cross section at energies far below the barrier could be associated with events that happen after the nuclei have passed through the barrier and their densities begin to merge. When the densities overlap a potential description may fail, even when coupled-channels effects are included. Despite these concerns, it is of great interest to see whether the fusion hindrance can be explained by a potential model.

Dasso and Pollarolo (2003) found that a shallow potential is needed to describe the experimental data for the fusion of $^{60}Ni + {}^{89}Y$. Mişicu and Esbensen (2006, 2007) used the double-folding technique to construct the ion-ion potential from the Reid parametrization of the M3Y effective interaction (Bertsch *et al.*, 1977), and they used realistic densities of the reacting nuclei. The resulting ion-ion potential is, however, unphysical for overlapping nuclei where it produces an entrance channel potential that is deeper than the ground-state energy of the compound nucleus. The potential must therefore be supplemented with a repulsive term as described in Sec. II.A.2.

The repulsive potential is also calculated from the double-folding integral, Eq. (9), but the densities that are used have a small diffusivity ($a_r \leq 0.4$). The effective NN interaction that produces the repulsion is modeled by a zero-range form $v_{NN}^{\mathrm{rep}}(r) = v_0\delta(r)$ with strength v_0, following the suggestion of Uegaki and Abe (1993). The strength of the repulsion is calibrated so that the total nuclear potential for overlapping nuclei is consistent with the nuclear incompressibility predicted by Myers and Światecki (2000). The resulting ion-ion potential is referred to as the M3Y + repulsion (or M3Y + rep) potential. It produces a relatively shallow potential and thicker barrier in the entrance channel (see Fig. 1) of the one proposed by Dasso and Pollarolo (2003) and it has been used in coupled-channels calculations to describe the experimental data rather well (see Figs. 4, 12, and 13). The shallow potential recipe is in principle a sudden-limit model. A further discussion of the effects of the shallow potential can be found in Sec. IV.B.

Ichikawa, Hagino, and Iwamoto (2007) suggested a two-step model of fusion where the first part is determined by the coupled-channels method and the second part is the penetration of a one-dimensional adiabatic potential barrier, which takes over after the reacting nuclei start to touch. In a later study, Ichikawa, Hagino, and Iwamoto (2009) proposed a smooth transition from sudden to adiabatic states in heavy-ion fusion reactions at deep sub-barrier energies. They used the coupled-channels technique and simulated the smooth transition, from sudden to adiabatic states, and gradually damping the off-diagonal part of the coupling potential. This approach reproduces the data as well as the sudden approximation in the deep sub-barrier region of $^{64}\mathrm{Ni} + {}^{64}\mathrm{Ni}$ and $^{16}\mathrm{O} + {}^{208}\mathrm{Pb}$ (Mişicu and Esbensen, 2006).

Although the results of the two models (i.e., the Mişicu and Ichikawa models) are nearly the same in the energy region of the measured data, they are very different at lower energies. While the logarithmic derivative $L(E)$ of Ichikawa's model saturates at very low energies, and the resulting $S(E)$ factor becomes flat, the $S(E)$ factor of Mişicu's model develops a maximum and falls off steeply with decreasing energy. The steep falloff and increasing value of $L(E)$ obtained in Mişicu's model are consequences of the increased thickness of the barrier, due to the repulsive part of the M3Y + rep potential. Moreover, the $S(E)$ factor develops a maximum because the incoming-wave boundary conditions do not allow any fusion to take place at energies below the minimum of the pocket in the entrance channel potential.

Dasgupta *et al.* (2007) considered the current scheme of coupled-channels calculations to be inadequate. Besides describing capture reactions, which are realized by applying either an imaginary potential or IWBC, when the two colliding nuclei approach a specific distance, the coupled-channels approach uses a quantum mechanical formulation. The total wave function is expressed in this formulation as a linear superposition of states (or channel wave functions), and these states are coupled to each other with matrix elements in a symmetric manner. The total wave function is therefore coherent and the interactions between the different channels are reversible before the incoming flux is absorbed, by either an imaginary potential or reaching the boundary for incoming waves. Dasgupta *et al.* (2007) proposed that one should consider a gradual onset of decoherence, due to giant resonances, deep inelastic scattering, etc.

Diaz-Torres (2010a) developed a coupled-channels density-matrix approach to describe the low-energy nuclear collision dynamics. His goal was to quantify the effect of quantum decoherence on reaction observables and he used the scattering of $^{16}\mathrm{O} + {}^{154}\mathrm{Sm}$ as an example. The influence of decoherence on fusion and inelastic scattering was shown to be strong but the calculations were not compared to experiments. The decoherence is caused by the irreversible dissipation of flux or probability to the environment, which dilutes the incoming flux that otherwise would lead to fusion or inelastic scattering. It remains to be seen whether this mechanism can explain quantitatively the hindrance of fusion that has been observed experimentally in many systems at extreme sub-barrier energies.

There are many other papers in the literature that discuss the reason for the fusion hindrance behavior. Some of them are las follows: Ramamurthy *et al.* (1990), Hagino, Rowley, and Dasgupta (2003), Jiang *et al.* (2003), Lin (2003), Giraud *et al.* (2004), Seif (2004), Sastry *et al.* (2005), Chamon, Hussein, and Canto (2007), Umar and Oberacker (2008), Sargsyan *et al.* (2010, 2011), Shilov (2012), and Kuzyakin *et al.* (2012). A different hindrance mechanism, that can occur in light-ion fusion reactions, was recently proposed by Jiang, Back *et al.* (2013). It is the hindrance that occurs when the level density of the compound nucleus is low, more specifically, for small values of Γ/D, which is the ratio of level width to level distance in the compound nucleus. This mechanism will be discussed in Sec. V.

IV. NEW RESULTS AT ENERGIES ABOVE THE COULOMB BARRIER

One of the major goals of coupled-channels calculations is to provide a consistent description of all reaction channels including fusion, elastic and inelastic scattering, and transfer reactions. In general, this goal is difficult to reach because it appears that different types of reactions require different parametrizations of the ion-ion potential. However, there are exceptions where a consistent set of coupled-reaction-channels (CRC) calculations have provided a good description of fusion, elastic scattering, and other reaction channels. These are usually for lighter or asymmetric systems where the data can be described fairly well by the couplings to the direct reaction channels. Keeley *et al.* (1998), for example, obtained a consistent description of the fusion and scattering data for $^{16}\mathrm{O} + {}^{58,62}\mathrm{Ni}$, and Santra (2001) obtained a comprehensive description of the elastic scattering and the different reaction channels, including transfer, for $^{12}\mathrm{C} + {}^{208}\mathrm{Pb}$.

A consistent coupled-channels description of the fusion, multineutron transfer, and (inclusive) elastic scattering of $^{58}\mathrm{Ni} + {}^{124}\mathrm{Sn}$ was developed by Esbensen, Jiang, and Rehm (1998). It was assumed that transfer and inelastic excitations are independent processes and the calculations included up to three-neutron transfer channels. The transfer was modeled as successive one-neutron transfers combined with a direct pair transfer, which was described by a form factor of the type defined in Eq. (24). By adjusting the strength of the

one-neutron transfer and the strength and the range of the pair-transfer form factor it was possible to reproduce the measured multineutron transfer data by Jiang *et al.* (1998). Moreover, the calculations provided a comprehensive description of the measured reaction and elastic scattering data. In particular, it was found that the couplings to the transfer channels cause an enhancement of the calculated capture cross section at sub-barrier energies.

The real part of the empirical ion-ion potential that is commonly used to describe the elastic scattering of heavy nuclei is fairly well established (Broglia and Winther, 1991). It is parametrized as a Woods-Saxon potential with a diffuseness of $a \approx 0.6$ to 0.7 fm. It agrees quite well with the M3Y double-folding potential at relative distances that are outside the Coulomb barrier. However, these potentials do not always provide a good description of fusion data, neither at extreme sub-barrier energies as discussed in Sec. III nor at energies far above the Coulomb barrier as discussed below. The data often fall below calculations that are based on the empirical ion-ion potential for elastic scattering. A large effort has gone into identifying where the inconsistencies with elastic scattering data occur and what causes them. Some of these inconsistencies and possible remedies are discussed next.

A. Suppression of fusion at high energies

The analysis of fusion data at energies far above the Coulomb barrier has often resulted in parameters of the ion-ion potential that are different from those that are used to describe elastic and quasielastic scattering data. A systematic analysis was performed by Newton *et al.* (2004a, 2004b). It showed that the required diffuseness of a Woods-Saxon–type potential increases with an increasing value of the product Z_1Z_2 of the atomic numbers of the reacting nuclei. The average diffuseness ranges from 0.75 to 1.5 fm, from light to heavy systems, but with large fluctuations. The analysis was performed with a fixed depth of the potential $V_0 = -100$ MeV, whereas the radius and the diffuseness were adjusted to optimize the fit to the data. For this purpose the computer code CCMOD by Dasgupta *et al.* (1992) was used.

Another way to illustrate that the empirical Woods-Saxon potential cannot explain the high-energy data is to plot the suppression factor of the data $S = \sigma_{\mathrm{exp}}/\sigma_{\mathrm{ref}}$, with respect to a reference calculation σ_{ref}. Newton *et al.* (2004a, 2004b) chose a modified empirical potential, which has a realistic diffuseness of $a \approx 0.67$ fm and the depth $V_0 = -100$ MeV. The suppression factor that was obtained is close to unity for lighter systems but it is reduced to about 0.6 for heavy systems. The suppression may in some cases be due to a reduced detection efficiency but the general trend suggests that this is not the only reason. It is expected that dynamical effects, which are beyond the one-dimensional penetration, are the cause of the suppression as suggested early on by Hanappe *et al.* (1974).

The need for a large diffuseness of the ion-ion potential to explain the high-energy fusion data implies that the fusion and the elastic scattering data cannot be reproduced simultaneously with the same Woods-Saxon potential. The apparent inconsistency of the two observables persists even when they are compared to coupled-channels calculations as discussed by Dasgupta *et al.* (2007) and Mukherjee *et al.* (2007).

The apparent inconsistency in the description of fusion and elastic scattering, with fusion data requiring a large diffuseness and elastic scattering data requiring a smaller diffuseness of the Woods-Saxon potential, stems from the fact that the two reactions probe different parts of the ion-ion potential. While the elastic scattering is primarily sensitive to the ion-ion potential at large distances that are outside the Coulomb barrier, the trajectories that probe smaller distances will lead to direct or more complicated reactions, including fusion. The inconsistency can therefore be resolved by modifying the empirical ion-ion potential for overlapping nuclei while keeping it unchanged at larger distances.

B. Sensitivity of CC calculations to the ion-ion potential

There are several examples of experimental observables that are sensitive to the ion-ion potential for overlapping nuclei. Next we discuss some of them.

1. Relation to the fusion hindrance at low energies

Since the first experimental demonstration of the hindrance phenomenon at energies far below the Coulomb barrier (Jiang *et al.*, 2002) many people have tried to explain why the fusion cross sections are suppressed when compared to coupled-channels calculations that are based on the empirical ion-ion potential for elastic scattering.

Early on, Hagino, Rowley, and Dasgupta (2003) pointed out that the fusion data far below the Coulomb barrier, where the fusion hindrance occurs, can be reproduced by applying an ion-ion potential of the Woods-Saxon type with a large diffuseness. This suggests that there may exist a connection between the suppression of fusion at high energies and the hindrance at extreme sub-barrier energies. A large diffuseness is often used to improve the description of fusion data at energies close to and far below the Coulomb barrier [see, for example, Montagnoli *et al.* (2010)].

Dasso and Pollarolo (2003) suggested that low-energy fusion is sensitive to the ion-ion potential at short distances between the reacting nuclei, and that the fusion hindrance phenomenon offers the opportunity to study the ion-ion potential for overlapping nuclei. The onset of the fusion hindrance could therefore be related to the depth of the ion-ion potential, and an early onset of the hindrance (i.e., at an energy closer to the Coulomb barrier) would indicate that the pocket in the entrance channel is shallow.

2. Theoretical explanation of the suppression

A theoretical description that is consistent with the suggestions of Dasso and Pollarolo (2003) was developed by Mişicu and Esbensen (2006). They calculated the M3Y + repulsion potential using the double-folding technique and adjusting it such that it produced a relatively shallow potential in the entrance channel. The fusion was determined by ingoing-wave boundary conditions, and the fusion hindrance would therefore set in as the relative energy of the colliding nuclei approached the minimum of the pocket in the entrance channel. In this way it became possible (as discussed in Sec. III) to reproduce the fusion data for many heavy-ion

systems at energies far below the Coulomb barrier (Mişicu and Esbensen, 2006).

It turns out that the shallow entrance channel potential, produced by the M3Y + repulsion potential, can also be used to explain the suppression of the fusion data at high energies. An example is the fusion of $^{16}O + ^{208}Pb$, which is illustrated in Fig. 22. The WS and the M3Y + rep potentials that have been used in the coupled-channels calculations produce the same height of the Coulomb barrier. The depth of the shallow M3Y + rep potential has been adjusted to optimize the fit to the measured fusion cross sections at sub-barrier energies and the result is shown as the solid curve in Fig. 12. It turns out that this calibration also provides an excellent reproduction of the data at high energies when applied in the coupled-channels calculation, which has 24 channels (Ch-24) and includes couplings to surface excitation modes and one-neutron transfer (Esbensen and Mişicu, 2007).

The calculated cross section that is based on the M3Y + rep potential in Fig. 22 exhibits small oscillations at high energies. The oscillations are caused by the penetration of individual centrifugal barriers and are related to the structures that are discussed in Sec. IV.B.3. The predicted cross section in Fig. 22 that is based on the empirical Woods-Saxon potential exceeds the data by about 10%, consistent with the findings of Newton *et al.* (2004a, 2004b).

It is interesting to note that the shallow M3Y + repulsion potential has been approximated with a Woods-Saxon potential in the barrier region by Ghodsi and Zanganeh (2010). The best fit has a diffuseness that is generally larger than the diffuseness of the empirical Woods-Saxon potential for elastic scattering. Since it is the height of the Coulomb barrier and the couplings in the vicinity of the Coulomb barrier that determine the fusion cross section, according to the constant-coupling model, the observation made by Ghodsi and Zanganeh provides a qualitative explanation as to why one can use either a shallow ion-ion potential, such as the M3Y + repulsion, or a Woods-Saxon potential with a large diffuseness, when fitting the fusion data at energies far above or far below the Coulomb barrier.

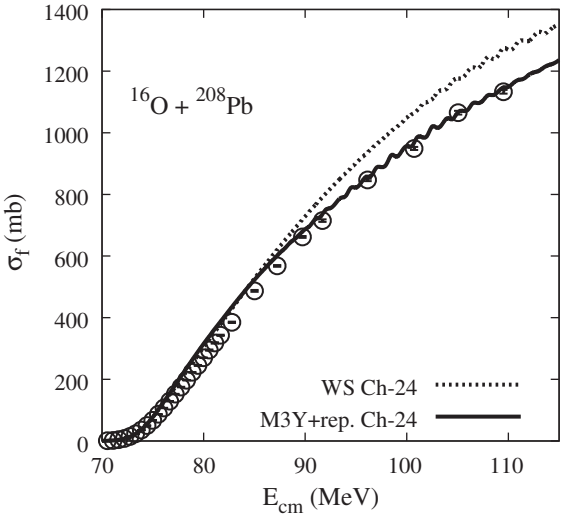

FIG. 22. The $^{16}O + ^{208}Pb$ fusion data (Morton *et al.*, 1999) are compared to coupled-channels calculations (Ch-24) that include 24 channels and are based on an empirical Woods-Saxon (WS) potential and the *M3Y* + repulsion potential that has been adjusted to reproduce the data at sub-barrier energies. From Esbensen and Mişicu, 2007.

3. Structures in high-energy fusion data

Another probe of the ion-ion potential are the oscillations or structures that have been observed in light-ion fusion reactions at energies above the Coulomb barrier. Some of the best examples are the fusion cross sections for $^{12}C + ^{12}C$, $^{12}C + ^{16}O$, and $^{16}O + ^{16}O$ which were measured by several groups. The structures were observed in the late 1970s but it was not completely clear at first what caused them. Similar structures were seen in elastic and inelastic scattering data and were associated with quasimolecular orbits of the two-body system.

The quasimolecular resonances that were observed in elastic scattering data could be explained by applying a fairly shallow ion-ion potential. A good example is the elastic scattering of $^{16}O + ^{16}O$ which was analyzed by Gobbi *et al.* (1973). The depth of the shallow potential that was used is similar to the depth of the M3Y + repulsion potential that was determined by Esbensen (2008) to reproduce the measured low-energy fusion cross sections for the same system.

It turned out that the M3Y + repulsion potential that was adjusted to reproduce the low-energy fusion data also provides a good description of the high-energy fusion data that were measured by Tserruya *et al.* (1978). The structures that are observed in the calculation at high energies can be associated with surpassing the centrifugal barriers for successive angular momenta (Esbensen, 2012). A good way to determine the energies of the L-dependent effective barriers is to plot the first derivative of the energy-weighted cross section,

$$D(E) = \frac{d(E\sigma_f)}{dE}. \tag{43}$$

This quantity is illustrated in Fig. 23 for the fusion of $^{16}O + ^{16}O$. The peak positions indicate the energies of the

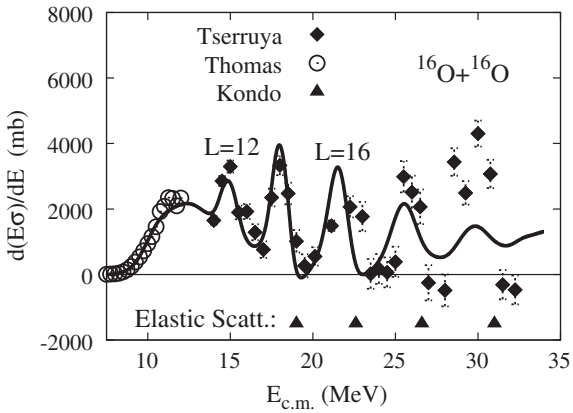

FIG. 23. Comparison of resonances extracted from the fusion data (Tserruya *et al.*, 1978) and the elastic scattering (Kondo, Bromley, and Abe, 1980) of $^{16}O + ^{16}O$. The solid curve is a coupled-channels calculation that is based on the M3Y + repulsion potential. From Esbensen, 2012.

effective centrifugal barriers, and the peaks associated with the angular momenta $L = 12$ and 16 are indicated in the figure. It was argued (Esbensen, 2012) that $D(E)$ represents the sum of the centrifugal barrier distributions at high energies, whereas the distribution $B(E)$ defined in Eq. (21) represents the $L = 0$ barrier distribution.

The above interpretation of the structures observed in high-energy fusion data was actually proposed previously by several authors, e.g., Poffe, Rowley, and Lindsay (1983), who observed similar structures in the fusion of $^{20}Ne + {}^{20}Ne$. An even earlier example is by Kondo, Bromley, and Abe (1980) who established the relationship to the quasimolecular resonances extracted from the elastic scattering data of $^{16}O + {}^{16}O$. The energies of the resonances they determined are indicated in Fig. 23 for $L = 14$, 16, 18, and 20 by the large triangles. They are located slightly above the corresponding barriers extracted from the fusion data. This is consistent with the expectation that the L-dependent phase shift varies quickly and goes through 90° as the energy exceeds the height of the L-dependent barrier; Kondo, Bromley, and Abe (1980) referred to this feature as an anticorrelation of the structures observed in the fusion and in the 90° elastic scattering excitation functions.

The above discussion shows that there is a close relationship between the quasimolecular resonances discussed in the late 1970s and the structures observed in light-ion fusion data at high energies. Both phenomena are best described by a shallow potential in the entrance channel. Moreover, the shallow M3Y + repulsion potential that has been calibrated to reproduce the low-energy fusion data for $^{16}O + {}^{16}O$ also provides a good description of the structures that are observed in the high-energy fusion data for the same system. It should be mentioned, however, that some of the high-energy fusion data for the same system show significant discrepancies between different data sets (Kovar *et al.*, 1979).

C. Influence of couplings to transfer

Transfer reactions can have a large impact on elastic scattering and fusion, in particular, at energies above the Coulomb barrier. The impact is particularly dramatic because it is, besides fusion, the main source of the absorption. This has been utilized in the construction of an imaginary ion-ion potential from the first-order single-particle transfer probabilities, which, in conjunction with the empirical real part of the ion-ion potential, provides a good description of the elastic scattering (Broglia and Winther, 1991).

The description of heavy-ion fusion reactions in terms of coupled-channels calculations becomes increasingly difficult as the beam energy increases above the Coulomb barrier, and an increasing number of transfer channels and other reaction channels open up. Transfer reactions are particularly challenging because there are so many of them and they are often poorly described at forward angles in the rotating frame approximation (Esbensen and Landowne, 1989). A complete coupled-channels calculation therefore becomes very demanding or even impractical. There are a few cases where this has been pursued, for example, the study by Santra (2001) who used the CRC method to describe the reactions of $^{12}C + {}^{208}Pb$.

These calculations included the direct couplings to a large number of excitation and transfer channels. The fusion of $^{12}C + {}^{208}Pb$ was simulated by a fairly strong but short-ranged imaginary potential. An interesting feature of the CRC calculations is that they produce essentially identical barrier distributions for fusion and quasielastic scattering. Moreover, they are in good agreement with the experimental barrier distribution for quasielastic scattering, whereas the barrier distribution for fusion could not be determined with the same accuracy.

The description of the fusion of $^{16}O + {}^{208}Pb$ has been a challenge to theory for several decades. Early attempts to explain the data by CRC calculations (Thompson *et al.*, 1989) did not succeed. It was realized that α transfer could play a role as well. Fortunately, the fusion data for $^{16}O + {}^{208}Pb$ have improved over the years (Morton *et al.*, 1999), and they have now been extended down to very small cross sections (Dasgupta *et al.*, 2007).

Although the fusion data for $^{16}O + {}^{208}Pb$ have now been reproduced fairly well by coupled-channels calculations that include the effect of excitations and one-neutron transfer (Esbensen and Mişicu, 2007), there are still some discrepancies. One problem that was first recognized by Morton *et al.* (1999) is that no calculation has yet provided a consistent description of the measured fusion cross sections for $^{16}O + {}^{208}Pb$ and the extracted barrier distribution. The problem is that the calculated peak of the barrier distribution is always higher than the peak of the measured distribution.

D. Multinucleon transfer reactions

As mentioned earlier, it is difficult to describe high-energy fusion data by coupled-channels calculations because of the large number of reaction channels that open up at these energies, as observed experimentally in $^{16}O + {}^{208}Pb$ collisions by Evers *et al.* (2011). The data showed large yields of one- and two-proton transfer over a broad range of Q values, even at energies close to the Coulomb barrier. The good agreement of the data with simplified coupled-channels calculations based on the M3Y + repulsion potential that are shown in Fig. 22 may therefore be accidental.

In order to reproduce both the fusion and scattering data for a given system within an incomplete coupled-channels calculation, it is necessary to supplement the ion-ion potential with an imaginary part that simulates the influence of the reaction channels that are not included explicitly in the calculations. This is in line with CRC calculations which include couplings to a large number of direct reaction channels but usually ignore multistep processes and higher-order couplings for practical reasons. The fusion process is described by the absorption in a short-ranged imaginary potential that acts primarily after the heavy ions have penetrated the Coulomb barrier. This description of fusion is equivalent to ingoing-wave boundary conditions.

The application of an imaginary potential is not a very satisfactory solution but it is often necessary because it is difficult to handle a large number of transfer channels. There are, however, other methods that may provide a better description of data at high energies. The computer code GRAZING, which was developed by Winther (1995), is based

on a semiclassical description and has been successful in describing elastic and quasielastic scattering, and transfer reactions in heavy-ion collisions at energies above the Coulomb barrier. The application to transfer reactions was recently reviewed by Corradi, Pollarolo, and Szilner (2009), and recent examples on the application of this method can be found in Montanari *et al.* (2011).

The time-dependent Hartree-Fock method was recently applied by Sekizawa and Yabana (2013) to describe multinucleon transfer processes between heavy nuclei. The transfer probabilities were calculated after the collision by the operator projection method that were proposed earlier by Simenel (2010). The calculations confirm the existence of a fast charge-equilibration mode in reactions of nuclei that have different values of N/Z. The calculations also show the formation of a neck at smaller impact parameters, and that the breaking of the neck is responsible for the transfer of protons and neutrons in the same direction. They found that the qualitative features of their calculations are similar to those obtained in calculations with the computer code GRAZING mentioned above.

E. Quasielastic and deep-inelastic scattering

The computer code GRAZING mentioned above was used by Pollarolo (2008) to analyze the barrier distributions that were extracted from the quasielastic scattering experiments performed by Mitsuoka *et al.* (2007). The systems that were considered are relatively heavy, ranging from Ti + Pb to Ge + Pb. The calculations showed that transfer reactions constitute a sizable fraction of the quasielastic scattering and have, as a consequence, a large influence on the calculated barrier distributions.

This code was also applied to calculate the capture cross sections for ^{58}Ni + ^{124}Sn (defined as the sum of the fusion and deep inelastic cross sections) as well as the quasielastic scattering cross sections and the cross sections for one-, two-, and three-neutron transfer reactions. The calculations are in good agreement with the capture data of Wolfs (1987) and with the quasielastic and transfer data by van den Berg *et al.* (1988) and Jiang *et al.* (1998). They are also in good agreement with the coupled-channels calculations by Esbensen, Jiang, and Rehm (1998) that were developed to provide a comprehensive description of the reaction data that were available for this system, from far below to well above the Coulomb barrier.

F. Complete and incomplete fusion

The fusion of weakly bound nuclei on stable targets is of current interest in heavy-ion fusion research and will be discussed in more detail in Sec. VI. In connection with the influence of transfer reactions discussed above, one should also consider the influence of transfer to the continuum or the breakup of the weakly bound projectile. An excellent example, that has been studied in great detail, is the complete and incomplete fusion of ^{9}Be on a number of stable targets.

An attractive feature of ^{9}Be in connection with breakup is that it has only one bound state (the ground state). Moreover, the threshold for the three-body breakup into $\alpha + \alpha + n$ is only 1.574 MeV, and neither ^{8}Be nor ^{5}He are stable. In a discussion of fusion one should therefore consider the complete fusion, where both α particles and the neutron fuse with the target, and the incomplete fusion, where only one of the α particles fuses with the target. In one of the first measurements Dasgupta *et al.* (1999) observed a reduction of about 30% in the complete fusion of ^{9}Be with a ^{208}Pb target in comparison to their expectations for the total fusion cross section. Moreover, a large cross section for incomplete fusion was observed. This was taken as evidence that the suppression of complete fusion was caused by the breakup of ^{9}Be before it reached the fusion barrier. This expectation was confirmed in a new measurement by Hinde *et al.* (2002) who observed a prompt breakup component at sub-barrier energies that could explain the previously observed suppression of the complete fusion of ^{9}Be with ^{208}Pb.

There are some uncertainties in the concept of incomplete fusion because it could as well arise from transfer processes. In the case of ^{9}Be, one could have a breakup followed by the fusion of one of the α particles, or one α particle could be transferred directly from an intact ^{9}Be nucleus. The situation is also uncertain with respect to the influence of breakup on complete fusion, because a breakup could (besides reducing the complete fusion probability) result in the fusion of both α particles. The fate of the released neutron is another subtle issue because it is usually not measured. These and other issues related to the interpretation of the data were discussed by Hinde *et al.* (2002), Dasgupta *et al.* (2004), and Gomes *et al.* (2011). These works also include a discussion of the many experiments that have been performed.

In order to obtain deeper insight into the many reaction mechanisms that govern the breakup of ^{9}Be on heavy targets, Rafiei *et al.* (2010) measured two α particles in coincidence. By plotting the data as functions of the relative energy between the two α particles and the reconstructed Q value of the breakup event, which assumed that the two α particles were the only fragments that were produced, they could separate the breakup probability into four or five different reaction mechanisms. This allowed them to identify the neutron transfer component, which resulted in the production of the unstable ^{8}Be ground state. They could also see events originating from the decay of excited states in ^{9}Be, referred to as inelastic breakup events. There were also various prompt breakup events with large relative energies between the two α particles.

They concluded that the breakup following neutron transfer dominates the total breakup yield. They also found that the prompt breakup probability is insensitive to the target Z when plotted as a function of the minimum surface-surface distance. These observations provide important constraints and tests of models that try to describe the competition between the complete and incomplete fusion of ^{9}Be.

G. Studies that have not been pursued recently

Several studies at energies far above the Coulomb barrier were pursued in the 1970s and 1980s but they were abandoned partly because of the growing interest in sub-barrier fusion. However, a number of problems remain largely unsolved and

with the improved techniques that have been developed it would be of interest to revive these studies.

One open question is the limiting angular momentum for fusion which was investigated for a few systems. As the spin and the excitation energy of the compound system approach the critical angular momentum and the critical excitation energy for fusion, it becomes unstable and starts to emit fast nucleons before it equilibrates by statistical particle and γ emission. These preequilibrium processes were studied in the 1970s and 1980s. The situation is related to the fusion of unstable nuclei that can quite easily release a few valence nucleons before the core nucleus fuses with the target.

V. NEW RESULTS IN NUCLEAR ASTROPHYSICS

Fusion in nuclear astrophysics is usually associated with the conversion of four protons into ^{4}He via the so-called pp reaction chain $^1\mathrm{H}(p,e^+\nu)^2\mathrm{H}(p,\gamma)^3\mathrm{He}(^3\mathrm{He},2p)^4\mathrm{He}$. While important for the energy production in stars and, thus, for the existence of life on Earth, the pp chain does not fall under the category of heavy-ion fusion reactions and will therefore not be discussed in this article. A review about this topic can be found in Adelberger *et al.* (2011).

A. Fusion reactions in nuclear astrophysics

The number of heavy-ion fusion reactions which are critical to nuclear astrophysics is quite small. In a hydrogen-rich environment the light elements such as Li, Be, and B have all positive (p,α) Q values, with the result that these nuclei are easily destroyed at low temperatures, before fusion reactions start to play a role. The stable carbon isotopes ^{12,13}C are the first p-shell nuclei with sufficiently negative (p,α) Q values. This makes $^{12}\mathrm{C}+{}^{12}\mathrm{C}$ the first fusion reaction that needs to be considered in nuclear astrophysics. ^{13}C has only about $1/100$ of the abundance of ^{12}C and therefore plays only a minor role in astrophysical fusion reactions [although it is crucial for neutron production via the (α,n) process]. Continuing toward heavier nuclei fusion reactions involving ^{16}O, the thirdmost abundant element in the Universe, suffer from the strong Z dependence of the quantum-mechanical tunneling probability. Oxygen fusion therefore plays a role only at higher temperatures occurring, e.g., in explosive environments. All this makes fusion of $^{12}\mathrm{C}+{}^{12}\mathrm{C}$ the most important heavy-ion fusion reaction in nuclear astrophysics.

Fusion of $^{12}\mathrm{C}+{}^{12}\mathrm{C}$ occurs in at least three astrophysical environments as discussed by Barnes *et al.* (1985) and Wallerstein *et al.* (1997).

- In nonexplosive scenarios carbon fusion takes place in the center of massive stars toward the end of their lifetime during the carbon-burning phase at temperatures of about 0.6–1 GK and densities of a few 10^5 g/cm^2. For a 15 solar-mass star this burning phase lasts about 10^3 yr (Woosley, Heger, and Weaver, 2002).
- In stellar explosions carbon fusion plays a role during the ignition phase of type Ia supernovae when a carbon-oxygen white dwarf (WD) accretes hydrogen and helium from a companion star on its surface (Hillebrandt and Niemeyer, 2000). If the mass of the WD exceeds the Chandrashekhar limit, it triggers an explosion which destroys the whole star. The temperatures associated with these conditions (1–10 GK) are higher than the ones experienced during carbon burning. Since type Ia supernovae are being used in cosmology as "standard candles" to study the expansion of the Universe (Astier, 2012) a good understanding of the type Ia supernovae explosions is critical.
- Carbon fusion has also been associated with so-called superbursts which occur in x-ray binary systems (Cumming and Bildsten, 2001). Superbursts are explosions in neutron stars which last longer (hours) than typical x-ray bursts (10 seconds).

In the following our present understanding of carbon fusion under these astrophysical conditions is discussed.

B. Experimental difficulties in measuring fusion reactions at astrophysical energies

The temperatures associated with the astrophysical scenarios mentioned above ($T\sim 1$ GK) are all so small that the respective Gamow energies ($E_G = 2.42\pm 0.75$ MeV for $T = 1$ GK) are well below the Coulomb barrier for C + C scattering ($V_C\sim 6.66$ MeV). Thus, fusion occurs via quantum mechanical tunneling with cross sections that are typically in the subnanobarn range. In stars, these small reaction rates are compensated by the large amount of carbon present in these environments (the Sun has carbon with a mass equivalent of about 1000 Earths) and by the long astronomical time scales. In terrestrial experiments the small cross sections result in yields (fusion events per incident carbon ion) of the order of 10^{-18} which require high-intensity particle accelerators and/or detection systems with good efficiencies.

The principal reactions occurring in $^{12}\mathrm{C}+{}^{12}\mathrm{C}$ fusion are

$$\begin{aligned} {}^{12}\mathrm{C}+{}^{12}\mathrm{C} &\rightarrow {}^{20}\mathrm{Ne}+\alpha+4.617\ \mathrm{MeV},\\ &\rightarrow {}^{23}\mathrm{Na}+p+2.241\ \mathrm{MeV},\\ &\rightarrow {}^{16}\mathrm{O}+2\alpha-0.113\ \mathrm{MeV},\\ &\rightarrow {}^{23}\mathrm{Mg}+n-2.599\ \mathrm{MeV}. \end{aligned} \tag{44}$$

In astrophysical environments the first two channels dominate the reaction due to their positive Q values. The protons and α particles produced in these two reactions are very important for nucleosynthesis since they further interact with the material present in the stellar environment generating other nuclei (e.g., ^{21,22}Ne, ^{25,26}Mg, ^{26,27}Al, ^{28,29,30}Si, etc.) which need to be included in network calculations.

In the following we briefly discuss some of the technical challenges encountered in measuring $^{12}\mathrm{C}+{}^{12}\mathrm{C}$ fusion cross sections at astrophysical energies. More details can be found in the literature.

Accelerators: Accelerators producing ^{12}C beams with intensities exceeding 15 particle μA (about 10^{14} particles/s) are now available. Excellent voltage stability and a precise voltage (energy) calibration are essential for measurements in an energy range where the cross sections fall off exponentially. The effects of energy shifts on measurements of steeply falling cross sections have been discussed by Barnes *et al.* (1985) and Aguilera *et al.* (2006).

Targets: The high beam currents in these measurements put extra constraints on the targets. Both thin (transmission) and thick targets have been used. In thick target experiments,

energy-integrated cross sections are obtained which need to be measured in small energy steps, in order to extract $\sigma(E)$ via point-to-point differentiation. For thin target experiments the thickness and structure of the target might change during the irradiation due to sputtering or through the deposition of hydrocarbons from the residual gas in the vacuum system. While the deposition of hydrocarbons on the target can be minimized by surrounding the target with a cryogenically cooled shroud, the presence of hydrogen and deuterium in the targets cannot be completely avoided. This can lead to background reactions as pointed out by Strieder (2010) and Zickefoose (2011).

Detection techniques: A variety of detection techniques have been developed to measure fusion cross sections for the $^{12}C + ^{12}C$ system:

- Detection of the evaporation residues (Kovar *et al.*, 1979).
- Detection of the γ rays (High and Cujec, 1977; Kettner, 1980; Dasmahaptra *et al.*, 1982; Rosales *et al.*, 2003; Aguilera *et al.*, 2006; Barron-Palos *et al.*, 2006; Spillane *et al.*, 2007).
- Detection of the light particles, protons, or α particles (Patterson *et al.*, 1969; Mazarakis and Stephens, 1973; Becker *et al.*, 1981) that are emitted from the evaporation residues.

At astrophysical energies only the latter two techniques have been used since the low energies of the residues make a direct detection impractical. Detecting the γ rays is straightforward and the good energy resolution of Ge detectors provides a clean signature of the nuclei produced in the fusion process. The main disadvantage is the low detection efficiency (even a 4π array such as GAMMASPHERE has only 6%–7% detection efficiency for the detection of the 1.63 MeV γ ray from ^{20}Ne). Furthermore, fusion-evaporation reactions populating the ground states in the final nuclei, which can be the strongest channel at the lowest energies, are not detected by this technique. Passive (Aguilera *et al.*, 2006; Barron-Palos *et al.*, 2006) and active (Spillane *et al.*, 2007) shielding techniques have been used in the experiments to reduce the backgrounds from cosmic rays. A further reduction can be achieved by locating the accelerator and the detectors underground, as planned at underground laboratories such as LUNA (Costantini *et al.*, 2008) or DUSEL (Winklehner *et al.*, 2013).

With particle detectors, higher detection efficiencies can be achieved, albeit at the expense of a reduced energy resolution. In order to identify the main (p and α) evaporation channels from the $^{12}C + ^{12}C$ fusion reaction ΔE-E telescopes with Si or gas detectors have been used in the experiments (the latter might introduce additional hydrocarbons to the system).

A major difficulty in these experiments is the presence of hydrogen and, thus, deuterium in the carbon targets. In the case of particle detection, background protons can be produced in a two-step process consisting of elastic deuterium scattering $d(^{12}C, d)$ followed by the proton transfer reaction $d(^{12}C, p)^{13}C$ with the recoil deuterons from the first step. This problem was discussed by Zickefoose (2011), where it was shown that the use of highly ordered pyrolytic graphite can strongly reduce this kind of background.

Other techniques that have been tried more recently are the use of a superconducting solenoid (Fang *et al.*, 2013). This avoids the need for large-area ΔE-E detector telescopes, since with this spectrometer particle identification is achieved through cyclotron motion which provides the m/q value of the detected particle, independent of its energy (Wuosmaa *et al.*, 2007). Particle-γ coincidences with high-efficiency γ-ray detector arrays were proposed by Jiang *et al.* (2012, 2013). This technique can provide very clean coincidence spectra and should allow for the extension of cross section measurements down to the 10 pb level using beam currents of the order of 100 particle μA.

C. $^{12}C + ^{12}C$ general behavior

In order to eliminate the strong energy dependence of the tunneling process in heavy-ion fusion reactions, the cross sections are usually converted into S factors (see Sec. III.A.). The S factor represents the fusion cross sections corrected for the tunneling through a Coulomb barrier generated by a pointlike nucleus for angular momentum $L = 0$. The S factors for fusion of ^{12}C, on a variety of systems ranging from ^{10}B to ^{17}O as a function of E/V_C, measured during the last 40 years are shown in Fig. 24. The data are obtained from the literature [a compilation of the various references can be found in Jiang, Rehm *et al.* (2007) and the values for the Coulomb barriers V_C are from Stokstad *et al.* (1976)].

Several characteristics can be observed from Fig. 24(a). Starting from energies above the Coulomb barrier, the S factors exhibit an exponential increase followed by a change in slope at $E/V_C \sim 0.8$. Regarding the importance of the various fusion reactions in astrophysical environments it has to be

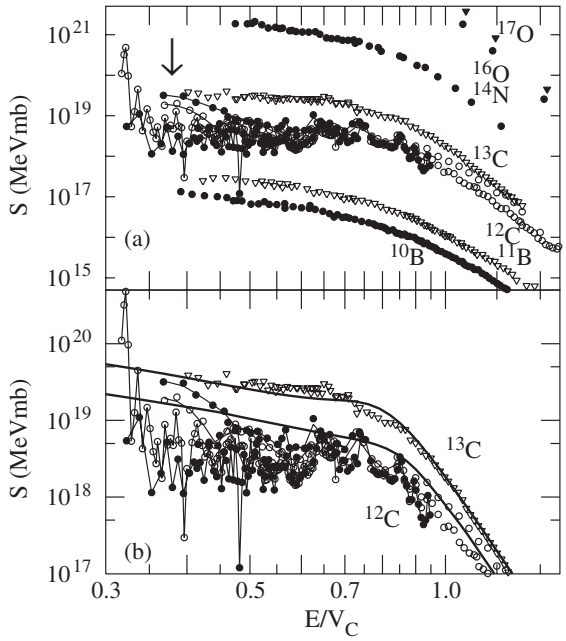

FIG. 24. (a) S factors of fusion reactions between ^{12}C and ^{10,11}B, ^{12,13}C, ^{14}N, and ^{16,17}O plotted as a function of E/V_C where V_C is the Coulomb barrier. (b) S factors of fusion between ^{12}C and ^{12,13}C as a function of E/V_C. The two solid lines are theoretical predictions (Esbensen, Tang, and Jiang, 2011) from coupled-channels calculations. The arrow indicates the center-of-mass energy corresponding to the Gamow window for a stellar temperature of $T = 1$ GK.

kept in mind that the abundance of boron in stars is very small and therefore C + B fusion reactions can be neglected. This demonstrates the importance of the $^{12}C + ^{12}C$ system in nuclear astrophysics. Because of its significance it has therefore been studied to the lowest energies reaching the Gamow window whose location (for $T = 1$ GK) is indicated by the arrow in Fig. 24(a).

The most conspicuous characteristics seen in Fig. 24(a), however, are the oscillations observed in the $^{12}C + ^{12}C$ system. While most fusion systems show a smooth behavior of $S(E)$, the $^{12}C + ^{12}C$ system exhibits fluctuations with widths of about 50–100 keV at energies below $E/V_C \sim 0.9$. A possible origin of this structure is discussed later.

Figure 24(a) also exposes the large differences among the various $^{12}C + ^{12}C$ experiments at the lowest energies. The techniques employed in fusion experiments and their respective advantages or disadvantages have been discussed previously. For the $^{12}C + ^{12}C$ system at energies above the Coulomb barrier the differences among the experiments are typically ±15%. At the lowest energies, however, these differences can reach 100%. A method to reconcile some of these measurements at higher energies was discussed by Aguilera *et al.* (2006). The questions about the possible existence of the resonant structure at $E_{\mathrm{c.m.}} = 2.14$ MeV, detected by Spillane *et al.* (2007) at the lowest energies, are not yet settled, since later measurements by the same group gave much smaller yields (Strieder, 2010; Zickefoose, 2011).

The curves in Fig. 24(b) for the astrophysically important reactions $^{12}C + ^{12}C$ and $^{12}C + ^{13}C$ are the result of coupled-channels calculations from Esbensen, Tang, and Jiang (2011) taking the strongest inelastic scattering channels into account. Details of these calculations have been discussed in Sec. II.A. These calculations give an excellent description of the behavior of the experimental S factors for $^{13}C + ^{12}C$. It is interesting to note that the calculations also agree with the maxima of the resonancelike structure seen in the experimental data for $^{12}C + ^{12}C$. This is discussed in more detail in Sec. V.D. Similar behavior of the S factor for $^{12}C + ^{12}C$ has been found in calculations by Denisov and Pilipenko (2010) using a barrier penetration model which includes quadrupole and hexadecapole surface deformations.

D. $^{12}C + ^{12}C$ resonant behavior at low energies

As shown in Fig. 24(a) the main difference of the $^{12}C + ^{12}C$ S factor compared to other systems is the occurrence of strong fluctuations at center-of-mass energies below ∼6 MeV with widths of 50–100 keV. Similar resonant structures have been observed in this system at higher energies in other reaction channels whose origins have been discussed since the early days of heavy-ion physics (Almqvist *et al.*, 1963; Kondo, Bromley, and Abe, 1980). In the astrophysical energy range discussed here these oscillations were described by Aguilera *et al.* (2006) in terms of a nonresonant background, calculated with the Krappe, Nix, and Sierk (KNS) potential (Krappe, Nix, and Sierk, 1979) using IWBC, and an additional contribution from a series of resonances of Breit-Wigner form σ_{BW} with the relation $\sigma_f = \sigma_{\mathrm{bkg}} + \sigma_{\mathrm{BW}}$. In this description, it is assumed that the appearance of resonances provides an additional mechanism over and above that associated with the normal fusion cross section, the latter being represented by the IWBC calculation. The resonance peaks in this system are explained in terms of molecular-resonance doorway states that absorb the incoming flux and allow for a competition of the decay strength between complete fusion and rescattering into outgoing channels.

A recent coupled-channels calculation by Esbensen, Tang, and Jiang (2011) gives a good description of the smooth cross sections of the neighboring $^{12}C + ^{13}C$ and $^{13}C + ^{13}C$ systems. The fact that it also agrees with the maxima of the cross sections of $^{12}C + ^{12}C$ (see Fig. 24) has led to an alternative explanation of the observed structures in the S factor (Jiang, Back *et al.*, 2013). There it was argued that the structures in the fusion cross sections are not caused by the presence of additional resonant states, but rather through the lack of compound states in the nucleus ^{24}Mg. For the $^{12}C + ^{12}C$ system, several factors conspire to make the paucity of compound levels an effect to consider in the fusion cross section. First, the fusion Q value for this system ($Q = 13.934$ MeV) is smaller than that for the two neighboring C + C systems ($Q = 16.318$ MeV for $^{12}C + ^{13}C$ and $Q = 22.465$ MeV for $^{13}C + ^{13}C$), leading to relatively low excitation energies in the fused ^{24}Mg system relative to the Coulomb barrier. Second, because ^{24}Mg is an even-even system, the level spacing at a given excitation is increased because of the pairing gap, and third, since the entrance channel is comprised of identical spin-zero nuclei, only states with positive parity and even spin can be populated. These three factors result in a reduction of the effective compound-nucleus level density by more than an order of magnitude for this system relative to $^{12}C + ^{13}C$.

In order to quantify the effect of the limited number of compound levels in ^{24}Mg, the average spacing $\langle D \rangle$ and the total width $\langle \Gamma \rangle$ as a function of spin J and excitation energy

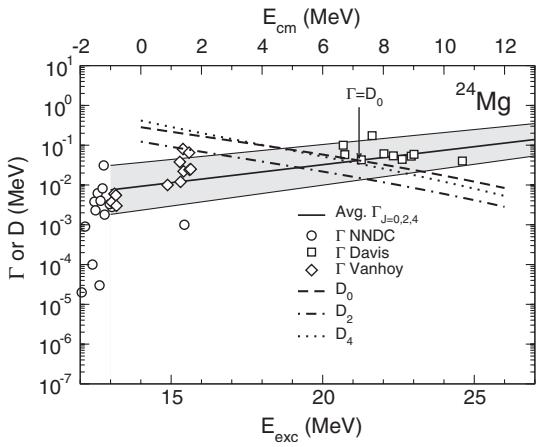

FIG. 25. Widths and level spacings of 0^+, 2^+, and 4^+ levels in ^{24}Mg. The experimental widths are shown as open symbols with data from Davis (1981) (squares), Vanhoy *et al.* (1987) (diamonds), and the NNDC (2013) compilation (circles). The solid line and the shaded region represent the estimated average trend for excitation energies $E_{\mathrm{exc}} \geq 13$ MeV. The average level spacings D_J for levels of spin $J^\pi = 0^+$, 2^+, and 4^+ are represented by the dashed, dot-dashed, and dotted curves, respectively. The corresponding center-of-mass energy $E_{\mathrm{c.m.}}$ for $^{12}C + ^{12}C$ is given on the top. The energy E_g at which $\Gamma = D_0$ is indicated by an arrow.

TABLE II. The fusion Q value, the center-of-mass energy E_g at which $\langle\Gamma\rangle = \langle D_0\rangle$, the Coulomb barrier V_C, and the ratio $\langle\Gamma\rangle_C/\langle D\rangle_C$ at the Coulomb barrier are listed for five light heavy-ion systems. Here E_g and $\langle\Gamma\rangle_C/\langle D\rangle_C$ are all given for the lowest J for the compound system.

System	Q (MeV)	E_g (MeV)	V_C (MeV)	$\langle\Gamma\rangle_C/\langle D\rangle_C$
$^{12}C + ^{12}C$	13.934	7.3	6.66	0.7
$^{12}C + ^{13}C$	16.318	−1.1	6.56	120
$^{13}C + ^{13}C$	22.465	−8.5	6.48	2210
$^{12}C + ^{16}O$	16.765	1.8	8.45	12
$^{16}O + ^{16}O$	16.542	0.8	10.76	94

$E_{\rm exc}$ were calculated [see Jiang, Back *et al.* (2013) for details]. The results together with experimental data from Davis (1981) and Vanhoy *et al.* (1987) and the NNDC (2013) compilation are shown in Fig. 25. The energy E_g at which the average level width $J = 0$, 2, 4, equals the average spacing of $J = 0$ levels D_0 is indicated by the arrow in Fig. 25. Around and below this energy ($E_{\rm c.m.} \sim 7$ MeV) $\Gamma < D$, and it is therefore expected that the fusion cross section is reduced relative to the one obtained from a CC (M3Y + rep) IWBC calculation. This value is in good agreement with the experimental data which show a start of the oscillating structure in the S factor at energies below 7–8 MeV. This also explains the special behavior of the $^{12}C + ^{12}C$ system with respect to the occurrence of fluctuations in the fusion cross sections.

Table II summarizes the values of the fusion Q values, the Coulomb barriers V_C, the crossover energies E_g, and the ratios $(\Gamma/D)_C$ at the Coulomb barrier for $^{12}C + ^{12}C$ and other neighboring systems. As can be seen from the table, $^{12}C + ^{12}C$ has the highest crossover energy of 7 MeV which is well within the center-of-mass energies accessible in today's experiments. The next highest energy is observed for the $^{12}C + ^{16}O$ system where indications of oscillations in the cross sections have been observed as well. These two systems also have the smallest values for $(\Gamma/D)_C$ with 0.7 and 12, respectively. $^{13}C + ^{12}C$ and $^{13}C + ^{13}C$, on the other hand, have $(\Gamma/D)_C$ values of 120 and 2210, respectively, and, thus, should not exhibit cross-section fluctuations in agreement with experimental observations.

If this explanation for the cross-section fluctuations is confirmed, one should be able to predict the structure of the fusion cross sections for $^{12}C + ^{12}C$ without direct measurements by using parameters of the appropriate low-spin resonances obtained, e.g., by $\alpha + ^{20}Ne$ experiments (Davis, 1981), which have much higher cross sections than $^{12}C + ^{12}C$ fusion reactions.

Other approaches that have been used to describe the resonant structure of the $^{12}C + ^{12}C$ fusion excitation function include the time-dependent wave-packet method by Diaz-Torres and Wiescher (2012). While the calculated S factor agrees with a subset of the published data, it generally overpredicts the cross sections at the lower energies.

E. $^{12}C + ^{12}C$ nonresonant behavior at low energies and influence on nuclear astrophysics

The temperature range associated with carbon burning in massive stars ($T \sim 0.5 - 1$ GK) and the corresponding Gamow energies (1–2 MeV) are in a range where no reliable cross-section measurements can be made with present technologies. For this reason, theoretical calculations or extrapolations starting with data at higher energies are needed. This was realized early on and a variety of S-factor parametrizations have been used for extrapolations. Many of them (Fowler, Caughlan, and Zimmerman, 1975; Caughlan and Fowler, 1988; Yakovlev *et al.*, 2006) provide a good description of the average trend of the $^{12}C + ^{12}C$ S factor, i.e., an exponential increase in $S(E)$ with a change in slope at $E/V_C \sim 0.8$. Whether this behavior continues to energies of $E \sim 1$ MeV has been questioned recently (Jiang, Rehm *et al.*, 2007). As discussed in Sec. III.B, fusion reactions with medium-mass nuclei experience a fusion suppression at the lowest energies which is caused by the fact that for systems with a negative fusion Q value, energy conservation requires $\sigma_f = 0$ for energies $E_{\rm c.m.} \leq -Q_f$. As a consequence, the S factor has to be zero at $E_{\rm c.m.} \leq -Q_f$ resulting in a maximum of $S(E)$, also discussed in Sec. III.B. For medium-mass nuclei this maximum has been experimentally observed at excitation energies of the compound system of $E_{\rm exc} \sim 15$ MeV. The question as to whether this behavior is also found for fusion systems with positive Q values is still being debated. Several experiments (Jiang *et al.*, 2010a) observed a change in slope for $S(E)$. In none of the systems, however, have the experiments been extended to sufficiently low energies to identify the existence of a true maximum.

The consequences of a reduced fusion cross section for the $^{12}C + ^{12}C$ reaction on the evolution of massive stars on the ignition of accreting white dwarfs which then explode as type Ia supernovae, and on the so-called superbursts have been discussed (Gasques, Evers *et al.*, 2007; Bravo and Martinez-Pinedo, 2012; Pignatari *et al.*, 2013). Here we summarize only the main conclusions achieved in these calculations. Details about the stellar evolution codes and the nuclear networks used in the publications can be found in the respective references.

Gasques, Brown *et al.* (2007) used the S-factor predictions by Jiang, Rehm *et al.* (2007) for $^{12}C + ^{12}C$, $^{12}C + ^{16}O$, and $^{16}O + ^{16}O$ to estimate possible effects in various astrophysical scenarios. In white dwarfs and in accreting neutron stars producing superbursts the reduced rates lead, as expected, to an increase in the carbon ignition temperature. For massive ($M = 20M_\odot$) stars a smaller $^{12}C + ^{12}C$ reaction rate leads to reduced (50%) abundances of ^{40}Ca, ^{46}Ti, and ^{50}Cr. Of particular interest are the effects on the production of the long-lived γ-ray emitters ^{26}Al and ^{60}Fe, which have been predicted by Limongi and Chieffi (2006) to be produced in large amounts in massive stars. Due to a higher neutron flux one obtains increased yields of ^{60}Fe and ^{26}Al in calculations using the reduced fusion cross sections. While an enhanced ^{26}Al production would match the observed ^{26}Al abundance, which is higher than predicted by nucleosynthesis calculations, the inverse is true for ^{60}Fe which is overpredicted by present calculations.

The effect of variations of the $^{12}C + ^{12}C$ fusion rates for type Ia supernovae was calculated by Bravo and Martinez-Pinedo (2012). These calculations indicate that a reduction in the $^{12}C + ^{12}C$ cross section leads to a corresponding increase in yield for CNO nuclei. The yield for ^{56}Ni, however, which is

the important nucleus powering the type Ia supernovae, was found to be quite robust.

The influence of reduced $^{12}C + {}^{12}C$ fusion rates on *s*-and *p*-process nucleosynthesis was recently discussed by Pignatari *et al.*, 2013. In addition to smaller effects on the production yields for *s*-process nuclei caused by the reduced neutron exposure, this calculation also finds increased yields for the long-lived radio isotopes ^{60}Fe and ^{26}Al, similar to the calculations of Gasques, Brown *et al.* (2007). It has, however, been argued that the yield for ^{26}Al could be affected by the particular stellar model used in the calculations.

In addition to $^{12}C + {}^{12}C$ fusion there are other heavy-ion fusion reactions which have recently been discussed in connection with x-ray bursts. Fusion reactions between neutron-rich carbon, oxygen, and neon isotopes such as $^{24}O + {}^{24}O$ or $^{34}Ne + {}^{34}Ne$ are predicted to occur in the in crust of accreting neutron stars. Studies of these reactions are clearly outside the reach of present experimental facilities and their cross sections rely on a theoretical description. Several papers on this topic have been published recently (Horowitz and Berry, 2009; Beard *et al.*, 2010; Umar, Oberacker, and Horowitz, 2012). First experimental studies to confirm these calculations using radioactive beams are discussed in Sec. VI.G.

VI. NEW RESULTS WITH RADIOACTIVE BEAMS

Many studies with stable ions have shown that there is a connection between the fusion mechanism and the underlying nuclear structure of projectile and target. As discussed in Sec. II, fusion cross sections were found to depend on the collective properties of the nuclei, on the Q values and the strength of neutron transfer reactions, or on the availability of weakly bound particles in the colliding nuclei. A theoretical framework to describe the connections between these processes was found in coupled-channels calculations which have been presented in Sec. II.A.

The availability of radioactive beams has greatly broadened our ability to investigate the relation between nuclear structure and reaction mechanism in more detail. Radioactive beams can be tailored to optimize certain nuclear properties that are found to influence the fusion process. Examples are nuclei with weakly bound neutrons or protons, sometimes called "halo nuclei" (e.g., ^{8}B, ^{11}Li, ^{15}C, ^{17}F), nuclei that exhibit strong transfer channels (e.g., ^{6,8}He), nuclei with a large neutron excess (e.g., ^{132}Sn), or nuclei with a pronounced vibrational structure (e.g., ^{76}Kr). Access to these exotic short-lived nuclei has expanded during the last two decades at several first-generation facilities and dedicated new radioactive beam facilities are being built at several laboratories. A description of the various production techniques for generating beams of short-lived nuclei can be found in several review articles (Mueller and Sherrill, 1993; Smith and Rehm, 2001). Here we discuss only those properties of radioactive beams that apply to measurements of fusion reactions.

A. Techniques of radioactive beam production

The isotope-separation-online (ISOL) technique, first developed in the 1950s by Kofoed-Hansen and Nielsen (1951), is the oldest method for producing radioactive beams. An intense beam of neutrons or charged particles hits a "thick" production target, producing a variety of radioactive nuclei. If these particles have a sufficiently long half-life, a high vapor pressure, and do not experience chemical reactions within the production target, they will effuse out of the target, where they can be ionized and accelerated in a secondary accelerator. Details of this technique can be found in Ravn (1979). Due to the underlying production mechanism, these ISOL beams have properties (beam-spot size, emittance, energy width) that are similar to the ones obtained with stable beams. The beam energy is in most cases in the range needed for measuring heavy-ion fusion reactions. The difficulties originating from isobaric impurities, a problem inherent to all secondary beams, can in some cases be overcome by using the mass selectivity of, e.g., a cyclotron as discussed by Cogneau *et al.* (1999) or by accelerating a particular charge state (e.g., $^{18}F^{9+}$), which eliminates contributions from the stable isobar ^{18}O. Because of its chemical dependence and the finite effusion times, the isotopic access of the ISOL technique is, however, somewhat limited. Facilities that presently use the ISOL technique are ISOLDE (CERN), ISAC (TRIUMF, Canada), and SPIRAL (GANIL, France).

The fragmentation of heavy ions, i.e., bombarding a "thin" production target with an energetic beam of heavy ions, was first used in the 1970s for the production of secondary beams (Symons *et al.*, 1979). Since there is no time delay for effusion out of the target, this technique has the widest range of secondary nuclei without any chemical dependence. The radioactive nuclei are separated from the primary beam with a set of ion-optical elements before they are transferred to the reaction target. Since many reaction products are produced in the fragmentation process, the beam purity is in many cases inferior to the one obtained with the ISOL technique. The main difficulty for measurements of fusion reactions is the relative high energy of the secondary beams (typically 40–100 MeV/u), which may require an energy degradation by foils depending on the application. Furthermore, the poor beam properties (beam spot size, energy width, and emittance) need to be taken into account when designing the detection system. The high beam energy, on the other hand, allows the user to individually tag each incoming particle according to their mass Z, position, and direction. Facilities that presently use the fragmentation technique are at GANIL (France), GSI (Germany), Lanzhou (China), NSCL (USA), and RIBF (Japan).

The in-flight technique uses transfer reactions such as (p, n), (d, n), (d, p), or $(d, {}^{3}\mathrm{He})$ performed with stable beams in inverse kinematics to produce secondary beams close to the valley of stability. A transfer line or a recoil separator transports the secondary beam from the production target to the experimental station. Because the energies involved in these reactions are usually lower than typical fragmentation energies, the secondary beams do not need to be attenuated by degrader foils in many cases. The beam properties of in-flight beams at the ATLAS accelerator are close to the ones observed for stable beams with beam spots of about 5×5 mm and an energy definition better than 0.6% (Harss *et al.*, 2000). Disadvantages of this technique are the limited mass and Z range of the secondary beams and the presence of beam

impurities which can be reduced using radio-frequency sweeper techniques. Because the equipment needed to produce secondary beams can be easily installed at existing low-energy stable beam facilities, many laboratories worldwide have been producing secondary beams with this technique. In-flight beams are available at ANL (USA), ANU (Australia), CIAE (China), FSU (USA), INS Tokyo (Japan), LLN (Italy), Notre Dame (USA), RIBRAS (Brazil), and TAMU (USA). More detailed descriptions of these facilities can be found in the literature.

Another method used to produce beams of certain long-lived radioactive particles is the so-called two-accelerator technique where a reasonably long-lived radio isotope is produced at a production accelerator (or reactor), followed by chemical separation, transport to a second accelerator, and insertion into the ion source. Examples of this technique cover half-lives ranging from $^{14}C(T_{1/2} = 5700\ \mathrm{yr})$, ^{44}Ti $(T_{1/2} = 59\ \mathrm{yr})$, ^{3}H $(T_{1/2} = 12.32\ \mathrm{yr})$, ^{7}Be $(T_{1/2} = 53.2\ \mathrm{d})$ down to ^{18}F $(T_{1/2} = 1.829\ \mathrm{h})$, and ^{11}C $(T_{1/2} = 20.3\ \mathrm{min})$ (Smith and Rehm, 2001).

The main difficulty present in all secondary beam experiments is the low beam intensity that can be achieved with the various production methods. Typical beam intensities are in the range of 10^3–10^7 particles/s, i.e., 3–6 orders of magnitude lower than what is typically available with stable beams. To compensate for these low beam intensities, detection systems with high efficiencies have to be employed or the experiments are limited to reactions with large cross sections. Because of these difficulties, it is not surprising that discrepancies among the various data have been observed, which in many cases have not been fully resolved. It is not the goal of this review to make a judgment about the reliability of the various measurements. The discrepancies observed in some of these experiments, however, emphasize the need for a reliable assessment of the underlying systematic uncertainties.

In the previous review by Liang and Signorini (2005), which covered radioactive beam experiments until 2005, nine different radioactive beams (^{6,8}He, ^{10,11}Be, ^{11}C, ^{17}F, ^{29,31}Al, ^{38}S, and ^{132}Sn) had been used for studies of heavy ion fusion reactions. Since that time, additional fusion experiments using fourteen different secondary beams (^{6,8}He, ^{8,9,11}Li, ^{7,10,11}Be, ^{8}B, ^{14,15}C, ^{20}O, ^{38}S, and ^{132}Sn) have been published, which are briefly summarized in Secs. VI.B–VI.I.

For a comparison of the cross sections obtained in the different experiments we use a renormalization proposed by Gomes *et al.* (2005) which eliminates the so-called geometrical effects, namely,

$$\sigma^{\mathrm{red}} = \sigma_f/(A_1^{1/3} + A_2^{1/3})^2 \tag{45}$$

and

$$E_{\mathrm{c.m.}}^{\mathrm{red}} = E_{\mathrm{c.m.}}(A_1^{1/3} + A_2^{1/3})/Z_1Z_2. \tag{46}$$

Other renormalizations can be found in the literature (Canto *et al.*, 2009). Since these renormalizations depend on additional parameters (e.g., radius parameters, curvature of the interaction potential, optical potentials), they will not be used in this review.

B. Fusion reactions with ^{6,8}He beams

The large neutron excess and the underlying halo structure have made the two helium isotopes ^{6,8}He prime candidates for nuclear reaction studies. ^{6}He, in particular, has high effusivity, chemical inertness, and is located close to the valley of β stability. For these reasons it can be produced with all production methods mentioned above [see, e.g., Becchetti *et al.* (1991), Fomichev *et al.* (1995), Watanabe *et al.* (1998), Trotta *et al.* (2000), Navin *et al.* (2004), Wuosmaa *et al.* (2005), Benjamim *et al.* (2007), and Rafiei (2011)]. Many experiments have been performed with this nucleus in the past decade. In this review we concentrate on experiments involving low-energy ^{6,8}He beams. Depending on the production technique, the beam properties can differ substantially. At Dubna (Fomichev *et al.*, 1995), the secondary ^{6}He beam was produced via the fragmentation technique using a 34 MeV/u ^{11}B beam, which was then slowed down to the energies of interest using degrader foils resulting in poor energy definition. The beam quality [e.g., a beam spot of 20 mm in diameter (Fomichev *et al.*, 2009)] is inferior to the one obtained for a ^{6}He beam produced with the ISOL technique. At Louvain-la-Neuve (Wolski *et al.*, 2011) and at Dubna (Lukyanov *et al.*, 2009), the ^{6}He beams are now produced using two cyclotrons. A proton beam from the first cyclotron produces ^{6}He via the $^7\mathrm{Li}(p,2p)^6\mathrm{He}$ reaction. The ^{6}He is then ionized in an electron-cyclotron resonance ion source and postaccelerated in the second cyclotron. This technique provides excellent beam properties with intensities of $\sim 10^{5-6}$ particles/s. The main problem with ^{6}He beams produced via the in-flight technique is the beam purity which requires special detection techniques.

The majority of ^{6,8}He induced fusion reactions performed during the past 8 years used heavier targets such as ^{197}Au or ^{206,208}Pb. The results of fusion studies with lighter targets (^{64}Zn or ^{63,65}Cu) have already been discussed by Liang and Signorini (2005) and will not be repeated. More recently Scuderi *et al.* (2011) revisited the question of a possible fusion enhancement for the system $^6\mathrm{He} + {}^{64}\mathrm{Zn}$ at low energies using new data from $^4\mathrm{He} + {}^{64}\mathrm{Zn}$ measured in the same energy range. Eliminating contributions from one- and two-neutron transfer reactions in the analysis, no fusion enhancement or suppression is observed at energies above the Coulomb barrier. Plotting the cross sections in so-called reduced coordinates, which eliminates static size effects, an enhanced cross section is still observed at energies below the Coulomb barrier.

Many studies of ^{6}He induced fusion reactions on heavier targets are marred by disagreements among the various experiments. The origins of these disagreements are not clear, but they might arise from the various detection techniques used in the experiments. Examples are fusion-fission cross sections for $^6\mathrm{He} + {}^{209}\mathrm{Bi}$ studied by Fomichev *et al.* (1995) and Kolata *et al.* (1998) or by Trotta *et al.* (2000) and Raabe *et al.* (2004).

More recent experiments in the system $^6\mathrm{He} + {}^{206}\mathrm{Pb}$ show similar discrepancies. First measured by Penionzhkevich *et al.* (2006) with a 60.3 MeV ^{6}He beam that was attenuated to barrier energies of 12–22 MeV with degrader foils, a large enhancement of the sub-barrier fusion cross section

(dominated by the $2n$-evaporation channel producing ^{210}Po) was observed. However, the need to use degrader foils resulted in large energy spreads of ± 3 MeV full width at half maximum (FWHM). A second experiment by Lukyanov *et al.* 2009)) using two cyclotrons for production and reacceleration resulted in a much improved energy spread ($\Delta E \pm 400$ keV) and gave similar cross sections. These two measurements, however, are at variance with the results obtained by Wolski *et al.* (2011) performed with the two cyclotrons at Louvain-la-Neuve; see Fig. 26.

In this context it should also be mentioned that the fusion data for the systems ^{4,6}He + ^{197}Au measured by Penionzhkevich *et al.* (2007) and plotted in the same coordinates are close to the ^{206}Pb data.

Much fewer fusion experiments with the "neutron-skin" nucleus ^{8}He can be found in the literature. While ^{6}He has a two-neutron binding energy of only 970 keV, this value increases to 2.089 MeV for ^{8}He. There are no well-suited transfer reactions to produce ^{8}He with the in-flight technique and, thus, the only method to produce low-energy ^{8}He beams with good beam properties is the ISOL technique. At SPIRAL, isotopically pure ^{8}He beams are produced by fragmentation of a 75 MeV/u ^{13}C beam in a thick graphite target followed by reacceleration in the CIME cyclotron. The energy resolution is better than 2×10^{-3} with a beam spot size of $\sim$5 mm in diameter and intensities of 4×10^{5} particles/s. With these beams, two fusion experiments have been performed (Lemasson *et al.*, 2009, 2010). In the second experiment (Lemasson *et al.*, 2010) elastic, quasielastic, and fusion reactions at energies of about twice the Coulomb barrier in the system ^{8}He + ^{65}Cu were investigated. Of particular interest for this review are the results from the first experiment (Lemasson *et al.*, 2009), where an excitation function for fusion in the system ^{8}He + ^{197}Au at energies in the vicinity of the Coulomb barrier was measured. The results are shown in Fig. 27 and compared to the results obtained for the neighboring isotopes ^{4,6}He. As can be seen, the three systems fall on a universal curve. Only at the lowest energies (corresponding to fusion cross sections of a few mb) one obtains deviations from the yields obtained with the stable ^{4}He beam.

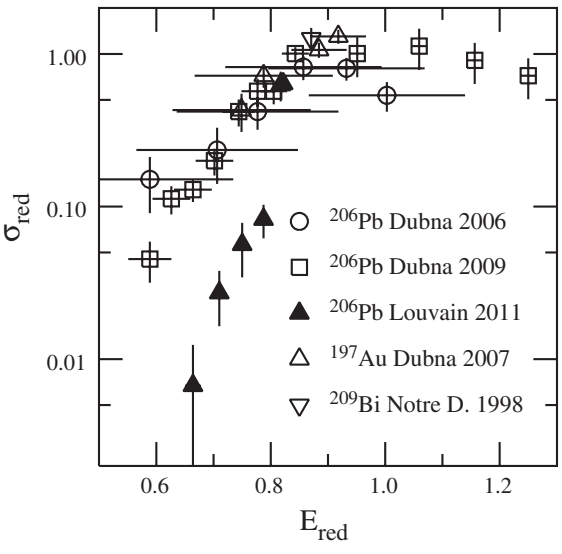

FIG. 26. ^{6}He induced fusion cross sections, plotted in reduced coordinates, on various targets in the vicinity of ^{208}Pb. The data are from Penionzhkevich *et al.* (2006), Lukyanov *et al.* (2009), and Wolski *et al.* (2011) for ^{206}Pb and from Penionzhkevich *et al.* (2007) and Skobelev *et al.* (2013) for ^{197}Au and Kolata *et al.* (1998) for ^{209}Bi.

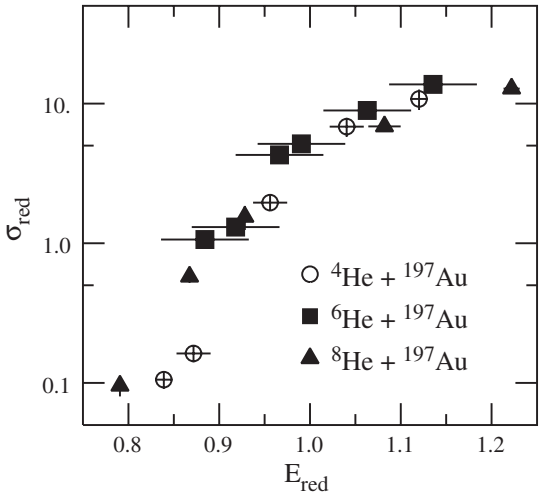

FIG. 27. Solid symbols: fusion cross sections for the systems ^{6}He (squares) and ^{8}He (triangles) on ^{197}Au plotted in reduced coordinates. The open symbols represent the fusion cross sections for the stable isotope ^{4}He. The data are from Lemasson *et al.* (2009) for ^{8}He, Penionzhkevich *et al.* (2006) and Skobelev *et al.* (2013) for ^{6}He and Basunia *et al.* (2007) for ^{4}He.

C. Fusion reactions with ^{8,9,11}Li beams

Although low-energy beams of ^{8}Li with intensities of 10^{5-6} particles/s have been available for about two decades at several laboratories, fusion studies with this isotope have been performed only in the last few years. One of the reasons might be that ^{8}Li always stood in the shadow of its more exotic neighbor ^{11}Li which has been at the center of radioactive beam studies since 1985 when its abnormally large interaction radius was discovered by Tanihata *et al.* (1985). A two-neutron halo nucleus with a binding energy of only 0.3 MeV, it has been the subject of many theoretical fusion studies (Signorini, 1997) predicting both enhancement and suppression of the fusion cross sections. These calculations differ by almost 4 orders of magnitude for the predicted cross sections. However, the short half-life of ^{11}Li ($T_{1/2} = 8.7$ ms) and its location at the neutron drip line have made fusion studies at energies in the vicinity of the Coulomb barrier very challenging and it was only recently that the first measurements were performed (Vinodkumar *et al.*, 2013). The beam of ^{11}Li was produced with the ISOL method and accelerated to energies $E = 29$–40 MeV at the ISAC2 facility at TRIUMF with intensities of $\sim 10^{3}$ particles/s.

In the study of fusion of ^{11}Li + ^{208}Pb, the ^{11}Li beam bombarded a stack of four 0.4–1 mg/cm^2 thick ^{208}Pb foils, which were backed by Al degraders so that four energies could be measured simultaneously. The ^{11}Li beam was pulsed with a 5 ns beam-on and 172 ns beam-off period. The evaporation residues formed in the ^{11}Li + ^{208}Pb reaction

are astatine isotopes ($^{212-216}$At), whose α decays were measured during the beam-off period (Vinodkumar *et al.*, 2013). The efficiency was calibrated using the previously measured ^{7}Li + ^{208}Pb reaction. One of the problems encountered in this experiment is the separation of the complete fusion reaction from the incomplete fusion processes generated by the breakup of ^{11}Li into ^{9}Li + $2n$ followed by the fusion of ^{9}Li + ^{208}Pb, which was measured separately. The cross sections for complete fusion of ^{11}Li + ^{208}Pb measured in this experiment were 73 ± 33 mb at $E_{\mathrm{c.m.}} = 37.9$ MeV while at lower energies only upper limits with cross sections below 10–20 mb could be obtained. Only about 11% of the total interactions was found to lead to complete fusion in this experiment.

Fusion cross sections in the system ^{8}Li + ^{208}Pb at high energies were studied by Aguilera *et al.* (2009) with ^{8}Li beams of energies between 32 and 37.5 MeV and intensities of 2×10^{5} particles/s. The (delayed) α decay of the evaporation residues ^{211,212}At was measured with an efficiency of ∼20% using a pulsed beam. The main problem in this experiment originated from the ^{4}He^{2+} beam contaminants having the same magnetic rigidity as ^{8}Li. Fusion of ^{208}Pb with ^{4}He can produce α activities such as ^{209,210}Po which can interfere with the α decay from the residues of interest. In the energy range covered in this experiment, the cross sections for complete fusion are still quite large (∼250–650 mb) resulting in a fusion suppression factor of about 0.7. From a comparison with the fusion cross sections for the neighboring stable ^{6,7}Li isotopes, which have both smaller (^{6}Li) and larger (^{7}Li) breakup thresholds S_A, a correlation between the fusion suppression and the breakup energy S_A was deduced.

Fusion reactions with ^{9}Li on ^{70}Zn (Loveland, Peterson *et al.*, 2006) were studied at TRIUMF as a first step toward experiments with a ^{11}Li beam. In these experiments the produced radioactivities (Ge and As isotopes for ^{70}Zn) were measured offline using α, β, and γ techniques. The fusion cross sections for the ^{9}Li + ^{70}Zn system plotted in reduced coordinates are shown in comparison with ^{6,7}Li induced fusion reactions on similar target nuclei in Fig. 28. A slight cross-section enhancement in the sub-barrier energy range is observed. This behavior is different from the one observed for ^{9}Li + ^{208}Pb (Loveland, 2011) where the differences in fusion cross sections observed for ^{6,7,9}Li are purely geometrical in origin (Vinodkumar, 2010).

D. Fusion reactions with ^{7,10,11}Be beams

The experiments with the long-lived radioisotope ^{7}Be were utilizing two different production techniques. Fusion of ^{7}Be + ^{27}Al was studied with a beam produced via the in-flight technique using the ^{1}H(^{7}Li, ^{7}Be)n reaction and the recoil separator at the IUAC New Delhi to separate the secondary ^{7}Be particles from the primary ^{7}Li beam (Kalita *et al.*, 2006). A very clean (≥ 99% purity), but low-intensity (10^{4} particles/s) beam was obtained which allowed the researchers to measure only fusion cross sections at higher energies where the data are well described by coupled-channels calculations. No indication of fusion suppression was found.

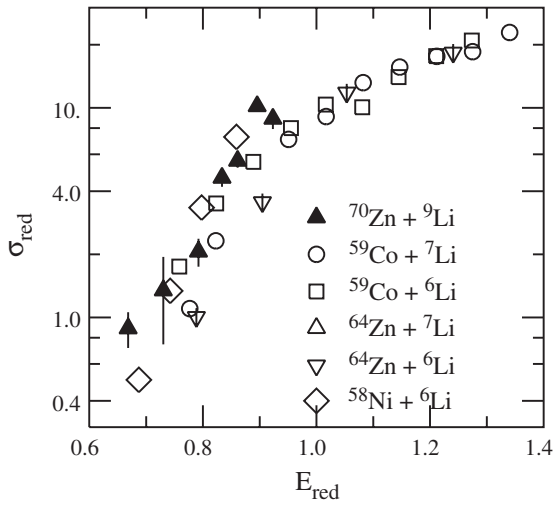

FIG. 28. Solid triangles: fusion cross sections for the system ^{9}Li on ^{70}Zn plotted in reduced coordinates. The open symbols represent fusion cross sections for ^{6,7}Li induced reactions on neighboring targets ^{58}Ni, ^{59}Co, and ^{64}Zn. The data are from Loveland *et al.* (2006) (^{70}Zn), Beck *et al.* (2003) (^{59}Co), Gomes *et al.* (2004) (^{7}Li + ^{64}Zn), Torresi *et al.* (2011) (^{6}Li + ^{64}Zn), and Aguilera *et al.* (2011) (^{58}Ni).

An experiment studying the heavier ^{7}Be + ^{238}U system was performed with a ^{7}Be beam produced via the two-accelerator technique using the two cyclotrons at Louvain-la-Neuve (Raabe *et al.*, 2006). Very pure beams with excellent properties were obtained with intensities around 5×10^{6} ions/s, which allowed for measurements of cross sections down to about 2 mb. Contrary to the lighter system mentioned above, a suppression of the fusion cross sections at higher energies was observed, while at the lowest energies no fusion enhancement due to coupling of direct channels could be found.

In this context it should be mentioned that a reanalysis of fusion measurements of ^{9,10,11}Be on ^{209}Bi suggests a significant suppression of complete fusion in these systems (Hinde and Dasgupta, 2010), despite the large variations in the α breakup thresholds for these three systems. Clearly a remeasurement of the ^{10,11}Be + ^{209}Bi systems with improved beam qualities is warranted.

E. Fusion reactions with ^{8}B beams

Two recent fusion measurements with ^{8}B beams and ^{28}Si (Pakout *et al.*, 2013) or ^{58}Ni (Aguilera, Martinez-Quiroz *et al.*, 2009; Aguilera *et al.*, 2011) targets have been reported. ^{8}B is an odd-odd proton halo nucleus with a very low proton separation energy of 0.138 MeV. In both experiments the beam was produced with the in-flight technique using the ^{3}He(^{6}Li, ^{8}B)n reaction with ^{6}Li beams from tandem accelerators. Since the production of ^{8}B requires a two-particle transfer reaction, the in-flight beams have considerable contaminations from neighboring nuclei (e.g., ^{3}He, ^{6}Li, and ^{7}Be). Taking the cross sections given in the two publications and plotting them in "reduced coordinates," the two systems (see solid points in Fig. 29) are in quite good agreement. It should be noticed that fusion cross sections of neighboring particles such as ^{6}Li or ^{7}Be (given by the open symbols) are above the

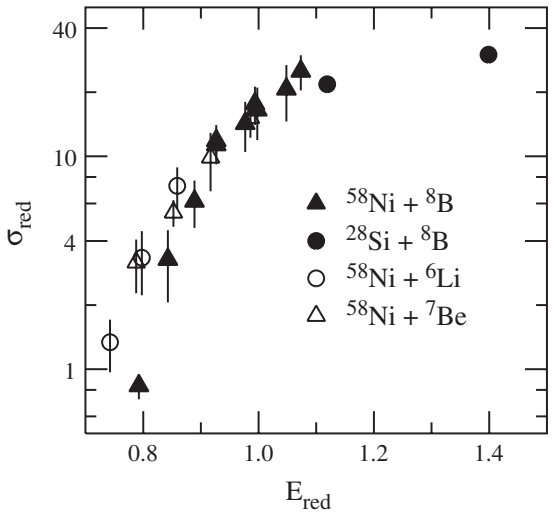

FIG. 29. Solid symbols: fusion cross sections for the systems ^{8}B on ^{28}Si (circles) or ^{58}Ni (triangles) plotted in reduced coordinates. The open symbols represent fusion cross sections for the neighboring systems ^{6}Li or ^{7}Be on ^{58}Ni. The data are from Aguilera *et al.* (2011) (^{58}Ni) and Pakout *et al.* (2013) (^{28}Si + ^{8}B).

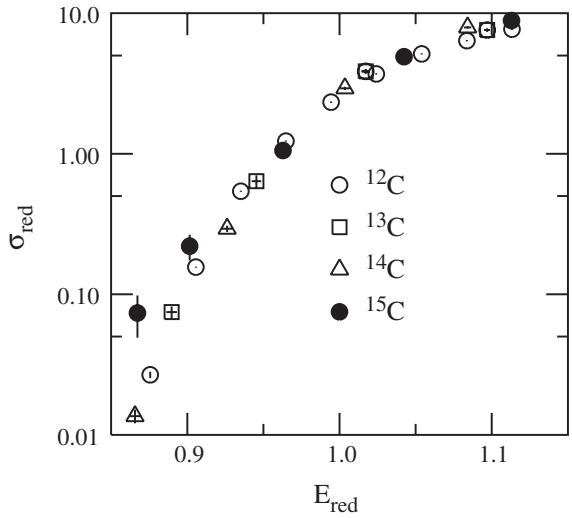

FIG. 30. Fusion cross sections induced by ^{12,13,14,15}C on ^{232}Th plotted in reduced coordinates. The fusion cross sections for the tightly bound nuclei ^{12,13,14}C coincide (open symbols), while at the lowest energies an enhancement is observed for the neutron-halo nucleus ^{15}C (solid points). From Alcorta *et al.*, 2011.

yields observed for the proton-halo nucleus ^{8}B, indicating that no special enhancement of fusion for ^{8}B is observed. This is similar to the results obtained for the proton-halo nucleus ^{17}F (Rehm *et al.*, 1998).

F. Fusion reactions with ^{14,15}C beams

Measurements with the two carbon isotopes ^{14,15}C have allowed a detailed study of the influence of a weakly bound neutron in the fusion process. The isotope ^{14}C ($T_{1/2} = 5700$ yr) has a closed neutron shell with its excited states starting above an excitation energy of $E_x \sim 6$ MeV. The Q values for neutron transfer on ^{14}C are quite negative which makes this nucleus a good reference without major contributions from inelastic scattering or transfer reactions. The ^{15}C nucleus, on the other hand, with a weakly ($B_n = 1.218$ MeV) bound $s_{1/2}$ neutron outside the closed $N = 8$ shell exhibits a large interaction cross section when compared to its nearest neighbors. Because of these properties, ^{15}C has been considered as a one-neutron halo nucleus (Al-Khalili, 2004). In the experiment by Alcorta *et al.* (2011) the fusion-fission processes of ^{13,14,15}C interacting with a ^{232}Th target were investigated. The beam for the long-lived ^{14}C ($T_{1/2} = 5700$ yr) was produced with the two-accelerator technique with properties identical to stable beams. For the shorter-lived ^{15}C($T_{1/2} = 2.45$ s) the in-flight production method with the inverse-kinematics $d(^{14}\mathrm{C}, ^{15}\mathrm{C})p$ reaction was used. The beam intensities were between 10^5 and 10^6 particles/s with a beam spot of about 5×5 mm^2. In order to expedite the energy changes for the secondary ^{15}C beam, Au degrader foils were used. For all beams, the energy of the beam was continuously monitored through its deflection in a calibrated magnetic spectrograph located after the target. A plot of the reduced cross sections for the four carbon isotopes ^{12,13,14,15}C is shown in Fig. 30. In these reduced coordinates the three isotopes ^{12,13,14}C coincide over the full energy range measured in the experiment. The one-neutron halo nucleus ^{15}C, on the other hand, exhibits an enhancement in cross sections by up to a factor of 6 at the lowest energies. This increase cannot be described in a simple valence-neutron model description.

G. Fusion reactions with ^{20}O beams

Studies of x-ray bursts performed during the last four decades have given us valuable information about nuclear reactions occurring on the surface of neutron stars (Schatz and Rehm, 2006). X-ray bursts occur in binary star systems if the neutron star accretes material from an evolved companion star on its surface. Once sufficient hydrogen and helium has accumulated, it ignites in a thermonuclear explosion forming heavier elements up to about mass 100 in the rapid proton capture process, which slowly sink deeper into the star. In addition to these standard x-ray bursts, which last tens of seconds and have recurrence times of hours to days, some x-ray binaries have been found to produce so-called superbursts lasting hours and emitting about 10^3 times more energy. While the main energy source of superbursts comes from $^{12}\mathrm{C} + ^{12}\mathrm{C}$ burning, detailed simulations have difficulties with reproducing the ignition phase of the superburst. Consequently, additional heat sources have been proposed, which include at the higher densities electron capture reactions producing neutron-rich isotopes that subsequently can undergo pycno-nuclear fusion reactions (Horowitz and Berry, 2009). Theoretical estimates have predicted increases in fusion cross sections by several orders of magnitude if fusion occurs between neutron-rich isotopes such as ^{24}C, ^{26}O, or ^{28}Ne (Beard *et al.*, 2010). While experimental verifications of these predictions are beyond our technical capabilities, some first steps have been made to study fusion of neutron-rich nuclei involving nuclei closer to stability. The system $^{12}\mathrm{C} + ^{20}$O was studied recently at GANIL (Rudolph *et al.*, 2012). The ^{20}O beam was produced through the ISOL method by

bombarding a carbon production target with a 79 MeV/u ^{22}Ne beam. The ^{20}O particles were ionized and reaccelerated in the CIME cyclotron to an energy of 60 MeV. Typical beam intensities were $(1–2) \times 10^4$ particles/s with a small isobaric contamination from ^{20}F. A gas-filled degrader ion chamber served to attenuate the secondary beam down to energies of about 20 MeV. The detection system consisted of a multichannel plate detector at 0° and two annular double-sided Si strip detectors covering the angular range $\theta_{\rm lab} = 3.5°–21.8°$. With this setup, the fraction of the fusion cross sections, which is followed by the emission of at least one charged particle, could be measured. The extrapolation of these yields to the total fusion cross section is model dependent, and, thus, an improved setup is needed in order to answer the question as to whether fusion enhancement occurs in these neutron-rich systems.

H. Fusion reactions with ^{38}S beams

The measurement of the ^{38}S + ^{208}Pb system is a follow-up on earlier fusion studies of ^{32,38}S + ^{181}Ta (Zyromski *et al.*, 2001) to investigate the possible fusion enhancement of neutron-rich nuclei in heavy systems. The ^{38}S beams were obtained by fragmentation of 40–140 MeV/u ^{40}Ar beams followed by a slow-down in Al degraders resulting in a 10% energy resolution for the degraded beam (Loveland *et al.*, 2006). The beam intensities achieved in these experiments were in the range of 1000–4500 particles/s. The energies of the degraded ^{38}S particles were measured via time of flight with a ~100 cm long flight path giving a ~2.5 MeV energy resolution for the beam. Limited by the beam intensity fusion-fission cross sections down to about only 800 mb could be measured. The interaction barrier for the neutron-rich beam of ^{38}S obtained from these data is about 15 MeV smaller than the one measured for the stable ^{32}S, although with an uncertainty of 10 MeV. More typical values for similar neutron-rich systems (^{31}Al, ^{132}Sn) (Zyromski *et al.*, 2001; Liang *et al.*, 2003) are around 4–5 MeV. Improvements in beam intensities are needed to answer the question about a possible lowering of the barrier heights in these systems.

I. Fusion reactions with ^{132}Sn beams

Beams of the doubly closed-shell nucleus ^{132}Sn have been available from the ISOL facility at the HRIBF since 2003. These beams have excellent beam properties and intensities up to 2×10^5 particles/s (Liang *et al.*, 2007). The detector used for measurements of evaporation residues and fission fragments consisted of a multianode ionization chamber and multichannel plate system where the residues where identified by their time-of-flight and energy-loss signals, while the fission fragments were detected in coincidence in an annular double-sided Si strip detector (Liang *et al.*, 2007). The first fusion experiments with ^{132}Sn were performed in 2003 addressing the question whether the eight extra neutrons in this closed-shell nucleus would lead to a fusion enhancement in the system ^{64}Ni + ^{132}Sn (Liang *et al.*, 2003). While in this publication the system is shown to exhibit considerable fusion enhancement at low energies, later revisions that attributed this behavior to problems with the measurements of the incident beam intensities have corrected this behavior (Liang *et al.*, 2006) and the cross sections of all Sn isotopes when plotted in reduced coordinates fall on a universal curve, as shown in Fig. 11 of Liang *et al.* (2007). Since these pioneering experiments, several other fusion studies with neutron-rich Sn beams (^{126,127,128,132}Sn) have been performed (Kohley *et al.*, 2011; Kolata *et al.*, 2012; Liang *et al.*, 2012). Of particular interest to this review are the experiments for the systems ^{132}Sn + ^{40,48}Ca. Contrary to the systems ^{132}Sn + ^{58,64}Ni which, when plotted in reduced coordinates, exhibit a universal behavior, an increase in cross sections is observed for ^{132}Sn + ^{40}Ca similar to the one observed for the stable system ^{124}Sn + ^{40}Ca which was studied by Scarlassara *et al.* (2000). Although it was argued that this behavior might be caused by the large number of neutron transfer reactions with positive-Q values for the ^{124,132}Sn + ^{40}Ca systems, a comparison with the system ^{132}Sn + ^{58}Ni shows that for the Ni + Sn systems all fusion cross sections fall on the same universal curve. Later Rowley and Hagino (2010) attributed this behavior to the excitation of a strongly excited 3^- state in ^{40}Ca, which leads to a strong peak in the barrier distribution originating from the 3^- state in ^{40}Ca located at $E_{\rm c.m.}/V_C = 0.97$. The extent to which this enhances the fusion process is not so clear, however, since no strong sub-barrier fusion enhancement is observed in ^{40}Ca + ^{90}Zr.

VII. FUSION IN HEAVY SYSTEMS

In the light and medium mass systems that were discussed in the previous sections, it is relatively straightforward to identify events associated with complete fusion by measuring the evaporation residues that remain after the completely fused compound nucleus has released its angular momentum and excitation energy by evaporating neutrons, charged particles, and finally a cascade of γ rays. Alternatively, the characteristic γ rays emitted in the last steps of this decay chain can be measured to identify a fusion event.

In heavier systems, however, the excited compound system can also decay by fission and this decay channel becomes more prominent with the overall fissility Z^2/A of the fused system. In addition, the fission decay branch increases with excitation energy and angular momentum of the system. There is a caveat, however, with associating the observation of fission fragments with complete fusion in heavy systems because of the quasifission reaction that does not proceed via the compound nucleus stage. In the following, we discuss some of the properties of the fission fragment distributions that can reveal the presence of quasifission.

A. Fusion fission or quasifission?

The conclusion that fissionlike fragments do not always originate from compound fusion reactions was based on several different observations. First, it was recognized that the fission cross section exceeded the upper bound imposed by the existence of a stabilizing pocket in the ion-ion potential. Consequently, a fraction of the fission cross section must originate from partial waves that do not proceed through a compound nucleus. Also, the fission mass distribution in these cases was observed to be wider than expected on the basis of a

compound nucleus model. Heusch *et al.* (1978) measured the cross section for fissionlike processes in $^{132}Xe + ^{56}Fe$ at 5.73 MeV/u to 1040 mb, which corresponds to a maximum spin of $120\hbar$ (in the sharp cutoff model). This result agreed well with the expectation for the total fusion cross section from contemporary models (Bass, 1973, 1974; Błocki *et al.*, 1977), but they also realized that not all of these fragments come from an equilibrated compound nucleus, since the fission barrier disappears for spins larger than about $72\hbar$ according to the rotating liquid drop model of Cohen (1974). Therefore, the fissionlike processes originating from total angular momenta in the range $(72–120)\hbar$ must be characterized as "fission without a barrier," or what is now referred to as quasifission.

Concurrently, it was noted that the fission fragment anisotropy in heavy-ion induced fission substantially exceeds expectations based on the transition state model; see Back *et al.* (1981, 1983) and Back (1985). Subsequent studies of the two-dimensional mass-angle distribution of fission fragments clearly demonstrated that these fragments are the result of a dynamic process, in which the system evolves toward mass symmetry on a time scale that is commensurate with the rotational period of the complex (Bock *et al.*, 1982; Tōke *et al.*, 1985; Shen *et al.*, 1987). Further precise experiments have been conducted (Hinde *et al.*, 2008; du Rietz *et al.*, 2011; Hinde, du Rietz, and Dasgupta, 2011), which provide further constraints on our understanding of these complex processes that also play a critical role in attempts to synthesize heavy and superheavy nuclei via heavy-ion fusion processes.

Extensive studies of the fusion-evaporation cross sections for near-symmetric systems involving beams of ^{86}Kr, $^{90,96}Zr$, ^{100}Mo, ^{110}Pd, and ^{124}Sn impinging onto targets of $^{90,92,94,96}Zr$, $^{92,94,96,100}Mo$, ^{104}Ru, and ^{110}Pd in various combinations have been carried out using the SHIP separator at GSI by Sahm *et al.* (1984), Keller *et al.* (1986), Morawek *et al.* (1991), and Quint *et al.* (1993). These studies provided direct early evidence for the dynamical suppression of complete fusion in heavy systems and the findings from these and other experiments have been summarized by Schmidt *et al.* (1991).

Early theoretical work explaining the strong suppression of the complete fusion channel and the occurrence of quasifission emphasized the dynamical effects in the interaction between the two nuclei and led to the concept of an "extra push" being needed to achieve complete fusion (Świątecki, 1981, 1982; Bjørnholm and Świątecki, 1982; Błocki, Feldmeier, and Świątecki, 1986). Recently, much progress in the theoretical description of this process has been reported (Abe, Grégoire, and Delagrange, 1986; Fröbrich and Yu, 1988; Abe *et al.*, 2000; Błocki *et al.*, 2000; Giardina *et al.*, 2000; Abe, 2002). In addition, Zagrebaev and Greiner (2005, 2008, 2011) has further developed the dynamical calculations and proposed that the multinucleon transfer reaction can be used as an alternative method for populating nuclei in the region of the superheavy island of stability.

B. Evaporation residues: Discovery of new elements

In recent years, incontrovertible evidence for the synthesis of heavy elements formed via the so-called "hot fusion" reaction was found at Dubna and elsewhere [see, e.g., Oganessian *et al.* (2011), and references therein]. The formation of these elements occurs by several successive small branches of neutron evaporation in competition with fission. Clearly, some fusion-fission cross section must be present underneath the often much larger quasifission branch. From the fission measurements, one cannot obtain accurate estimates of this fusion-fission branch, but it is possible to set upper limits under the assumption that it follows the expected behavior in terms of width of the mass distribution and angular anisotropy.

One such analysis was carried out by Shen *et al.* (1987) for ^{238}U induced reactions on ^{26}Mg, ^{27}Al, ^{32}S, ^{35}Cl, $^{40,49}Ca$ and by Back *et al.* (1996) for reactions leading to the ^{214}Th system using three different entrance channels. In the latter study, it was found that only of the order of 10%–15% of the fissionlike cross section could come from fusion fission for the most mass symmetric system $^{60}Ni + ^{154}Sm$ although it could also be substantially smaller. A similar analysis of different entrance channels leading to the ^{220}Th compound system was later carried out by Hinde, Dasgupta, and Mukherjee (2002) giving similar results. Data analysis of the type mentioned above has not often been employed, but it may help provide some limits on fission barrier heights in systems populated in the hot fusion reactions that are successfully being used for the synthesis of the heaviest elements. Recently, Itkis *et al.* (2011) studied the systems $^{22}Ne + ^{249}Cf$, $^{26}Mg + ^{248}Cm$, $^{36}S + ^{238}U$, and $^{58}Fe + ^{208}Pb$ and Kozulin *et al.* (2010) studied the systems $^{64}Ni + ^{238}U$ and $^{48}Ca + ^{238}U$. In these studies strong suppression of the complete fusion reaction was found for $^{36}S + ^{238}U$, $^{58}Fe + ^{208}Pb$, $^{64}Ni + ^{238}U$, and $^{48}Ca + ^{238}U$.

C. Dynamical fusion theories

The early description of the heavy-ion dynamics that leads to the diversion of a large fraction of the reaction cross section into deep-inelastic and quasifission channels was based on dynamical calculations of the trajectories in a multidimensional space describing the geometrical shapes of the system from the initial approach of two, separated spherical nuclei through the mononucleus regime until either fusion or reseparation of two final fragments was observed (Świątecki, 1981, 1982; Bjørnholm and Świątecki, 1982; Błocki, Feldmeier, and Świątecki, 1986). While providing an overall understanding of the process, this description did not allow for a quantitative description of the probability of achieving complete fusion, i.e., formation of a CN inside the fission barrier. An alternative approach, based on the two-center shell model, considers the possibility that the approach of the interacting nuclei occurs on a time scale that is too short for the single particle structure to adjust adiabatically to the rapid changes in the ion-ion potential. This dissipative diabatic dynamics model (Lukasiak, Cassing, and Nörenberg, 1984) has been successful in reproducing the fusion cross sections for a number of reactions between near-symmetric $A \sim 100$ nuclei (Berdichevski *et al.*, 1989), but has not been applied to more recent experimental data.

A more refined description is called for, especially when the probability for complete fusion becomes very small. Recently, Świątecki (2003) suggested a somewhat different approach, in

which the probability for CN formation is composed of two factors, namely, (1) the probability for overcoming the ion-ion interaction barrier and (2) the probability of the system to diffuse from this, often mass asymmetric configuration, to the near spherical shape of the compound nucleus. The first step, referred to as "sticking," represents the cross section for overcoming the Coulomb barrier B and the second step, denoted "diffusion," represents the probability that the system reaches the CN stage. This step is described as a diffusion process in the landscape of the shape of the system. The probability for reaching the CN via diffusion depends crucially on this landscape, which changes substantially when going from relatively light to very heavy systems as illustrated in Fig. 31.

The cross section for complete fusion is given in Eq. (1). The cross section for evaporation residue formation involves, of course, an additional factor that accounts for the probability of survival against fission decay during the evaporation cascade. The cross section for evaporation residue formation becomes

$$\sigma_{\mathrm{CN}} = \pi\lambda\!\!\!^{-2} \sum_{L=0}^{\infty} (2L+1) T(L) P_{\mathrm{CN}}(L) P_{\mathrm{surv}}, \qquad (47)$$

where P_{surv} represents the probability for survival against fission in possibly multiple evaporation steps. This factor can be evaluated in a statistical model of the decay cascade assuming that the relevant parameters for this process are known.

This model was first used to describe the so-called "cold-fusion" reactions, namely, those involving ^{208}Pb and ^{209}Bi targets (Świątecki, Siwek-Wilczyńska, and Wilczyński, 2005). As shown in Fig. 32, this model accounts very well for the peak $1n$ cross sections for reactions using beams from

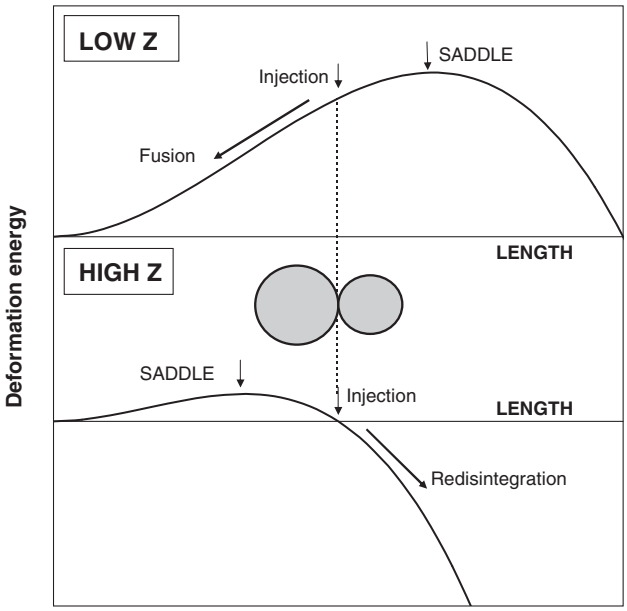

FIG. 31. The difference in the driving force of the ion-ion potential at the injection point for low Z (upper panel) and high Z (lower panel) systems.

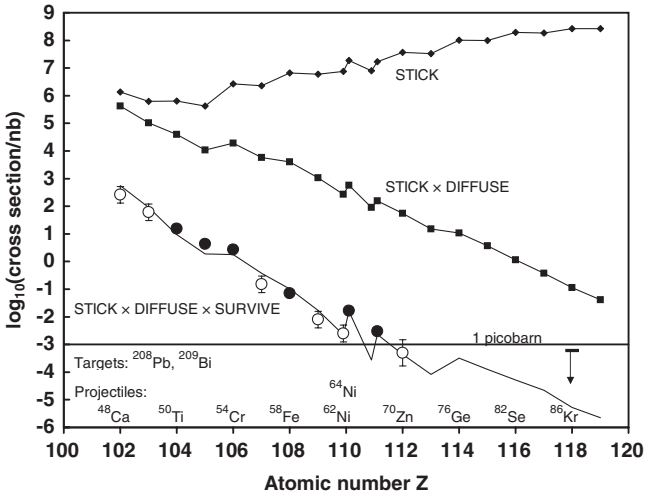

FIG. 32. Experimental peak cross sections for $1n$ evaporation residues in reactions on ^{208}Pb and ^{209}Bi targets, shown as solid and open circles, are compared to model calculations (sold curve); open circles are estimates since the peak may not have been reached. Model estimates for capture behind the interaction barrier (here labeled "stick") and compound nucleus formation (here labeled "stick x diffuse") are shown by diamond and square symbols, respectively.

^{48}Ca to ^{64}Ni, and it illustrates the fact that the P_{CN} drops precipitously with Z and A of the beam. Subsequently Cap and Siwek-Wilczyńska (2011) and Siwek-Wilczyńska *et al.* (2012) extended this description to include explicitly the L dependence [see Eq. (47)] and the multichance decay chains appropriate for hot fusion reactions that have been used successfully to synthesize the heaviest elements.

In a similar approach, Adamian *et al.* (1998) applied the dinuclear system concept to estimate the compound nucleus formation probability using nuclear diffusion to describe the dynamics in the mass equilibration degree of freedom [see also Adamian *et al.* (2012), and references therein].

In a parallel theoretical development, Arimoto *et al.* (1999) studied the synthesis of superheavy elements in a fluctuation-dissipation model that used the Smoluchowski equation as an approximation to the Kramers or Langevin diffusion equation to describe the fusion-fission dynamics. In this approach, the potential energy landscape includes contributions from temperature dependent shell and pairing effects in addition to the liquid droplet model energies. Initially, this approach was applied only to a hypothetical mass-symmetric entrance channel to illustrate the effects of fluctuation-dissipation dynamics to both the fusion process and fission-neutron evaporation competition in the later stages of the process. In a subsequent development (Arimoto *et al.*, 2012), this model was refined to include realistic entrance channels including deformed nuclei and the associated couped-channel effects. The fluctuation-dissipation dynamics is described using the Langevin equation and full dynamical development is followed to describe trajectories leading to fusion-fission and quasifission as well as a description of the final mass distributions of these processes. A more general review of stochastic approaches to describe nuclear dynamics was given by Abe, Grégoire, and Delagrange (1986). Additional work

exploring the Langevin equation for describing heavy-ion fusion, deep-inelastic scattering, and fission was summarized by Fröbrich and Gontchar (1998) and it has more recently been extensively applied by Zagrebaev and Greiner (2008) to calculate the fusion-evaporation cross section for synthesizing superheavy elements. They also emphasized the possibility of reaching the superheavy island of stability by multinulceon transfer reactions with actinide nuclei. See, e.g., Zagrebaev, Greiner, and Beck (2010) for a review of this theoretical approach.

VIII. SUMMARY AND OUTLOOK

The study of heavy-ion fusion continues to be an area of intense research. Recent work has provided insight into the reaction mechanism itself as well as the dependence on the shape and structure of the interacting nuclei. In this review, we summarized the most recent progress that includes the unanticipated sharp drop in the cross section at deep sub-barrier energies and the development and modification of theories to describe this phenomenon. Building on previous reviews, we provided updates on the present status of measurements of fusion excitation function over the range from deep sub-barrier to energies well above the interaction barrier and discussed the level to which these measurements can be understood in terms of current theories including refinements to the coupled-channels method as well as the most recent improvements to a TDHF description of heavy-ion fusion.

An important connection with the description of stellar evolution is discussed. The processes important for this occur at extremely low energies and the extension of experiments into these regions is clearly a challenge. The progress in both experimental measurements and the theoretical description in this range is discussed and proposals for analytical extrapolations into regions, that cannot be reached experimentally, are given.

The study of fusion reactions using radioactive beams is still in its infancy. The effects of loosely bound valence nucleons on the fusion process do not yet present a clear picture and further studies are needed to assess whether the fusion process is enhanced or hindered by using reaction partners with these properties.

It has been recognized for a long time that fusion between massive nuclei, needed to reach the heaviest elements, is impeded by dynamical effects associated with forming a compound system with a compact shape inside the fission barrier. Several approaches to include these effects into the theoretical description have been made. A recent model, based on a diffusion description of the probability to reach the near-spherical compound stage from the dinuclear shape of the system captured inside the interaction barrier, appears to provide a good description of many systems used to synthesize superheavy elements. Future experiments will show whether this approach also has predictive power.

In the future, it is expected that the study of fusion using radioactive beams will become an important focus as higher intensities become available from new facilities. This will enable a more detailed study of a fusion excitation function to assess the effects of loosely bound nucleons in such systems. With improved experimental techniques, further exploration of the fusion hindrance phenomenon as well as a further push into the Gamow window region for astrophysical fusion processes is anticipated. On the theoretical side, one may expect that further developments of both the coupled-channels and the TDHF approaches will attain a global description of this process. As fusion of the heaviest systems is strongly influenced by the dynamics of the process, it is expected that a fundamental theory for fusion in this region must also provide a description of the competition between complete fusion and various two-body, i.e., deep-inelastic or quasifission, exit channels.

ACKNOWLEDGMENTS

We acknowledge B. Kay's suggestions for improving the manuscript as well as illuminating discussions with P. R. S. Gomes, A. Navin, and Yu. E. Penionzhkevich. This work was supported by the U.S. Department of Energy, Office of Nuclear Physics, under Contract No. DE-AC02-06CH11357.

REFERENCES

Abe, Y., 2002, Eur. Phys. J. A **13**, 143.
Abe, Y., D. Boilley, B. Giraud, and T. Wada, 2000, Phys. Rev. E **61**, 1125.
Abe, Y., C. Grégoire, and H. Delagrange, 1986, J. Phys. **47**, 329.
Adamian, G. G., N. V. Antonenko, and W. Scheid, 2012, in *Clusters in Nuclei 2*, edited by C. Beck, Lecture Notes in Physics (Springer-Verlag, Berlin), Vol. 848, p. 165.
Adamian, G. G., N. V. Antonenko, W. Scheid, and V. V. Volkov, 1998, Nucl. Phys. **A633**, 409.
Adelberger, E., *et al.*, 2011, Rev. Mod. Phys. **83**, 195.
Aguilera, E. F., J. J. Kolata, and R. J. Tighe, 1995, Phys. Rev. C **52**, 3103.
Aguilera, E. F., E. Martinez-Quiroz, P. Rosales, J. J. Kolata, P. A. DeYoung, G. F. Peaslee, P. Mears, C. Guess, F. D. Becchetti, J. H. Lupton, and Yu Chen, 2009, Phys. Rev. C **80**,044605.
Aguilera, E. F., *et al.*, 2006, Phys. Rev. C **73**, 064601.
Aguilera, E. F., *et al.*, 2009, Phys. Rev. C **79**, 021601.
Aguilera, E. F., *et al.*, 2011, Phys. Rev. Lett. **107**,092701.
Akyüz, Ö., and A. Winther, 1981, in *Proceedings of the Enrico Fermi International School of Physics, 1979*, course on "Nuclear Structure and Heavy Ion Reactions," edited by R. A. Broglia *et al.* (North-Holland, Amsterdam).
Alcorta, M., *et al.*, 2011, Phys. Rev. Lett. **106**, 172701.
Aljuwair, H. A., R. J. Ledoux, M. Beckerman, S. B. Gazes, J. Wiggins, E. R. Cosman, R. R. Betts, S. Saini, and Ole Hansen, 1984, Phys. Rev. C **30**, 1223.
Al-Khalili, J. S., 2004, Lect. Notes Phys. **651**, 77.
Almqvist, E., D. A. Bromley, J. A. Kuehner, and B. Whalen, 1963, Phys. Rev. **130**, 1140.
Arimoto, Y., K. Hagino, K. Nishio, and S. Chiba, 2012, Phys. Rev. C **85**, 044614.
Arimoto, Y., T. Wada, M. Otha, and Y. Abe, 1999, Phys. Rev. C **59**, 796.
Astier, A., 2012, Rep. Prog. Phys. **75**, 116901.
Back, B. B., 1985, Phys. Rev. C **31**, 2104.
Back, B. B., R. R. Betts, K. Cassidy, B. G. Glagola, J. E. Gindler, L. E. Glendenin, and B. Wilkins, 1983, Phys. Rev. Lett. **50**, 818.

Back, B. B., H.-G. Clerc, R. R. Betts, B. G. Glagola, and B. D. Wilkins, 1981, Phys. Rev. Lett. **46**, 1068.
Back, B. B., P. B. Fernandez, B. G. Glagola, D. Henderson, S. Kaufman, J. G. Keller, S. J. Sanders, F. Videbaek, T. F. Wang, and B. D. Wilkins, 1996, Phys. Rev. C **53**, 1734.
Balantekin, A. B., and N. Takigawa, 1998, Rev. Mod. Phys., **70**, 77.
Barnes, C. A., S. Trentalange, and S. C. Wu, 1985, *Treatise on Heavy Ion Science*, edited by D. A. Bromley (Plenum, New York), Vol. 6, p. 3.
Barron-Palos, L., *et al.*, 2006, Nucl. Phys. **A779**, 318.
Bass, R., 1973, Phys. Lett. **47B**, 139.
Bass, R., 1974, Nucl. Phys. **A231**, 45.
Basunia, M. S., H. A. Shugart, A. R. Smith, and E. B. Norman, 2007, Phys. Rev. C **75**, 015802.
Beard, M., A. V. Afanasjev, L. C. Chamon, L. R. Gasques, M. Wiescher, and D. G. Yakovlev, 2010, At. Data Nucl. Data Tables **96**, 541.
Becchetti, F., *et al.*, 1991, Nucl. Instrum. Methods Phys. Res., Sect. B **56–57**, 554.
Beck, C., N. Keeley, and A. Diaz-Torres, 2007, Phys. Rev. C **75**, 054605.
Beck, C., *et al.*, 2003, Phys. Rev. C **67**, 054602.
Becker, H. W., K. U. Kettner, C. Rolfs, and H. P. Trautvetter, 1981, Z. Phys. A **303**, 305.
Beckerman, M., 1985, Phys. Rep. **129**, 145.
Beckerman, M., 1988, Rep. Prog. Phys. **51**, 1047.
Beckerman, M., M. Salomaa, A. Sperduto, H. Enge, J. Ball, A. DiRienzo, S. Gazes, Yan Chen, J. D. Molitoris, and Mao Nai-feng, 1980, Phys. Rev. Lett. **45**, 1472.
Beckerman, M., M. Salomaa, A. Sperduto, J. D. Molitoris, and A. DiRienzo, 1982, Phys. Rev. C **25**, 837.
Benjamim, E. A., *et al.*, 2007, Phys. Lett. B **647**, 30.
Berdichevski, D., W. Lukasiak, W. Nörenberg, and P. Rozmej, 1989, Nucl. Phys. **A502**, 395.
Bertsch, G., W. Borysowicz, H. McManus, and W. G. Love, 1977, Nucl. Phys. **A284**, 399.
Birkelund, J. R., and J. R. Huizenga, 1983, Annu. Rev. Nucl. Part. Sci. **33**, 265.
Birkelund, J. R., L. E. Tubbs, J. R. Huizenga, J. N. De, and D. Sperber, 1979, Phys. Rep. **56**, 107.
Bjørnholm, S., and W. J. Świątecki, 1982, Nucl. Phys. **A391** 471.
Błocki, J., H. Feldmeier, and W. J. Świątecki, 1986, Nucl. Phys. **A459**, 145.
Błocki, J., O. Mazonka, J. Wilczyński, Z. Sosin, and A. Wieloch, 2000, Acta Phys. Pol. B **31**, 1513.
Błocki, J., J. Randrup, W. J. Świątecki, and C. F. Tsang, 1977, Ann. Phys. (N.Y.) **105**, 427.
Bock, R., *et al.*, 1982, Nucl. Phys. **A388**, 334.
Bravo, E., and G. Martinez-Pinedo, 2012, Phys. Rev. C **85**, 055805.
Brink, D. M., 2004, Prog. Theor. Phys. Suppl., **154**, 268.
Broglia, R. A., C. H. Dasso, and S. Landowne, 1985, Phys. Rev. C **32**, 1426.
Broglia, R. A., C. H. Dasso, S. Landowne, and A. Winther, 1983, Phys. Rev. C **27**, 2433.
Broglia, R. A., and A. Winther, 1991, *Frontiers in Physics Lecture Notes Series: Heavy-ion Reactions*, Vol. 84 (Addison-Wesley, Redwood City, CA).
Burbidge, E. M., G. Burbidge, W. Fowler, and F. Hoyle, 1957, Rev. Mod. Phys. **29**, 547.
Canto, L. F., P. R. S. Gomes, R. Donangelo, and M. S. Hussein, 2006, Phys. Rep. **424**, 1.
Canto, L. F., P. R. S. Gomes, J. Lubian, L. C. Chamon, and E. Crema, 2009, Nucl. Phys. **A821**, 51.
Cap, T., and K. Siwek-Wilczyńska, 2011, Phys. Rev. C **83**, 054602.
Caughlan, G. R., and W. A. Fowler, 1988, At. Data Nucl. Data Tables **40**, 283.
Chamon, L. C., M. S. Hussein, and L. F. Canto, 2007, Braz. J. Phys. **37**, 1177.
Christensen, P. R., Z. E. Switkowski, and R. A. Dayras, 1977, Nucl. Phys. **A280**, 189.
Cogneau, M., P. Decrock, M. Gaelens, D. Labar, P. Leleux, M. Loiselet, and G. Ryckewaert, 1999, Nucl. Instrum. Methods Phys. Res., Sect. A **420**, 489.
Cohen, S., 1974, Ann. Phys. (N.Y.) **82**, 557.
Corradi, L., G. Pollarolo, and S. Szilner, 2009, J. Phys. G **36**, 113101.
Costantini, H., *et al.*, 2008, Nucl. Phys. **A814**, 144.
Cujec, B., and C. A. Barnes, 1976, Nucl. Phys. **A266**, 461.
Cumming, A., and L. Bildsten, 2001, Astrophys. J. **559**, L127.
Dasgupta, M., D. J. Hinde, A. Diaz-Torres, B. Bouriquet, Catherine I. Low, G. J. Milburn, and J. O. Newton, 2007, Phys. Rev. Lett. **99**, 192701.
Dasgupta, M., D. J. Hinde, N. Rowley, and A. M. Stefanini, 1998, Annu. Rev. Nucl. Part. Sci. **48**, 401.
Dasgupta, M., A. Navin, Y. K. Agarwal, C. V. K. Baba, H. C. Jain, M. L. Jhingan, and A. Roy, 1992, Nucl. Phys. **A539**, 351.
Dasgupta, M., *et al.*, 1999, Phys. Rev. Lett. **82**, 1395.
Dasgupta, M., *et al.*, 2004, Phys. Rev. C **70**, 024606.
Dasmahaptra, Binay, Bibiana Čujec, and Fouad Lahlou, 1982, Nucl. Phys. **A384**, 257.
Dasmahapatra, B., B. Cujec, and F. Lahlou, 1983a, Can. J. Phys. **61**, 657.
Dasmahapatra, B., B. Cujec, and F. Lahlou, 1983b, Nucl. Phys. **A394**, 301.
Dasso, C. H., and S. Landowne, 1987a, Phys. Lett. B **183**, 141.
Dasso, C. H., and S. Landowne, 1987b, Comput. Phys. Commun. **46**, 187.
Dasso, C. H., S. Landowne, and A. Winther, 1983, Nucl. Phys. **A407**, 221.
Dasso, C. H., and G. Pollarolo, 1985, Phys. Lett. **155B**, 223.
Dasso, C. H., and A. Vitturi, 1986, Phys. Rev. C **34**, 743.
Dasso, C. H., and G. Pollarolo, 2003, Phys. Rev. C **68**, 054604.
Davids, C. N., and J. Larson, 1989, Nucl. Instrum. Methods Phys. Res., Sect. B **40–41**, 1224.
Davids, C. N., and J. Larson, 1994 Nucl. Instrum. Methods Phys. Res., Sect. A **345**, 528.
Davis, C. A., 1981 Phys. Rev. C **24**, 1891.
Dayras, J., R. G. Stokstad, Z. E. Switkowski, and R. M. Wieland, 1976, Nucl. Phys. **A265**, 153.
Denisov, V. Yu., and N. A. Pilipenko, 2010, Phys. Rev. C **81**, 025805.
Diaz-Torres, A., 2010a, Phys. Rev. C **82**, 054617.
Diaz-Torres, A., 2010b, J. Phys. G **37**, 075109.
Diaz-Torres, A., 2011, Comput. Phys. Commun., **182**, 1100.
Diaz-Torres, A., L. R. Gasques, and M. Wiescher, 2007, Phys. Lett. B **652**, 255.
Diaz-Torres, A., D. J. Hinde, J. A. Tostevin, M. Dasgupta, and L. R. Gasques, 2007, Phys. Rev. Lett. **98**, 152701.
Diaz-Torres, A., I. J. Thompson, and C. Beck, 2003, Phys. Rev. C **68**, 044607.
Diaz-Torres, A., and M. Wiescher, 2012, AIP Conf. Proc. **1491**, 273, and references therein.
du Rietz, R., D. J. Hinde, M. Dasgupta, R. G. Thomas, L. R. Gasques, M. Evers, N. Lobanov, and A. Wakhle, 2011, Phys. Rev. Lett. **106**, 052701.
Esbensen, H., 1981, Nucl. Phys. **A352**, 147.
Esbensen, H., 2003, Phys. Rev. C **68**, 034604.

Esbensen, H., 2008, Phys. Rev. C **77**, 054608.
Esbensen, H., 2012, Phys. Rev. C **85**, 064611.
Esbensen, H., and B. B. Back, 1996, Phys. Rev. C **54**, 3109.
Esbensen, H., and C. L. Jiang, 2009, Phys. Rev. C **79**, 064619.
Esbensen, H., C. L. Jiang, and K. E. Rehm, 1998, Phys. Rev. C **57**, 2401.
Esbensen, H., C. L. Jiang, and A. M. Stefanini, 2010, Phys. Rev. C **82**, 054621.
Esbensen, H., and S. Landowne, 1987, Phys. Rev. C **35**, 2090.
Esbensen, H., and S. Landowne, 1989, Nucl. Phys. **A492**, 473.
Esbensen, H., S. Landowne, and C. Price, 1987a, Phys. Rev. C **36**, 1216.
Esbensen, H., S. Landowne, and C. Price, 1987b, Phys. Rev. C **36**, 2359.
Esbensen, H., and Ş. Mişicu, 2007, Phys. Rev. C **76**, 054609.
Esbensen, H., X. Tang, and C. L. Jiang, 2011, Phys. Rev. C **84**, 064613.
Evers, M., M. Dasgupta, D. J. Hinde, L. R. Gasques, M. L. Brown, R. Rafiei, and R. G. Thomas, 2008, Phys. Rev. C **78**, 034614.
Evers, M., M. Dasgupta, D. J. Hinde, D. H. Luong, R. Rafiei, R. du Rietz, and C. Simenel, 2011, Phys. Rev. C **84**, 054614.
Fang, X., *et al.*, 2013, J. Phys. Conf. Ser. **420**, 012151.
Fernandez-Niello, J., C. H. Dasso, and S. Landowne, 1989, Comput. Phys. Commun. **54**, 409.
Fomichev, A. S., I. David, Z. Dlouhy, S. M. Lukyanov, Yu. Ts. Oganessian, Yu. E. Penionzkevich, V. P. Perelygin, N. K. Skobelev, O. B. Tarasov, and R. Wolski, 1995, Z. Phys. A **351**, 129.
Fomichev, A. S., *et al.*, 2009, Eur. Phys. J. A **42**, 465.
Fowler, W. A., G. R. Caughlan, and B. A. Zimmerman, 1975, Annu. Rev. Astron. Astrophys. **13**, 69.
Fröbrich, 1984, Phys. Rep. **116**, 337.
Fröbrich, P., and I. I. Gontchar, 1998, Phys. Rep. **292**, 131.
Fröbrich, P., and S. Y. Yu, 1988, Nucl. Phys. **A477**, 143.
FUSION97, 1997, J. Phys. G **23**, 1157.
FUSION03, 2004, Prog. Theor. Phys. Suppl. **154**, 1.
FUSION06, 2006, *AIP Conf. Ser.* **853**, 1.
FUSION08, 2008, *AIP Conf. Ser.* **1098**, 1.
FUSION11, 2011, *Proceedings of "Tunneling through barriers,"* St. Malo, France, *EPJ Web of Conf.*, edited by A. Navin, H. Goutte, D. Lacroix, M. Rejmund, and C. Schmitt (European Physical Journal), Vol. **17** [http://www.epj-conferences.org/site].
Gasques, L. R., A. V. Afanasjev, E. F. Aguilera, M. Beard, L. C. Chamon, P. Ring, M. Wiescher, and D. G. Yakovlev, 2005, Phys. Rev. C **72**, 025806.
Gasques, L. R., E. F. Brown, A. Chieffi, C. L. Jiang, M. Limongi, C. Rolfs, M. Wiescher, and D. G. Yakovlev, 2007, Phys. Rev. C **76**, 035802.
Gasques, L. R., M. Evers, D. J. Hinde, M. Dasgupta, P. R. S. Gomes, R. M. Anjos, M. L. Brown, M. D. Rodríguez, R. G. Thomas, and K. Hagino, 2007, Phys. Rev. C **76**, 024612.
Ghodsi, O. N., and V. Zanganeh, 2010, Nucl. Phys. **A846**, 40.
Giardina, G., S. Hofmann, A. J. Muminov, and A. K. Nasirov, 2000, Eur. Phys. J. A **8**, 205.
Giraud, B. G., S. Karataglidis, K. Amos, and B. A. Robson, 2004, Phys. Rev. C **69**, 064613.
Gobbi, A., R. Wieland, L. Chua, D. Shapira, and D. A. Bromley, 1973, Phys. Rev. C **7**, 30.
Gomes, P. R. S., R. Linares, J. Lubian, C. C. Lopes, E. N. Cardozo, B. H. F. Pereira, and I. Padron, 2011, Phys. Rev. C **84**, 014615.
Gomes, P. R. S., J. Lubian, I. Padron, and R. M. Anjos, 2005, Phys. Rev. C **71**, 017601.
Gomes, P. R. S., *et al.*, 2004, Phys. Lett. B **601**, 20.
Gross, D. H. E., and H. Kalinowski, 1978, Phys. Rep. **45C**, 175.
Hagino, K., and N. Rowley, 2004, Phys. Rev. C **69**, 054610.
Hagino, K., N. Rowley, and M. Dasgupta, 2003, Phys. Rev. C **67**, 054603.
Hagino, K., N. Rowley, and A. T. Kruppa, 1999, Comput. Phys. Commun. **123**, 143.
Hagino, K., and N. Takigawa, 2012, Prog. Theor. Phys. **128**, 1001.
Hagino, K., N. Takigawa, M. Dasgupta, D. J. Hinde, and J. R. Leigh, 1997a, Phys. Rev. C **55**, 276.
Hagino, K., N. Takigawa, M. Dasgupta, D. J. Hinde, and J. R. Leigh, 1997b, Phys. Rev. Lett. **79**, 2014.
Hanappe, F., M. Lefort, C. Ngô, J. Péter, and B. Tamain, 1974, Phys. Rev. Lett. **32**, 738.
Harss, B., *et al.*, 2000, Rev. Sci. Instrum. **71**, 380.
Heusch, B., C. Volant, H. Freiesleben, R. P. Chestnut, K. D. Hildenbrand, F. Pühlhofer, W. F. W. Schneider, B. Kohlmeyer, and W Pfeffer, 1978, Z. Phys. A **288**, 391.
High, M. D., and B. Cujec, 1976, Nucl. Phys. **A259**, 513.
High, M. D., and B. Cujec, 1977, Nucl. Phys. **A282**, 181.
Hillebrandt, W., and J. C. Niemeyer, 2000, Annu. Rev. Astron. Astrophys. **38**, 191.
Hinde, D. J., A. C. Berriman, M. Dasgupta, J. R. Leigh, J. C. Mein, C. R. Morton, and J. O. Newton, 1999, Phys. Rev. C **60**, 054602.
Hinde, D. J., and M. Dasgupta, 2010, Phys. Rev. C **81**, 064611.
Hinde, D. J., M. Dasgupta, B. Fulton, C. Morton, R. Wooliscroft, A. Berriman, and K. Hagino, 2002, Phys. Rev. Lett. **89**, 272701.
Hinde, D. J., M. Dasgupta, and A. Mukherjee, 2002, Phys. Rev. Lett. **89**, 282701.
Hinde, D. J., R. du Rietz, and M. Dasgupta, 2011, Eur. Phys. J. Web Conf. **17**, 04001.
Hinde, D. J., R. G. Thomas, R. du Rietz, A. Diaz-Torres, M. Dasgupta, M. L. Brown, M. Evers, L. R. Gasques, R. Rafiei, and M. D. Rodriguez, 2008, Phys. Rev. Lett. **100**, 202701.
Hofmann, S., F. P. Hessberger, V. Ninov, P. Armbruster, G. Munzenberg, C. Stodel, A. G. Popeko, A. V. Yeremin, S. Saro, and M. Leino, 1997, Z. Phys. A **358**, 377.
Horowitz, C. J., and D. K. Berry, 2009, Phys. Rev. C **79**, 065803.
Hulke, G., C. Rolfs, and H. P. Trautvetter, 1980, Z. Phys. A **297**, 161.
Ichikawa, T., K. Hagino, and A. Iwamoto, 2007, Phys. Rev. C **75**, 057603.
Ichikawa, T., K. Hagino, and A. Iwamoto, 2009, Phys. Rev. Lett. **103**, 202701.
Itkis, I. M., *et al.*, 2011, Phys. Rev. C **83**, 064613.
Ito, M., K. Yabana, T. Nakatsukasa, and M. Ueda, 2006, Phys. Lett. B **637**, 53.
Ito, M., K. Yabana, T. Nakatsukasa, and M. Ueda, 2007, Nucl. Phys. **A787**, 267.
Jiang, C. L., 2011, *EPJ Web of Conf.* **17**, 01001.
Jiang, C. L., B. B. Back, H. Esbensen, R. V. F. Janssens, and K. E. Rehm, 2006, Phys. Rev. C **73**, 014613.
Jiang, C. L., B. B. Back, H. Esbensen, R. V. F. Janssens, K. E. Rehm, and R. Charity, 2013, Phys. Rev. Lett. **110**, 72701.
Jiang, C. L., H. Esbensen, B. B. Back, R. V. F. Janssens, and K. E. Rehm, 2004, Phys. Rev. C **69**, 014604.
Jiang, C. L., K. E. Rehm, B. B. Back, and R. V. F. Janssens, 2007, Phys. Rev. C **75**, 015803.
Jiang, C. L., K. E. Rehm, B. B. Back, and R. V. F. Janssens, 2009, Phys. Rev. C **79**, 044601.
Jiang, C. L., K. E. Rehm, H. Esbensen, D. J. Blumenthal, B. Crowell, J. Gehring, B. Glagola, J. P. Schiffer, and A. H. Wuosmaa, 1998, Phys. Rev. C **57**, 2393.
Jiang, C. L., *et al.*, 2002, Phys. Rev. Lett. **89**, 052701.
Jiang, C. L., *et al.*, 2003, Phys. Rev. Lett. **91**, 229202.
Jiang, C. L., *et al.*, 2004, Phys. Rev. Lett. **93**, 012701.

Jiang, C. L., *et al.*, 2005, Phys. Rev. C **71**, 044613.
Jiang, C. L., *et al.*, 2006, Phys. Lett. B **640**, 18.
Jiang, C. L., *et al.*, 2008, Phys. Rev. C **78**, 017601.
Jiang, C. L., *et al.*, 2010a, Phys. Rev. C **81**, 024611.
Jiang, C. L., *et al.*, 2010b, Phys. Rev. C **82**, 041601R.
Jiang, C. L., *et al.*, 2011, J. Phys. Conf. Ser. **312**, 042011.
Jiang, C. L., *et al.*, 2012, Nucl. Instrum. Methods Phys. Res., Sect. A **682**, 12.
Jiang, C. L., *et al.*, 2013, J. Phys. Conf. Ser. **420**, 012120.
Kalita, K., *et al.*, 2006, Phys. Rev. C **73**, 024609.
Kalkal, S., *et al.*, 2010, Phys. Rev. C **81**, 044610.
Keeley, N., J. S. Lilley, J. X. Wei, M. Dasgupta, D. J. Hinde, J. R. Leigh, J. C. Mein, C. R. Morton, H. Timmers, and N. Rowley, 1998, Nucl. Phys. **A628**, 1.
Keeley, N., R. Raabe, N. Alamanos, and J. L. Sida, 2007, Prog. Part. Nucl. Phys. **59**, 579.
Keller, J. G., K.-H. Schmidt, F. P. Hessberger, G. Münzenberg, W. Reisdorf, H.-G. Clerc, and C.-C. Sahm, 1986, Nucl. Phys. **A452**, 173.
Keser, R., A. S. Umar, and V. E. Oberacker, 2012, Phys. Rev. C **85**, 044606.
Kettner, K. U., 1980, Z. Phys. A **298**, 65.
Kofoed-Hansen, O., and K. O. Nielsen, 1951, Phys. Rev. **82**, 96 [http://prola.aps.org/pdf/PR/v82/i1/p96_2].
Kohley, Z., J. F. Liang, D. Shapira, C. J. Gross, R. L. Varner, J. M. Allmond, J. J. Kolata, P. E. Mueller, and A. Roberts, 2013, Phys. Rev. C **87**, 064612.
Kohley, Z., *et al.*, 2011, Phys. Rev. Lett. **107**, 202701.
Kolata, J. J., *et al.*, 1998, Phys. Rev. C **57**, R6.
Kolata, J. J., *et al.*, 2012, Phys. Rev. C **85**, 054603.
Kondo, Y., D. A. Bromley, and Y. Abe, 1980, Phys. Rev. C **22**, 1068.
Kovar, D. G., *et al.*, 1979, Phys. Rev. C **20**, 1305.
Kozulin, E. M., *et al.*, 2010, Phys. Lett. B **686** 227.
Krappe, H. J., J. R. Nix, and A. J. Sierk, 1979, Phys. Rev. C **20**, 992.
Kuzyakin, R. A., V. V. Sargsyan, G. G. Adamian, and N. V. Antonenko, 2012, Phys. At. Nucl., **75**, 439.
Lemasson, A., *et al.*, 2009, Phys. Rev. Lett. **103**, 232701.
Lemasson, A., *et al.*, 2010, Phys. Rev. C **82**, 044617.
Liang, J. F., C. J. Gross, Z. Kohley, D. Shapira, R. L. Varner, J. M. Allmond, A. L. Caraley, K. Lagergren, and P. E. Mueller, 2012, Phys. Rev. C **85**, 031601.
Liang, J. F., and C. Signorini, 2005, Int. J. Mod. Phys. E **14**, 1121.
Liang, J. F., *et al.*, 2003, Phys. Rev. Lett. **91**, 152701.
Liang, J. F., *et al.*, 2006, Phys. Rev. Lett. **96**, 29903.
Liang, J. F., *et al.*, 2007, Phys. Rev. C **75**, 054607.
Limongi, M., and A. Chieffi, 2006, Astrophys. J. **647**, 483.
Lin, C. J., 2003, Phys. Rev. Lett. **91**, 229201.
Loveland, W., D. Peterson, A. M. Vinodkumar, P. H. Sprunger, D. Shapira, J. F. Liang, G. A. Souliotis, D. J. Morrissey, and P. Lofy, 2006, Phys. Rev. C **74**, 044607.
Loveland, W., *et al.*, 2006, Phys. Rev. C **74**, 064609.
Loveland, W., 2011, Eur. Phys. J. Web Conf. **17**, 02003.
Lukasiak, A, W. Cassing, and W. Nörenberg, 1984, Nucl. Phys. **A426**, 181.
Lukyanov, S. M., *et al.*, 2009, Phys. Lett. B **670**, 321.
MacFarlane, M. H., and S. C. Pieper, 1978, Code Ptolemy: Argonne Laboratory Report No. ANL-76-11.
Mazarakis, M., and W. E. Stephens, 1973, Phys. Rev. C **7**, 1280.
Mişicu, Ş., and H. Esbensen, 2006, Phys. Rev. Lett. **96**, 112701.
Mişicu, Ş., and H. Esbensen, 2007, Phys. Rev. C **75**, 034606.
Mitsuoka, S., H. Ikezoe, K. Nishio, K. Tsuruta, S. C. Jeong, and Y. Watanabe, 2007, Phys. Rev. Lett. **99**, 182701.
Montagnoli, G., A. M. Stefanini, L. Corradi, S. Courtin, E. Fioretto, F. Haas, D. Lebhertz, F. Scarlassara, R. Silvestri, and S. Szilner, 2010, Phys. Rev. C **82**, 064609.
Montagnoli, G., *et al.*, 2012, Phys. Rev. C **85**, 024607.
Montagnoli, G., *et al.*, 2013, Phys. Rev. C **87**, 014611.
Montanari, D., *et al.*, 2011, Phys. Rev. C **84**, 054613.
Morawek, W., *et al.*, 1991, Z. Phys. A **341**, 75.
Morsad, A., J. J. Kolata, R. J. Tighe, and X. J. Kong, 1990, Phys. Rev. C **41**, 988.
Morton, C. R., A. C. Berriman, M. Dasgupta, D. J. Hinde, J. O. Newton, K. Hagino, and I. J. Thompson, 1999, Phys. Rev. C **60** 044608.
Mueller, A. C., and B. M. Sherrill, 1993, Annu. Rev. Nucl. Part. Sci. **43**, 529.
Mukherjee, A., M. Dasgupta, D. J. Hinde, K. Hagino, J. R. Leigh, J. C. Mein, C. R. Morton, J. O. Newton, and H. Timmers, 2002, Phys. Rev. C **66**, 34607.
Mukherjee, A., D. J. Hinde, M. Dasgupta, K. Hagino, J. O. Newton, and R. D. Butt, 2007, Phys. Rev. C **75**, 044608.
Myers, W. D., and W. J. Świątecki, 2000, Phys. Rev. C **62**, 044610.
Navin, A., *et al.*, 2004, Phys. Rev. C **70**, 044601.
Negele, J. W., 1982, Rev. Mod. Phys. **54**, 913.
Newton, J. O., R. D. Butt, M. Dasgupta, D. J. Hinde, I. I. Gontchar, C. R. Morton, and K. Hagino, 2004a, Phys. Lett. B **586**, 219.
Newton, J. O., R. D. Butt, M. Dasgupta, D. J. Hinde, I. I. Gontchar, and C. R. Morton, 2004b, Phys. Rev. C **70**, 024605.
Newton, J. O., C. R. Morton, M. Dasgupta, J. R. Leigh, J. C. Mein, D. J. Hinde, H. Timmers, and K. Hagino, 2001, Phys. Rev. C **64**, 064608.
NNDC (National Nuclear Data Center), 2013, http://www.nndc.bnl.gov/.
Notani, M., *et al.*, 2012, Phys. Rev. C **85**, 014607.
Oganessian, Yu. Ts., *et al.*, 2011, Phys. Rev. C **83**, 054315.
Pakout, A., *et al.*, 2013, Phys. Rev. C **87**, 014619.
Patterson, J. R., B. N. Nagorcka, G. D. Symoms, and W. m. Zuk, 1971, Nucl. Phys. **A165**, 545.
Patterson, J. R., H. Winkler, and C. S. Zaidins, 1969, Astrophys. J. **157**, 367.
Penionzhkevich, Yu. E., V. I. Zagrebaev, S. M. Lukyanov, and R. Kalpakchieva, 2006, Phys. Rev. Lett. **96**, 162701.
Penionzhkevich, Yu. E., *et al.*, 2007, Eur. Phys. J. A **31**, 185.
Piasecki, E., *et al.*, 2009, Phys. Rev. C **80**, 054613.
Piasecki, E., *et al.*, 2012, Phys. Rev. C **85**, 054608.
Pignatari, M., *et al.*, 2013, Astrophys. J. **762**, 31.
Poffe, N., N. Rowley, and R. Lindsay, 1983, Nucl. Phys. **A410**, 498.
Pollarolo, G., 2008, Phys. Rev. Lett. **100**, 252701.
Quint, A. B., *et al.*, 1993, Z. Phys. A **346**, 119.
Raabe, R., C. Angulo, J. L. Charvet, C. Jouanne, L. Nalpas, P. Figuera, D. Pierroutsakou, M. Romoli, and J. Sida, 2006, Phys. Rev. C **74**, 044606.
Raabe, R., *et al.*, 2004, Nature (London) **431**, 823.
Rafiei, R., 2011, Nucl. Instrum. Methods Phys. Res., Sect. A **631**, 12.
Rafiei, R., R. du Rietz, D. H. Luong, D. J. Hinde, M. Dasgupta, M. Evers, and A. Diaz-Torres, 2010, Phys. Rev. C **81**, 024601.
Ramamurthy, V. S., A. K. Mohanty, S. K. Kataria, and G. Rangarajan, 1990, Phys. Rev. C **41**, 2702.
Ravn, H., 1979, Phys. Rep. **54**, 201.
Rehm, K. E., 1991, Annu. Rev. Nucl. Part. Sci. **41**, 429.
Rehm, K. E., *et al.*, 1998, Phys. Rev. Lett. **81**, 3341.
Reisdorf, W., 1994, J. Phys. G **20**, 1297.

Rosales, P., *et al.*, 2003, Rev. Mex. Fis. **49**, 88.
Rowley, N., and K. Hagino, 2010, Nucl. Phys. A **834**, 110c.
Rowley, N., G. R. Satchler, and P. H. Stelson, 1991, Phys. Lett. B **254**, 25.
Rudolph, M. J., *et al.*, 2012, Phys. Rev. C **85**, 024605.
Sahm, C.-C., H.-G. Clerc, K.-H. Schmidt, W. Reisdorf, P. Armbruster, F. P. Heßberger, J. G. Keller, G. Münzenberg, and D. Vermeulen, 1984, Z. Phys. A **319**, 113.
Sakuragi, Y., M. Yahiro, and M. Kamimura, 1986, Prog. Theor. Phys. Suppl. **89**, 136.
Santra, S., 2001, Phys. Rev. C **64**, 024602.
Sargsyan, V. V., *et al.*, 2010, Eur. Phys. J. A **45**, 125.
Sargsyan, V. V., *et al.*, 2011, arXiv:1006.2705v1.
Sastry, S. V. S., S. Kailas, A. K. Mohanty, and A. Saxena, 2005, Pramana J. Phys. **64**, 47.
Scarlassara, F., S. Beghini, G. Montagnoli, G. F. Segato, D. Ackermann, L. Corradi, C. J. Lin, A. M. Stefanini, and L. F. Zheng, 2000, Nucl. Phys. **A672**, 99.
Schatz, H., and K. E. Rehm, 2006, Nucl. Phys. **A777**, 601.
Schmidt, K.-H., and W. Morawek, 1991, Rep. Prog. Phys. **54**, 949.
Scuderi, V., *et al.*, 2011, Phys. Rev. C **84**, 064604.
Seif, W. M., 2004, J. Phys. G **30**, 1231.
Sekizawa, K., and K. Yabana, 2013, Phys. Rev. C **88**, 014614.
Shen, W. Q., *et al.*, 1987, Phys. Rev. C **36**, 115.
Shilov, V. M., 2012, Phys. At. Nucl., **75**, 449.
Shrivastava, A., *et al.*, 2013, Phys. Lett. B **718**, 931.
Signorini, S., 1997, Nucl. Phys. **A616**, 262.
Simenel, C., 2010, Phys. Rev. Lett. **105**, 192701.
Simenel, C., 2014, in *Clusters in Nuclei 3*, edited by C. Beck, Lecture Notes in Physics (Springer-Verlag, Berlin), Vol. 875, p. 95.
Siwek-Wilczyńska, K., T. Cap, M. Kowal, A. Sobiczewski, and J. Wilczyński, 2012, Phys. Rev. C **86**, 014611.
Skobelev, N. K., *et al.*, 2013, Phys. Part. Nucl. Lett., **10**, 248.
Smith, M. S., and K. E. Rehm, 2001, Annu. Rev. Nucl. Part. Sci. **51**, 91.
Souza, F. A., *et al.*, 2009, Nucl. Phys. **A821**, 36.
Souza, F. A., *et al.*, 2010a, Nucl. Phys. **A834**, 420c.
Souza, F. A., *et al.*, 2010b, Eur. Phys. J. A **44**, 181.
Spillane, T., *et al.*, 2007, Phys. Rev. Lett. **98**, 122501.
Spinka, H., and H. Winkler, 1974, Nucl. Phys. **A233**, 456.
Steadman, S. G., and M. J. Rhoades-Brown, 1986, Annu. Rev. Nucl. Part. Sci. **36**, 649.
Stefanini, A. M., L. Corradi, A. M. Vinodkumar, Yang Feng, F. Scarlassara, G. Montagnoli, S. Beghini, and M. Bisogno, 2000, Phys. Rev. C **62**, 014601.
Stefanini, A. M., *et al.*, 1986, Nucl. Phys. **A456**, 509.
Stefanini, A. M., *et al.*, 1995, Phys. Rev. Lett. **74**, 864.
Stefanini, A. M., *et al.*, 2006, Phys. Rev. C **73**, 034606.
Stefanini, A. M., *et al.*, 2007, Phys. Rev. C **76**, 014610.
Stefanini, A. M., *et al.*, 2008, Phys. Rev. C **78**, 044607.
Stefanini, A. M., *et al.* 2009, Phys. Lett. B **679**, 95.
Stefanini, A. M., *et al.*, 2010, Phys. Rev. C **82**, 014614.
Stelson, P. H., 1988, Phys. Lett. B **205**, 190.
Stokstad, R. G., Z. E. Switkowski, R. A. Dayras, and R. M. Wieland, 1976, Phys. Rev. Lett. **37**, 888.
Strieder, F., 2010, *Symposium NIC XI, Heidelberg*, www.lsw.uni-heidelberg.de/nic2010/talks/Strieder.pdf.
Summers, N. C., F. M. Nunes, and I. J. Thompson, 2006, Phys. Rev. C **74**, 014505.
Światecki, W. J., 1981, Phys. Scr. **24**, 113.
Światecki, W. J., 1982, Nucl. Phys. **A376**, 275.
Światecki, W. J., 2003, Acta Phys. Pol. B **34**, 2049.
Światecki, W. J, K. Siwek-Wilczyńska, and J. Wilczyński, 2005, Phys. Rev. C **71**, 014602.
Switkowski, Z. E., R. G. Stokstad, and R. M. Wieland, 1976, Nucl. Phys. **A274**, 202.
Switkowski, Z. E., R. G. Stokstad, and R. M. Wieland, 1977, Nucl. Phys. **A279**, 502.
Symons, T. J. M., V. P. Viyogi, G. D. Westfall, P. Doll, D. E. Greiner, H. Faraggi, P. J. Lindstrom, D. K. Scott, H. J. Crawford, and C. McParland, 1979, Phys. Rev. Lett. **42**, 40.
Takigawa, N., K. Hagino, M. Abe, and A. B. Balantekin, 1994, Phys. Rev. C **49**, 2630.
Tanihata, I., H. Hamagaki, O. Hashimoto, Y. Shida, N. Yoshikawa, K. Sugimoto, O. Yamakawa, T. Kobayashi, and N. Takahashi, 1985, Phys. Rev. Lett. **55**, 2676.
Tanimura, O., 1987a, Phys. Rev. C **35**, 1600.
Tanimura, O., 1987b, Z. Phys. A **327**, 413.
Thomas, J., Y. T. Chen, S. Hinds, K. Langanke, D. Meridith, M. Olson, and C. A. Barnes, 1985, Phys. Rev. C **31**, 1980.
Thompson, I. J., 2006 (Fresco) [www.fresco.org.uk].
Thompson, I. J., M. A. Nagarajan, J. S. Lilley, and M. J. Smithson, 1989, Nucl. Phys. **A505**, 84.
Timmers, H., D. Ackermann, S. Beghini, L. Corradi, J. H. He, G. Montagnoli, F. Scarlassara, A. M. Stefanini, and N. Rowley, 1998, Nucl. Phys. **A633**, 421.
Timmers, H., J. R. Leigh, M. Dasgupta, D. J. Hinde, R. C. Lemmon, J. C. Mein, C. R. Morton, J. O. Newton, and N. Rowley, 1995, Nucl. Phys. **A584**, 190.
Tōke, J., *et al.*, 1985, Nucl. Phys. **A440**, 327.
Torresi, D., *et al.*, 2011, Eur. Phys. J. Web Conf. **17**, 16018.
Trotta, M., *et al.*, 2000, Phys. Rev. Lett. **84**, 2342.
Tserruya, I., Y. Eisen, D. Pelte, A. Gavron, H. Oeschler, D. Berndt, and H. L. Harney, 1978, Phys. Rev. C **18**, 1688.
Uegaki, E., and Y. Abe, 1993, Prog. Theor. Phys. **90**, 615.
Umar, A. S., and V. E. Oberacker, 2006a, Phys. Rev. C **73**, 054607.
Umar, A. S., and V. E. Oberacker, 2006b, Phys. Rev. C **74**, 021601.
Umar, A. S., and V. E. Oberacker, 2008, Phys. Rev. C **77**, 064605.
Umar, A. S., V. E. Oberacker, and C. J. Horowitz, 2012, Phys. Rev. C **85**, 055801.
van den Berg, A. M., W. Henning, L. L. Lee, K. T. Lesko, K. E. Rehm, J. P. Schiffer, G. S. F. Stephans, F. L. H. Wolfs, and W. S. Freeman, 1988, Phys. Rev. C **37**, 178.
Vandenbosch, R., 1992, Annu. Rev. Nucl. Part. Sci. **42**, 447.
Vanhoy, J. R., E. G. Bilpuch, C. R. Westerfeldt, and G. E. Mitchell, 1987, Phys. Rev. C **36**, 920.
Vaz, L. C., J. M. Alexander, and G. R. Satchler, 1981, Phys. Rep. **69**, 373.
Vinodkumar, A. M., 2010, Pramana J. Phys. **75**, 109.
Vinodkumar, A. M., *et al.*, 2013, Phys. Rev. C **87**, 044603.
Wallerstein, G., *et al.*, 1997, Rev. Mod. Phys. **69**, 995.
Washiyama, K., K. Hagino, and M. Dasgupta, 2006, Phys. Rev. C **73**, 034607.
Washiyama, K., and D. Lacroix, 2008, Phys. Rev. C **78**, 024610.
Watanabe, Y. X., *et al.*, 1998, RIKEN Annual Report 1998, p. 70.
Winklehner, D., A. Lemut, D. Leitner, M. Couder, A. Hodgkinson, and M. Wiescher, 2013, AIP Conf. Proc. No. 1525 (AIP, New York), p. 516.
Winther, A., 1995, Nucl. Phys. **A594**, 203.
Wolfs, F. L. H., 1987, Phys. Rev. C **36**, 1379.
Wolski, R., *et al.*, 2011, Eur. Phys. J. A **47**, 111.
Wong, C. Y., 1973, Phys. Rev. Lett. **31**, 766.

Woosley, S. E., A. Heger, and T. A. Weaver, 2002, Rev. Mod. Phys. **74**, 1015.
Wu, S. C., 1978, Ph.D. thesis, California Institute of Technology.
Wu, S. C., and C. A. Barnes, 1984, Nucl. Phys. **A422**, 373.
Wuosmaa, A. H., J. P. Schiffer, B. B. Back, C. J. Lister, and K. E. Rehm, 2007, Nucl. Instrum. Methods Phys. Res., Sect. A **580**, 1290.
Wuosmaa, A. H., *et al.*, 2005, Phys. Rev. C **72**, 061301.
Yakovlev, D. G., L. R. Gasques, A. V. Afanasjev, M. Beard, and M. Wiescher, 2006, Phys. Rev. C **74**, 035803.
Yusa, S., K. Hagino, and N. Rowley, 2010, Phys. Rev. C **82**, 024606.
Yusa, S., K. Hagino, and N. Rowley, 2012, Phys. Rev. C **85**, 054601.
Zagrebaev, V., and W. Greiner, 2005, J. Phys. G **31**, 825.
Zagrebaev, V., and W. Greiner, 2008, Phys. Rev. C **78**, 034608.
Zagrebaev, V., and W. Greiner, 2011, Phys. Rev. C **83**, 044618.
Zagrebaev, V., and W. Greiner, 2010, in *Clusters in Nuclei 2*, edited by C. Beck, Lecture Notes in Physics (Springer-Verlag, Berlin), Vol. 818, p. 267.
Zagrebaev, V. I., 2003, Phys. Rev. C **67**, 061601(R).
Zhang, H. Q., *et al.*, 2010, Phys. Rev. C **82**, 054609.
Zickefoose, J., 2011, Ph.D. thesis, University of Connecticut, 2011 (UMI Dissertation Publication No. 3485448 and references therein).
Zyromski, K. E., W. Loveland, G. A. Souliotis, D. J. Morrissey, C. F. Powell, O. Batenkov, K. Aleklett, R. Yanez, and I. Forsberg, 2001, Phys. Rev. C **63**, 24615.